ANALYSIS OF TWO-DIMENSIONAL TURBULENT WALL-JETS

A THESIS

Presented to

The Faculty of the Division of Graduate Studies and Research

By

Jaunan Liaw

In Partial Fulfillment

of the Requirements for the Degree

Doctor of Philosophy

in the School of Aerospace Engineering

Georgia Institute of Technology

June, 1975

ANALYSIS OF TWO-DIMENSIONAL

TURBULENT WALL-JET

Approved:

Prof. J. E. Hubbartt, Chairman

Dr. W. H. Bangert

Dr. H. G. Roper

Date approved by chairman: 4/30/75

ACKNOWLEDGMENTS

The author is deeply indebted to Professor James E. Hubbartt, his advisor, for his guidance, encouragement, cooperation and constant support during the author's graduate work. His contributions have been the most significant factor in bringing this thesis to its present state. In addition the author appreciates very much the successful efforts of Professor Hubbartt in overcoming the language barrier.

The cooperation and advice of Dr. R. G. Roper and Dr. L. H. Bangert, who served as members of the thesis committee, are gratefully acknowledged.

The author is also indebted to the Georgia Institute of Technology for providing a graduate research assistantship.

Finally, the patience and understanding provided by the author's parents, wife, and son are greatly appreciated.

TABLE OF CONTENTS

		Page
ACKNOWLEDGMENTS		ii
LIST OF TABLES		v
LIST OF ILLUSTRATIONS		vi
LIST OF SYMBOLS		viii
SUMMARY		xi
Chapter		
I.	INTRODUCTION AND LITERATURE REVIEW	1
	Introduction Literature Review Purpose of the Present Investigation	
II.	FUNDAMENTAL ASSUMPTIONS, EQUATIONS AND EXPERIMENTAL DATA	13
	General Equations Turbulent B. L. Equations Experimental Data	
III.	DATA ANALYSES	25
	Velocity Profiles Velocity Decay Temperature Data Shear Stress Eddy Viscosity and Mixing Length Maximum Shear Stresses Wall Sublayer	
IV.	ANALYTICAL SOLUTION	119
	Basic Technique and Assumptions Numerical Solution Numerical Results	
V.	CONCLUSIONS AND RECOMMENDATIONS	143

Page

REFERENCES 146

VITA 149

LIST OF TABLES

Table		Page
1.	Experimental Data	24
2.	Tabulation of Velocity Profile for Jet Layer	39
3.	Tabulation of Shear-Stress Similarity Functions	79

LIST OF ILLUSTRATIONS

Figure		Page
1.	Composite Wall Jet Development	20
2.	Wall Jet Velocity Profile and Definitions of δ_j and δ_w	27
3.	Jet Layer Velocity Profile	28
4.	Comparison of Analytic Curve with Clasic Curves	41
5.	Wake Layer Velocity Profile	43
6.	Wall Jet Velocity Decay	49
7.	Wall Jet Temperature Profile	55
8.	Temperature Profile for Series III; VR = 2.92; x = 286	56
9.	Wall Jet Temperature Decay	58
10.	Shear Stress Distribution for Series III; VR = 2.92; x = 341	60
11.	Inner Shear Layer Profile	61
12.	Submerged Shear Layer Profile	67
13.	Outer Shear Layer Profile	71
14.	Eddy Viscosity Profile	82
15.	Turbulent Reynolds Number Variation with x-Jet Layer	86
16.	Turbulent Reynolds Number Variation with x-Wake Layer	89
17.	Turbulent Reynolds Number Variation with U_e/U_m-Jet Layer	97
18.	Wall Sublayer Velocity Profile	100
19.	Wall Sublayer Velocity Profile	106
20.	Wall Sublayer Velocity Profile	108
21.	Wall Sublayer Velocity Profile	110

Figure		Page
22.	Wall Sublayer Velocity Profile, Series I, VR = ∞	111
23.	Wall Sublayer Velocity Profile; Series II; VR = 0	113
24.	Wall Sublayer Velocity Profile, Series III; VR = 2.07 . .	115
25.	Wall Sublayer Velocity Profile, Series IV; VR = 2.99 . . .	116
26.	Wall Sublayer Shear Stress Profiles	118
27.	Comparison of Shear Stress Cubic Profile with Experimental Data	122
28.	Boundary Layer Velocity Profile for Wieghardt Flat Plate Flow; U_∞ = 33 m/sec	130
29.	Boundary Layer Velocity Profile for Liedwieg and Tillman Mild Adverse Pressure Gradient	133
30.	Wall-Jet Velocity Profile Series II; VR = 3	135
31.	Wall-Jet Velocity Profile Series III; VR = 2.92	139

LIST OF SYMBOLS

f	velocity similarity function
g	shear-stress similarity function
h	jet slot height
P	pressure
R_e	Reynolds number
T	temperature
U	mean velocity in x direction
u	instantaneous velocity in x direction
v	mean velocity in y direction
ν	instantaneous velocity in y direction
U_τ	friction velocity
u^+	U/U_τ
x	cartesian coordinate (streamwise)
u'	$u - U$
ν'	$\nu - v$
X	x/h
y	Cartesian coordinate (normal to wall)
Ueo	edge velocity at jet exit plane in x direction
U_J	jet mean velocity in x direction
VR	ratio of U_j to Ueo
δs.L.	boundary layer thickness
δ	velocity profile thickness parameter

τ_w	local wall skin friction
τ	turbulent shear stress
ν	kinematic viscosity
ρ	gas density
λ	$\frac{\nu}{U_\tau^2} \frac{dU_\tau}{dx}$
π	$\frac{\nu}{\rho U_\tau^3} \frac{dP}{dx}$
y^+	$\frac{yU_\tau}{\nu}$
η	velocity similarity length scale
ϕ	shear similarity length scale
Series I	the wall jet injected into still air
Series II	the wall jet under a constant pressure main-stream flow
Series III	the wall jet subjected to an adverse pressure gradient imposed by a retarded main-stream flow with a substantially thickened initial boundary layer
Series IV	the wall jet subjected to an adverse pressure gradient imposed by a retarded main-stream flow with a thickened and distorted initial boundary layer

Subscripts

o	jet exit plane
2	jet layer half-velocity or submerged shear layer
3	minimum velocity or outer shear layer
4	half-velocity, wake layer
e	edge
j	jet

m	jet peak
w	wake

SUMMARY

An analytic investigation of the flowfield produced by two-dimensional, turbulent wall jets with and without a longitudinal free-stream pressure gradient is presented.

The investigation was conducted in two parts. In the first part, experimental data were analyzed to establish semi-empirical relations for

1. Velocity profile similarities
2. Shear stress similarities
3. Wall sublayer similarities, and
4. Maximum shear stresses

An analytic function for the velocity profiles in the jet and wake layers was obtained by least square fitting to experimental data. This analytic function was used in all subsequent data analysis to represent the experimental data with high accuracy.

The local shear stress data were calculated using the momentum equation, the continuity equation, experimental surface shear stresses, and the analytic function for the velocity profiles. Shear stress similarity relations for the wall, jet, and wake layers were then achieved by appropriately scaling the calculated shear stress results.

The velocity and shear profiles in the wall sublayer were obtained by using the mixing length theory which, as is shown, gives results that agree well with the experimental data.

A closed form expression for the maximum shear stress was derived from the turbulent energy equation assuming that the various turbulent quantities are related. The expression yields results which are in satisfactory agreement with the experimental data.

In the second part, similarity and semi-empirical results, as established in the first part, were utilized to develop an overall solution for turbulent boundary layer and wall jet flows. A step-by-step numerical solution of the partial differential equations was employed. Comparisons between the predicted and experimental data show encouraging agreement.

CHAPTER I

INTRODUCTION AND LITERATURE REVIEW

Introduction

The behavior of a jet blowing tangential to a solid surface is of great interest because of the applicability of such jets to film cooling (1), boundary layer control (B.L.C.) of ejectors as a means of substantially increasing the thrust augmentation (2) and B.L.C. of aircraft. Applied in the area of B.L.C. of aircraft, the jet supplies additional energy to a boundary layer in an adverse pressure gradient thereby not only delaying or eliminating separation but also producing increased circulation about the lifting body. Both of these effects contribute measurably to increase lift for any angle of attack and free stream velocity. It is important, then, to become familiar with the controlling parameters involved in the problem and to be able to predict the increase in lift for any reasonable set of operating conditions. Accomplishment of this suggests analytic approaches to solution of the development of a two-dimensional wall jet introduced into an initial boundary layer with a free stream pressure gradient.

A relatively large volume of literature pertaining to boundary layer control by means of external blowing exists. A great deal of this documents various experimental investigations in which certain trends have been observed; some of these are fairly well understood and some are not. Theoretical analyses are found less frequently and

are often less than satisfactory. Basically, the boundary layer control problem requires theoretical methods capable of analyzing the jet-boundary layer mixing in order to permit rational calculation of the optimum amount and distribution of blowing momentum needed to prevent separation of the boundary layer from an arbitrary airfoil. General basic methods of analysis are not found in the literature, mainly for the reason that there is as yet only incomplete understanding of the complicated interactions which occur when a jet is blown into a boundary layer tangentially to an arbitrarily curved surface, where it is influenced by the external velocity and external pressure gradient.

Wall jet flow is more complicated than most two-dimensional shear flows, incorporating as it does some features of a boundary layer and some features of jets and wakes. Any analytic approach must involve some impiricism and the best approach will be the one which makes maximum use of data and analytic methods for these and other related turbulent shear flows. There is already in existence in the literature much material of interest and usefulness regarding, or related to, the boundary layer control problem. However, a satisfactory method for analyzing turbulent wall jet flows with pressure gradients is not available.

Literature Review

This review, in an attempt to collect related systematic and chronological studies, includes experimental and theoretical works in which the wall jet is directed tangent to a flat downstream surface. The investigations in which no free stream was used are included along

with those in which a free stream existed with and without a streamwise pressure gradient.

Experimental Investigations

The earliest published experimental work on the two-dimensional wall jet with no main-stream flow was performed by Förthmann (3) as a supplement to his investigation of the plane free jet and partially expanding jet. Förthmann observed the apparent self-preserving nature of wall jet velocity profiles for short distances downstream of the jet slot. His data also indicated that the boundary layer thickness varies linearly with distance from the slot and that the maximum velocity varies inversely as the one half power of this distance. Further, he concluded from his data that the velocity in the wall layer (between the wall and velocity maximum) varies as the one seventh power of the height from the wall, an observation that is not substantiated by later experiments.

The first effort to concentrate experimentally on the wall jet with no free-stream flow was implemented by Bakke (4) in 1957. In an attempt to verify the analytic results of Glauert (5), Bakke measured velocity profiles to a distance of 20 slot widths from the point of injection for a Reynolds number based on slot height of approximately 30,000. The data provided a record of jet thickness growth and maximum velocity decay with distance from the slot. Bakke found agreement in his work with the results of Förthmann and Glauert and stated, "within the experimental range and accuracy the velocity profiles are similar and the rate of change of velocity and width of the jet can be expressed by simple power laws." Bakke's data was not sufficiently extensive to

reveal the variation of the growth and decay laws with Reynolds number based on slot height that Blauert had predicted.

In 1961 Patel and Newman (6) experimentally created the conditions necessary for the wall jet outer profiles (from the jet peak to the free stream) to remain similar. These "self-preserving" profiles were obtained by retarding the free-stream flow such that the ratio of local jet peak velocity to free-stream velocity was constant. They suggested that experimental evidence indicates that similarity exists in the outer layer and may extend to the outer region of the wall layer. It should be noted that evidence of an initial boundary layer did not appear in their data. Patel and Newman also measured wall jet profiles for zero pressure gradient cases. They found that for the zero pressure gradient cases the outer layer profiles demonstrated near similarity. They finally suggested that further profile detail is needed in the wall layer and that more complete skin friction measurements must be made for all wall jet cases.

In 1963, Eskinazi and Kruka (7) investigated the zero pressure gradient cases for a wide range of initial velocity ratios and confirmed that the similarity expressions for the wall layer and the outer layer require different velocity and length scales. Based on the results of their investigations, they concurred with the earlier findings of Bradshaw and Gee (8) that the point of zero turbulent shear stress is not located at the jet peak and that the points of partition of the profile are still open to question. Kruka and Eskinazi also investigated skin friction with a flattened Preston tube. Their data does not agree well with either earlier or later results.

Erian and Eskinazi (9) extended the work of Kruka and Eskinazi in 1964 to include velocity profile and skin friction measurements for a wall jet in a moving stream with a pressure gradient. The tests were performed for one initial velocity ratio and no attempt was made to systematically vary pressure gradient; the results were therefore considerably limited in scope.

In 1968, Kacker and Whitelaw (10) recognized the need for more data in the low velocity ratio range and performed their experiments for velocity ratios of 0.75 to 2.74 to a distance of 150 slot widths downstream. The work was done with no pressure gradient applied to the wall jet. Kacker and Whitelaw noted in their work that the trends observed in previous investigations for skin friction seem to be consistent; however, they still found sizeable differences in values measured.

In 1969, Gartshore and Newman presented their own data for several wall jet cases as follows:

1. A wall jet into still air.

2. A self-preserving wall jet for nominal velocity ratios of 1.3, 2.0 and 3.0.

3. A non-self-preserving wall jet in adverse pressure gradient for nominal velocity ratios of 2.0 and 4.0.

4. A wall jet in zero pressure gradient for nominal velocity ratios of 2.0, 3.0 and 4.0.

They included over all growth and decay information for comparison with calculations based on their own analytical model; however, they did not

present profile detail or skin friction measurements.

In 1971, Neale (12) presented an experimental study of various wall jet flows as follows:

1. The wall jet injected into still air.

2. The wall jet under a constant-pressure main-stream flow for nominal velocity ratios of 2.0, 3.0, 4.0 and 6.0.

3. The wall jet subjected to an adverse pressure gradient imposed by a retarded main-stream flow with a substantially thickened initial boundary layer for nominal velocity ratio of 1.5, 2.07, and 2.92.

4. The wall jet subjected to an adverse pressure gradient imposed by a retarded main-stream flow with a thickened and distorted initial boundary layer for nominal velocity ratio of 2.0 and 3.0.

Neale's investigations proceeded systematically from the simple to the more complex wall jet flows. The studies of wall jets in still air and wall jets in constant pressure free streams establish the characteristics of simple wall jet flows. With the behavior of these comparatively uncomplicated flows known, Neale provided with studies of more complex wall jets in adverse pressure gradients. These adverse pressure-gradient cases provide a study of wall jet flow in which the initial boundary layer momentum deficit is significant in comparison with the jet momentum excess. Evidence of this relatively large initial momentum deficit is present throughout his measured development of these wall jets. Neale made detailed velocity profile and local skin friction measurements for the case in which no main-stream flow was present; his studies were carried out for a wide range of slot Reynolds numbers. For the wall jets with main-stream flow, he investigated selected ratios

of free-stream velocity to jet nozzle velocity. In each of his studies measurements were performed at several streamwise distances from the point of jet injection. Neale demonstrated velocity profile similarity for all four series of wall jet test results. The measured growth of the half-velocity height and the decay of the jet peak velocity with distance from the jet slot agree qualitatively with theoretical predictions and quantitatively with comparable measurements of others (11), (6). The near wall profiles seemed to demonstrate similarity in the form of a single "law of the wall" for all measurements. The outer portion of the wall layer, however, does not conform to a simple expression of similarity. This outer region is influenced by the presence of local pressure gradients, by the local jet to free-stream velocity ratio and by the velocity deficit in the valley above it. Neale measured the friction data with a Preston tube for the wall jet in still air and his results agree closely with the data presented by Sigalla (13). His studies have provided a large body of experimental information concerning velocity profiles and wall jet development for the still air and free-stream cases with and without streamwise pressure gradient. Furthermore, the results show a good measure of consistency and concurrence with other high quality wall jet data.

In summary, Neale's studies have provided detailed presentation of a systematic study of wall jets developing under streamwise pressure gradient. Of the few studies that have been implemented, most are narrow in scope while the rest are lacking in comprehensive detail. Neale's experimental data were therefore utilized in the present study to establish semiempirical formula and similarity parameters.

Theoretical Investigations

In 1956, Glauert (5) used a similarity approach to solve the flow due to a jet spreading out over a plane surface, either radially or in two dimensions. Based on physical reasoning in this simple type of flow, Glauert was the first to postulate that the entire flow field of the wall jet cannot conform to one overall similarity solution. He divided the flow into a wall layer and a jet layer on either side of maximum velocity and treated the two regions separately.

In 1961, Carriere and Eichelbrenner (14) developed a more detailed calculation method. This method is incomplete, however, as certain empirical information about each flow is needed. A notable result of the analysis and experiments of Carriere and Eichelbrenner was the importance of velocity profiles with both a maximum and a minimum, characterizing the initial boundary layer effect. High velocity, narrow jets appeared to require smaller momentum, as only the inner part of the original boundary layer must be accelerated to prevent separation.

In 1965, Harris (15) conducted analytical work on the turbulent wall jet in a moving stream with arbitrary pressure gradient. His mathematical model consisted of a wall layer and a jet layer only, and further more, it was assumed in his analysis that slot velocity and slot height are very large compared to the free stream velocity and boundary layer thickness at the exit of the slot. In that case the momentum deficit of the upstream boundary layer at the slot lip is negligible and, thus, he could justify the assumption of no interference of external stream boundary layer on the flow development downstream.

In 1967, Patanker and Spalding (16) presented a solution for the wall jet problem using the finite difference technique and Prandtl's mixing length hypothesis. They expressed the eddy viscosity by

$$\mu_{eff} = \rho l^2 \left(\frac{\partial u}{\partial y} \right) \tag{1}$$

where l is the mixing length given by

$$0 < y \leq \lambda\, y_\ell / K \;:\; \ell = Ky \tag{2a}$$

$$\lambda\, y_\ell / K = y \;:\; \ell = \lambda\, y_\ell \tag{2b}$$

where λ and K are constants, y is the distance from the wall, and y_ℓ is a characteristic thickness of the layer. Calculations were provided for wall-jet flows, with various values of the constants K and λ; comparisons were made with the experimental data of Myers, Schauer and Eutis (17), and Schwartz and Cosart (18). The investigation showed that, the values $K = 0.435$, and $\lambda = 0.09$ gave fairly good agreement with experimental velocity profiles and wall shear stresses. They indicated that better pairs of values could be found for predicting each of these quantities individually; but these "better pairs" were not identical. For example $K = 0.6$, and $\lambda = 0.075$ fitted the velocity profile fairly well; but the pair, $K = 0.5$, $\lambda = 0.0625$, gave better predictions for the shear stress at the wall. It meant simply that the mixing-length hypothesis does not express the whole truth about turbulent boundary layers.

In 1969, Gertshore and Newman (11) developed a method for

calculating the growth of a turbulent wall jet in streaming flow. The flow is assumed to be two-dimensional incompressible and over a plane, smooth wall. The method incorporates four integral momentum equations taken from the wall to various points in the flow. The wall layer is represented by a classical turbulent boundary layer power law profile. The calculation of the outer shearing stress is based on the large-eddy equilibrium hypothesis. The remaining empiricism in the method is based on measurements in selfpreserving wall jets. However, their analysis is restricted to a simple wall jet.

In 1970, Verhoff (19) used a similarity solution approach to solve both plane turbulent wall jet and turbulent wall jet beneath a secondary uniform stream. He compared his solutions with experimental data and obtained excellent agreement over much of the profile for a wide range of velocity ratios and slots widths downstream of the jet slot. Verhoff attempted, however, to fit the complete velocity profile with his similarity solution and he did not meet with success in the outer region of the outer layer.

In 1970, Hubbartt and Bangert (20) analyzed turbulent wall jets in adverse pressure gradients leading to wall layer separation. The analyses utilize the integral momentum and mechanical energy equations with the wall jet divided into layers. In one limiting case the initial boundary layer is ignored (or rapidly consumed). In the other limit, the initial boundary layer is assumed to be separated forming a starting wake which persists downstream with the minimum velocity remaining zero. This uniquely specifies the allowable pressure gradient. They indicated that for a constant jet momentum, wall layer separation is relatively

insensitive to the jet to free-stream velocity ratio, the jet and wake layer dissipation rates, and the jet and wake layer profile shape factor. They also indicated that the jet and wake layer profile parameters, within the range predicted by similar flows have little effect on the wall jet growth and the influence of Reynolds number on the wall jet development is relatively small. In their analysis, they used several constant turbulent Reynolds numbers to define eddy viscosities in the various parts of the layer and adopted a simple power law for the wall layer.

In 1970, Goradia (21) developed a mathematical model for the wall jet flow from preliminary experimental data. Goradia divided the flow model into an initial region, main regions, and an ordinary turbulent boundary layer region. Furthermore he subdivided each region into various layers such as, wall layer, jet layer and wake layer, according to the characteristic of velocity profiles in the different layers; he derived integral equations for each region mentioned above and for the various layers in the specific region. Goradia obtained similarity functions for the various regions of flow from experimental data. These similarity expressions were checked against data published by others and the agreement was satisfactory. He also considered the initial region where the core flow exists and indicated that the length of the initial region is approximately 7 to 15 slot heights, depending upon pressure gradient and initial conditions at slot exit.

Purpose of the Present Investigation

The primary purpose of the present investigation is to study the

downstream development of wall jets with and without pressure gradient. This type of flow has not been studied in detail proceeding systematically from simple to complex. The present investigation contributes to the understanding in the following ways:

1. Establishes similarity parameters for velocity profiles and shear stress profiles.

2. Presents better agreement between theoretical prediction and experimental data in the wall sublayer.

3. Establishes a semiempirical formula for maximum shear stresses.

4. Develops a similarity approach using shear stresses coupled with wall sublayer analyses to refine and simplify the mathematical model in analysis of two dimensional turbulent wall jets.

CHAPTER II

FUNDAMENTAL ASSUMPTIONS, EQUATIONS AND EXPERIMENTAL DATA

General Equations

The measurable quantities which are usually of interest for a gas in motion are its pressure P, density ρ, temperature T and velocity $\vec{q}$. The equations governing these quantities are

1. The equation of state

$$f(P, \rho, T) = 0 \tag{3}$$

2. The equation of mass conservation

$$\frac{\partial \rho}{\partial t} + \text{div } (\rho \vec{q}) = 0 \tag{4}$$

3. The equation of momentum conservation

$$\rho \frac{D\vec{q}}{Dt} = \rho \vec{F} - \text{grad } p - \text{curl curl } \mu \vec{q}$$

$$+ \frac{4}{3} \text{grad } (\mu \text{ div } \vec{q})$$

$$+ \text{grad } (\vec{q} \cdot \text{grad } \mu) - \vec{q} \nabla^2 \mu$$

$$+ \text{ grad } \mu \times \text{ curl } \vec{q} - \text{ div } \vec{q} \text{ grad } \mu \qquad (5)$$

4. The equation of energy conservation

$$\rho \frac{DE}{Dt} = \Phi - p \text{ div } \vec{q} + \text{div } (K \text{ grad } T) \qquad (6)$$

where E is the internal energy per unit mass, Φ is the dissipation function, μ is the coefficient of viscosity, K is the thermal conductivity, and $\vec{F}$ the external force per unit mass. The underlying assumptions and implication of these equations are discussed by Lighthill (22), Thwaites, and others. A brief and illuminating discussion of their general applicability is contained in Liepmann and Roshko (23). As a consequence of their nonlinearity, the mathematical difficulties of solving the Navier-Stokes equations are severe, even for two-dimensional incompressible flow. In many cases, approximations of various kinds have been useful. Of these, the boundary layer concept, essentially the contribution of Prandtl, has proven to be immeasurably significant and fruitful. Under the boundary layer concept the Navier-Stokes and continuity equations reduce to the well-known boundary layer equation (24);

1. Momentum:

$$\rho u \frac{\partial u}{\partial x} + \rho v \frac{\partial u}{\partial y} = - \frac{dp}{dx} + \frac{\partial \mu \frac{\partial u}{\partial y}}{\partial y} \qquad (7)$$

and

$$\frac{\partial P}{\partial y} = 0 \tag{8}$$

2. Continuity:

$$\frac{\partial \rho u}{\partial x} + \frac{\partial \rho v}{\partial y} = 0 \tag{9}$$

where ρ is expressed in terms of T and P by the thermal state equation and T is from the energy equation (for the data reduction in the subsequent section T was determined from the experimental data and the final analysis was developed and applied for an incompressible flow because the change in T was small and the mathematical model could be simplified).

Turbulent B. L. Equations

Strictly speaking, the assumption of steady, two-dimensional motion is applicable only for laminar flow. In the more interesting turbulent case, turbulent fluctuation velocities of equal order of magnitude occur in all three coordinate directions. However, turbulent flows may be two-dimensional and time-independent in the mean. The turbulent boundary layer equations are indeterminant and must be complemented by additional hypotheses or equations regarding the Reynolds stresses. This problem is not yet solved satisfactorily, and crude approximations with known shortcomings are still in use, for lack of anything better. The classical approaches, more or less in the order of sophistication, are

1. Integral techniques employing only the momentum integral to eliminate all values of the shear stresses except at the wall,

2. Integral techniques employing the momentum integral and an integrated moment of the momentum equation which requires more shear stress detail but integrate this to obtain only one additional shear stress parameter which is evaluated experimentally,

3. Differential technique which uses the differential momentum equation with a mixing length concept (usually empirical) or an eddy viscosity (usually empirical or related by an empirical turbulent Reynolds number) and,

4. Differential techniques which attempt to close the momentum equation by using one or more approximate equations for turbulence quantities (e.g., mixing length, $\rho\overline{uv}$, $\overline{q^2}$, dissipation function).

Bradshaw (25) lists three difficulties associated with developing analyses for complex turbulent boundary layers. First, the simple behavior of eddy viscosity and mixing length in simple thin shear layers is not maintained in more complicated cases like three-dimensional flow, multiple shear layers, and flows with significant extra rates of strain. In cases where the rate of strain changes rapidly (in the x or y direction) the Reynolds stress will respond slowly and not at once as implied by the eddy-viscosity formula. Second, there is no independent exact equation for eddy viscosity or mixing length analogous to the transport equations for Reynolds stress, therefore any independent eddy-viscosity transport equation must be completely empirical. Third, any transport equation for the eddy viscosity or mixing length can be converted into a transport equation for Reynolds stresses by substituting

for the velocity gradients, obtained by differentiating the time-average Navier-Stokes equations. Bradshaw indicated the need for more fundamental data on turbulence quantities before developing turbulent closure equations.

In view of the shortage of fundamental turbulence data the present studies are directed toward extracting additional empirical results from experimental and flow data to establish, to the extent possible, semi-empirical formula and similarities. The boundary layer equations are expressed as

$$\rho U \frac{\partial U}{\partial x} + \rho V \frac{\partial U}{\partial y} = - \frac{\partial P}{\partial x} + \frac{\partial \tau}{\partial y} \tag{10}$$

$$\frac{\partial \rho U}{\partial x} + \frac{\partial \rho V}{\partial y} = 0 \tag{11}$$

Equations (10) and (11) were integrated to determine the shear stress τ from the experimental data. Subsequently these differential equations were used employing similarities in τ, except at the wall where the mixing length approach was used, to establish a numerical differential technique.

Experimental Data

The experimental data obtained by Neale were analyzed. These data included

1. Velocity profiles computed from measured total pressure and temperature profiles,

2. Wall friction coefficients evaluated from preston tube measure-

ments, and

3. Total temperatures measured by a copper-constantan thermocouple probe.

The wall jet flow is generated by introducing a two dimensional jet tangent to the test section floor immediately downstream of the boundary layer development section through a continuous slot (i.e., without spacers) running the full width of the test section. The test section is constructed with clear plexiglas side wall to facilitate observation of visual flow studies and probe locations. Static pressure taps are located along the centerline of the precision flat ground aluminum plate floor and are also located offset 7.5 inches to the right and left of the centerline. The floor is 30 inches wide and 36 inches long. In the test section the developing wall jet flow may be subject to longitudinal pressure gradients. These pressure gradients are created by the controlled bleed of main-stream air through a perforated sheet metal ceiling. This ceiling is matched at its leading edge to the ceiling of a boundary layer development section and may be deformed along its length to achieve additional pressure variations beyond those provided by main-stream bleed alone. The pressure potential is generated by a valve attached immediately downstream of the test section.

Experimental results from the following three series of tests have been analyzed in detail in the present study:

a. Series II - the wall jet under a constant-pressure mainstream flow.

b. Series III - the wall jet subjected to an adverse pressure gradient imposed by a retarded mainstream flow with a substantially

thickened initial boundary layer.

c. Series IV - the wall jet subjected to an adverse pressure gradient imposed by a retarded mainstream flow with a thickened and distorted initial boundary layer.

Typical velocity profiles for each of these series are shown in Figures 1(a) - (d). The various velocity ratios (initial jet-to-mainstream velocity ratio) and streamwise stations for which experimental data were obtained in Reference 12 and which were analyzed in the present study are tabulated in Table 1.

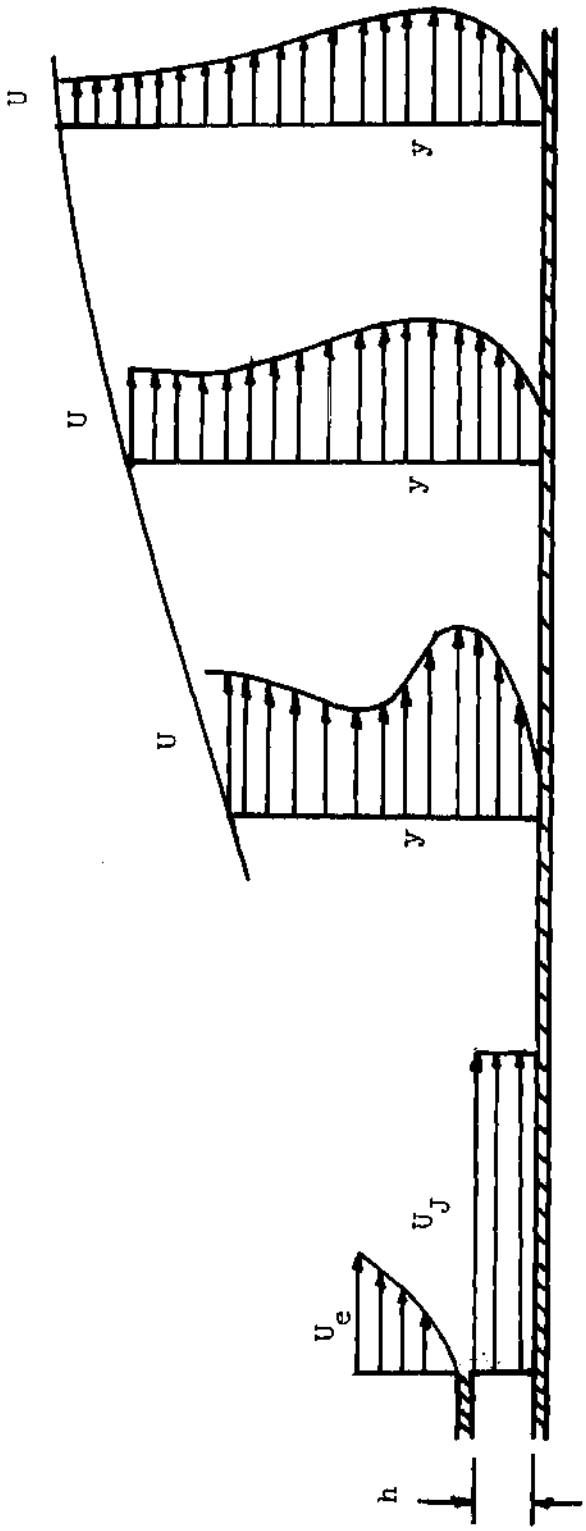

(a) Illustration of Velocity Decay

Figure 1. Composite Wall-Jet Development

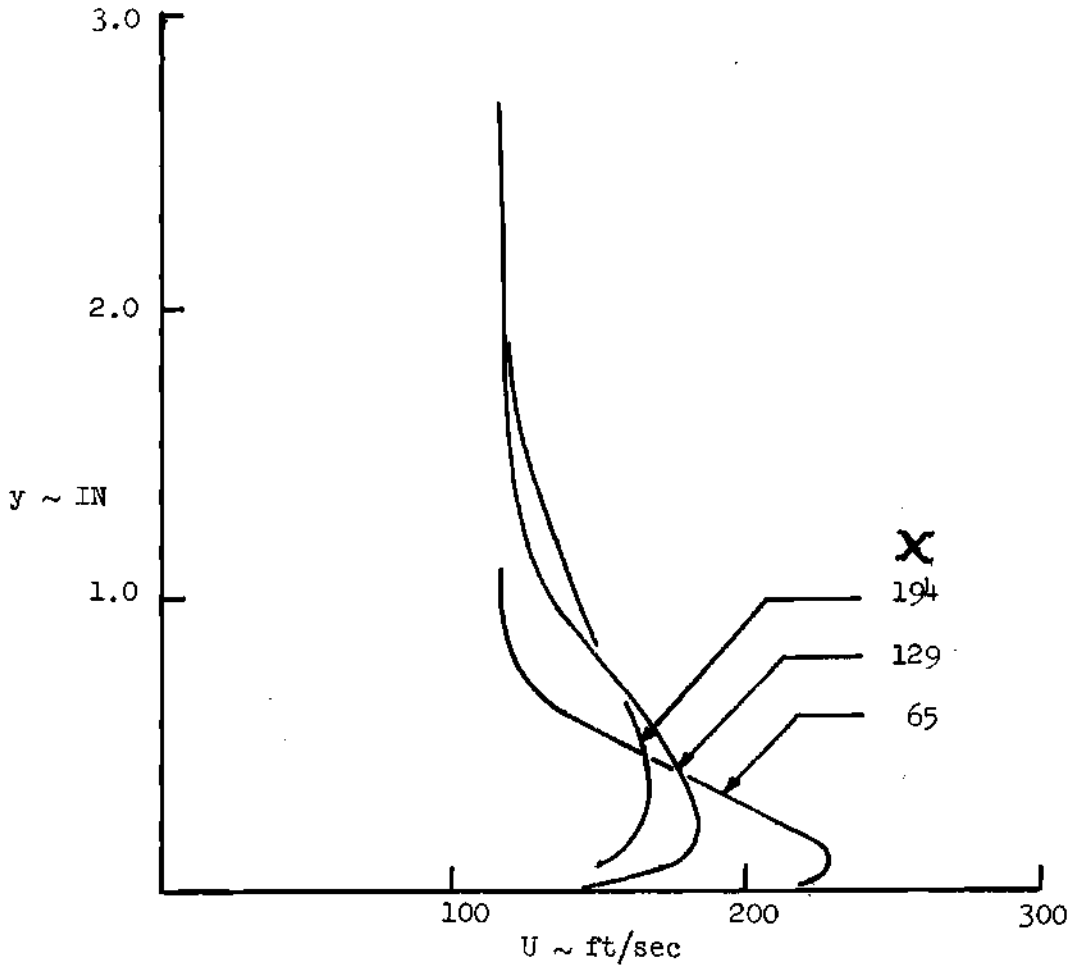

(b) Velocity Profiles for Series II, VR = 3.0

Figure 1. (Continued)

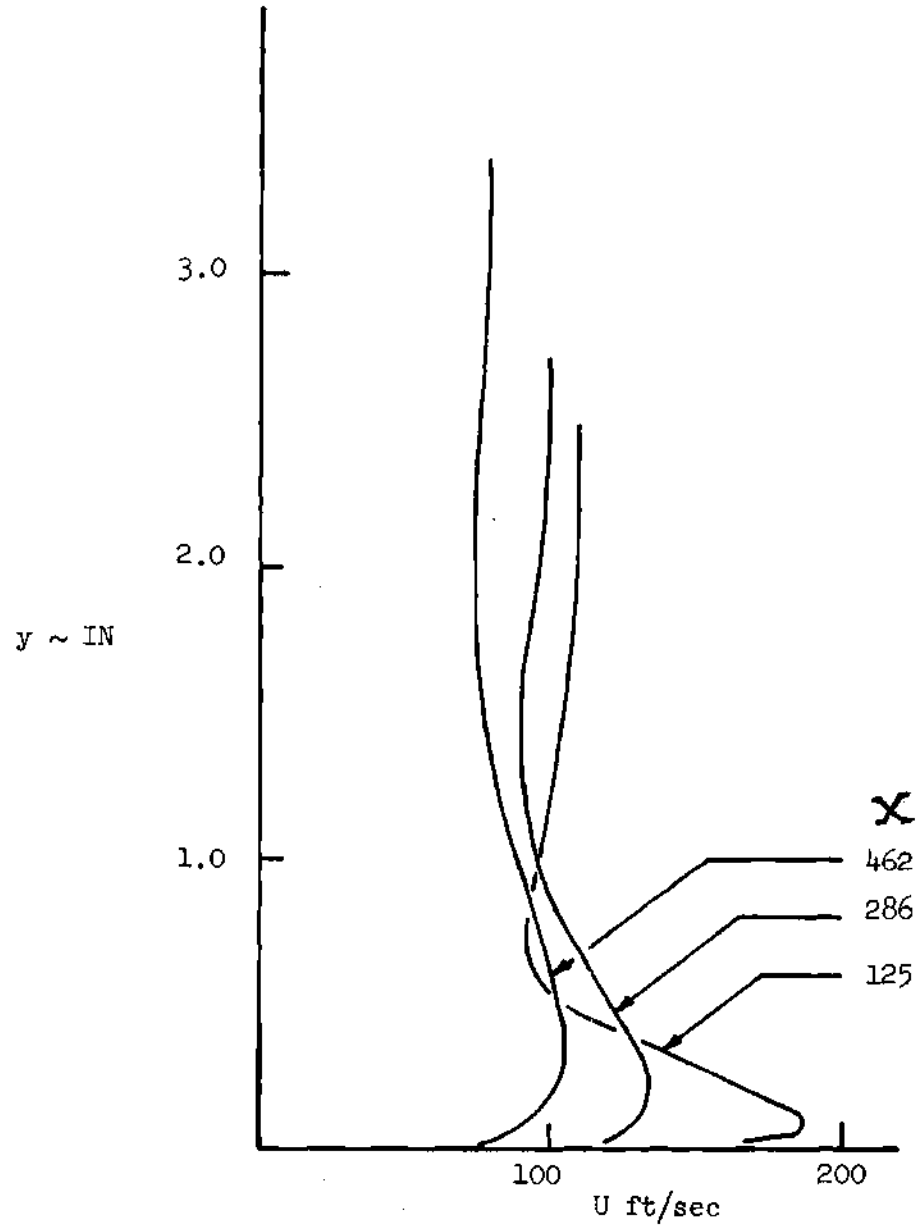

(c) Velocity Profiles for Series III, VR = 2.92

Figure 1. (Continued)

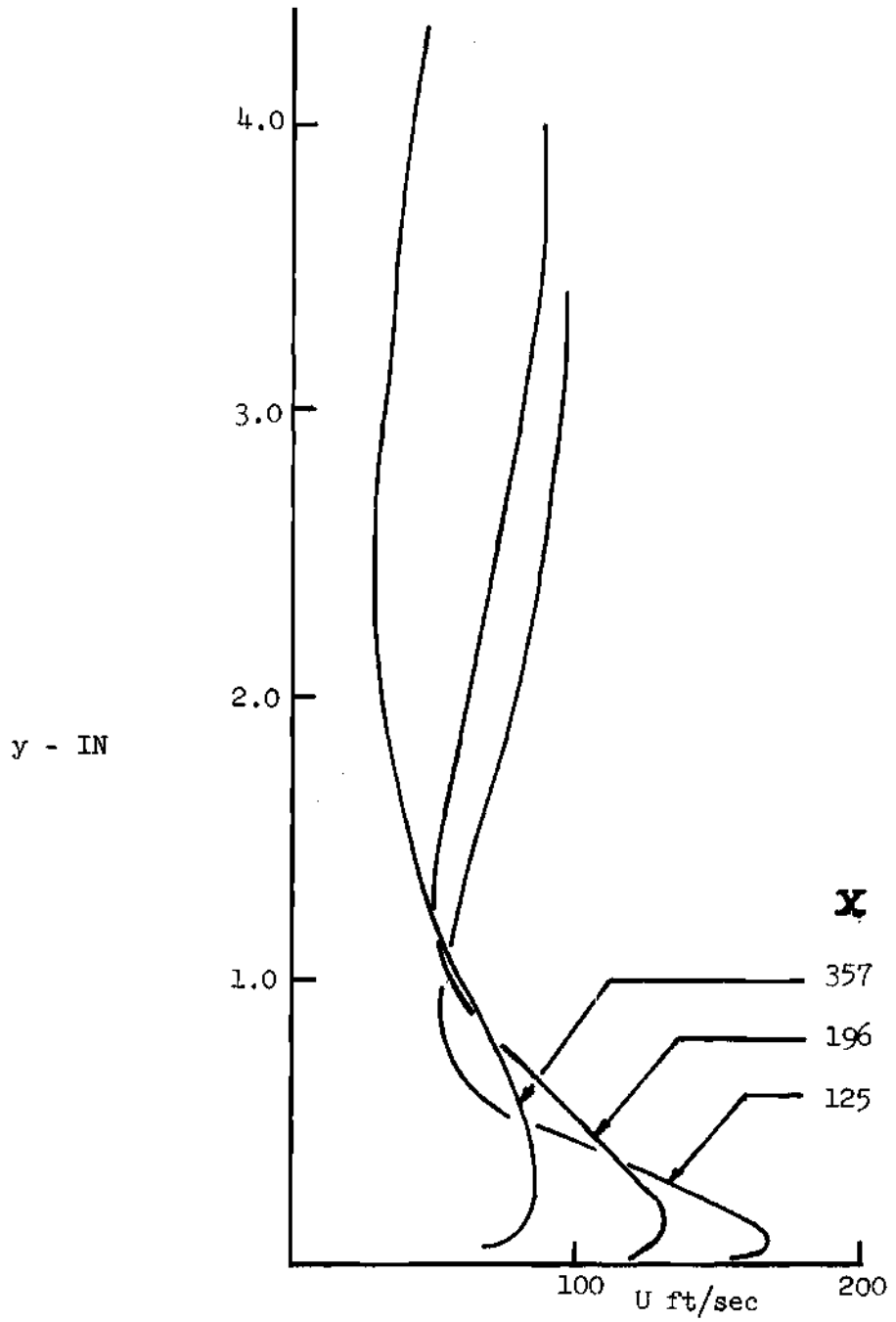

(d) Velocity Profiles for Series IV, VR = 2.99

Figure 1. (Continued)

Table 1. Experimental Data

SERIES	II				III		IV		
VR	2.0	3.0	4.0	6.0	2.07	2.92	1.97	2.0	3.0
	52	52	52	52	125	125	125	56	125
	65	65	65	65	197	197	196	92	196
X	97	97	97	97	286	286	287	125	287
	129	129	129	129	357	357	357	161	357
	161	161	161	161	462	462	463	196	
	194	194	194	194	554	554			

CHAPTER III

DATA ANALYSIS

The experimental data is carefully and systematically analyzed in this chapter in order to establish results useful for evaluating and predicting wall-jet flow. The experimental data are first analyzed in detail to establish flow similarities and smooth out the experimental results. Analytical expressions for the velocity profiles are achieved and then used to represent the experimental data. The shear stresses are obtained from the mean flow data using the integrated momentum and continuity equations. Fairing of the experimental data for the streamwise velocity decay and evaluations of the consistency of the data are conducted considering the overall conservation of momentum. A semi-empirical formula for maximum shear stresses is developed by employing the energy equation. The wall sublayer flow is analyzed in detail to demonstrate the applicability of the mixing length approach for this region.

Velocity Profiles

In order to simplify the analyses to obtain the shear stress profiles from the experimental data of reference (12) and, more importantly, to minimize errors due to data scatter, velocity profile similarities were first established from the experimental data. A total of 50 velocity profiles covering the complete range of operating conditions were analyzed. The results, as discussed in the subsequent paragraphs,

showed that velocity-profile similarities did exist in all of the regions except in the inner region (near the wall) which, as is well known, involves more than one length scale. Each of the regions resemble previously well understood cases for simpler flows. The velocity profiles are subdivided into three regions - an inner layer, a jet layer, and a wake layer - as shown in Figure 2(a). Analytic expressions are obtained for each region having similar velocity profiles using least square fitting to the experimental data. The analysis of these layers is discussed in the following paragraphs.

Inner Layer Velocity Profile

The velocity profile from the wall to the point where $U - U_3 / U_m - U_3 = .8$ was defined as the inner layer (see Figure 2). Velocity-profile similarity does not exist in this region as is evident from the results in Figures 3(a) - (i). Consequently a single function could not be used to represent the inner layer. Therefore, the experimental velocity profiles in this region were replaced by curves faired smoothly through each set of data. Least square fitting was not employed since it was felt that analytic expressions in this complex region would improperly prejudice the results.

Jet Layer Velocity Profile

The velocity profile in the jet layer is expressed as

$$\frac{U - U_3}{U_m - U_3} = f_j(\eta_j) \tag{12}$$

where $\eta_j = (y - \delta_{\frac{1}{2}})/\delta_j$, $\delta_{\frac{1}{2}}$ is the wall-jet thickness to $U = (U_m + U_3)/2$,

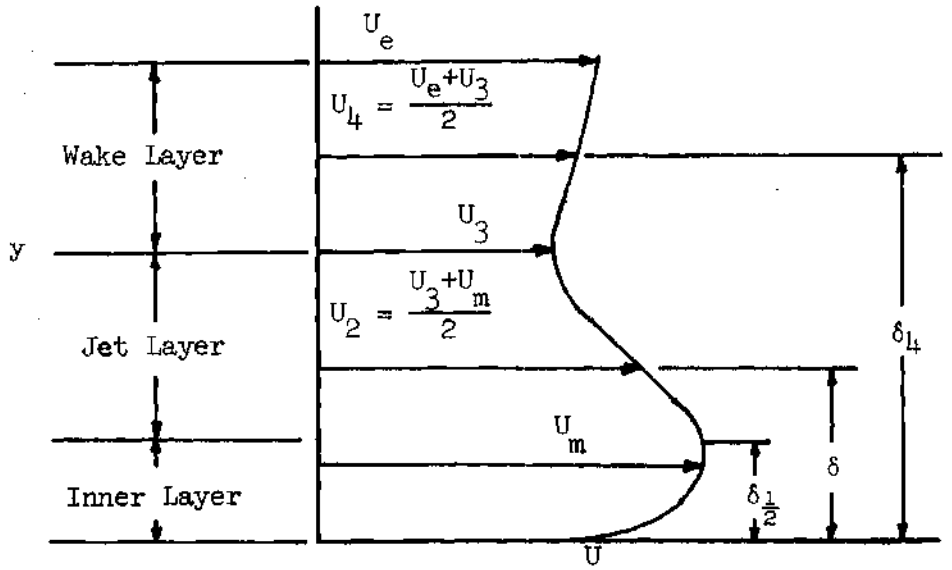

(a) Subdivisions of the Velocity Profile

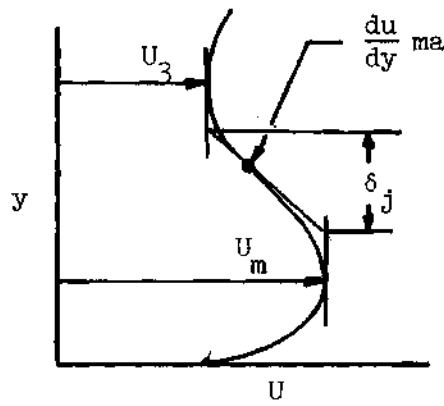

(b) Definition of δ_j

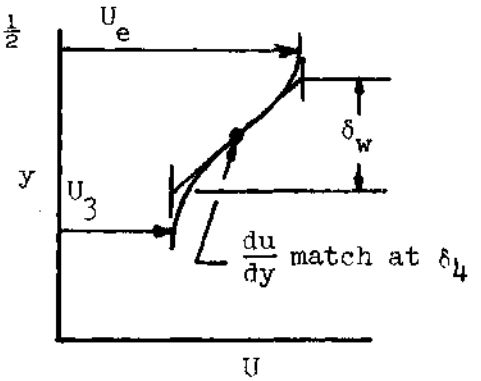

(c) Definition of δ_w

Figure 2. Wall Jet Velocity Profile and Definitions of δ_j and δ_w

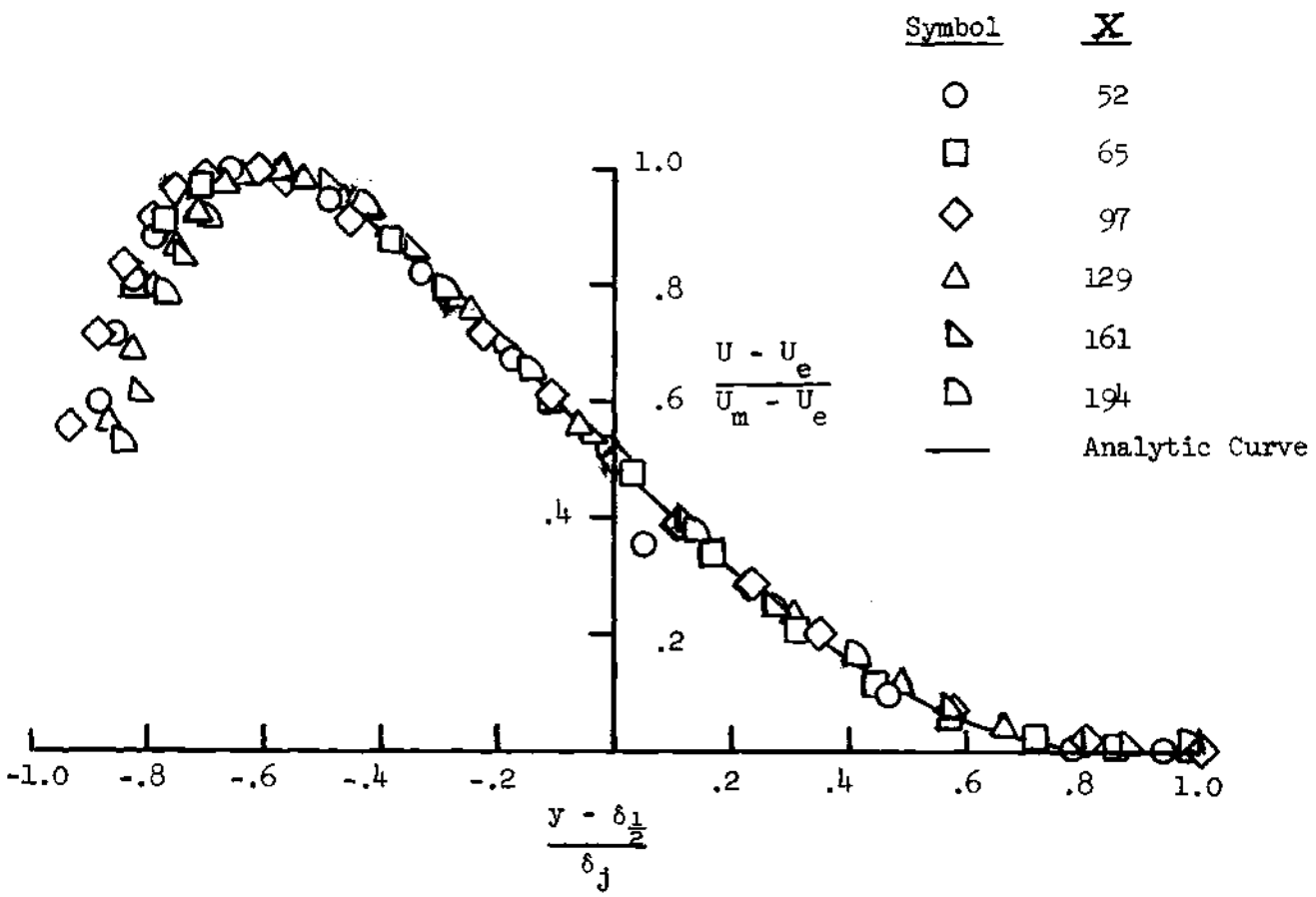

(a) Series II, VR = 2.0

Figure 3. Jet Layer Velocity Profile

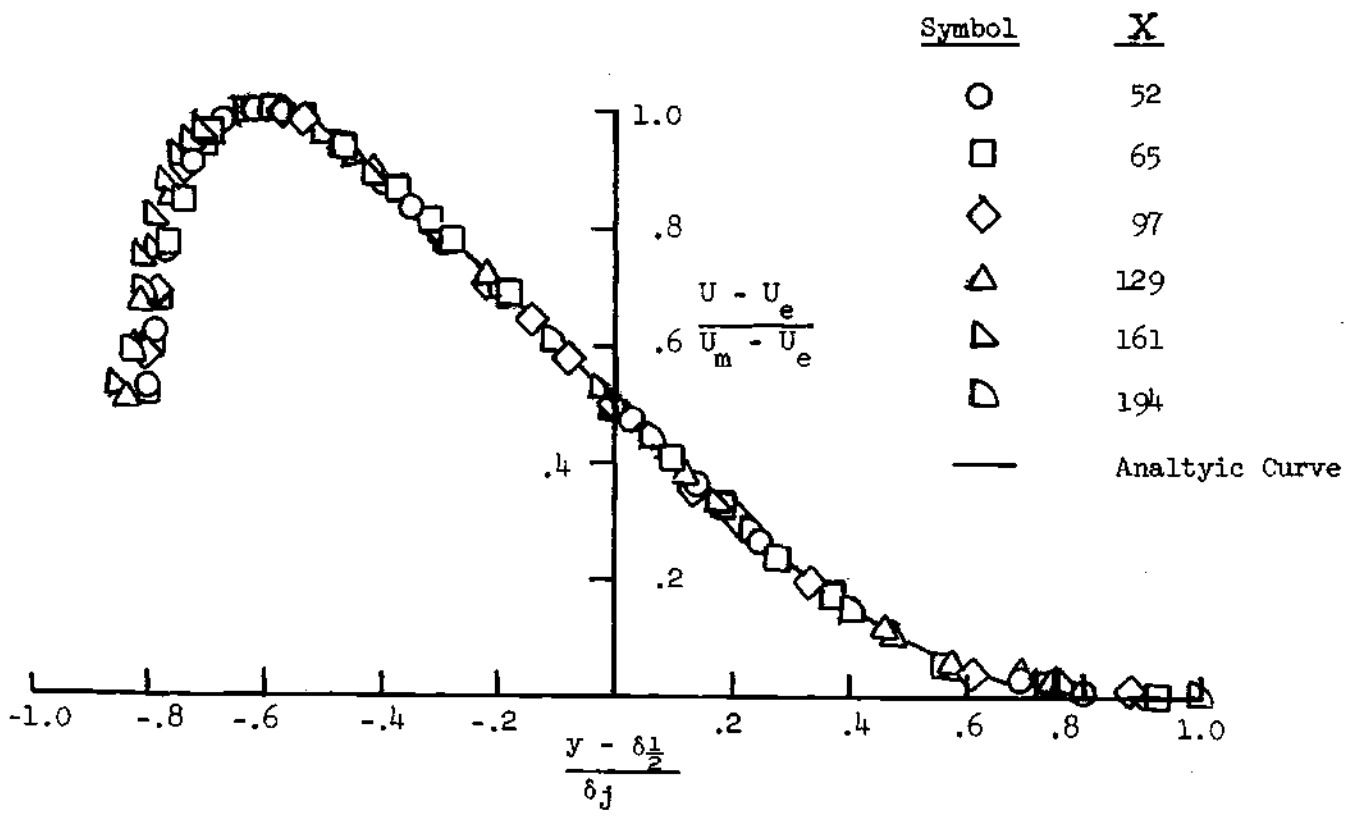

(b) Series II, VR = 3.0

Figure 3. (Continued)

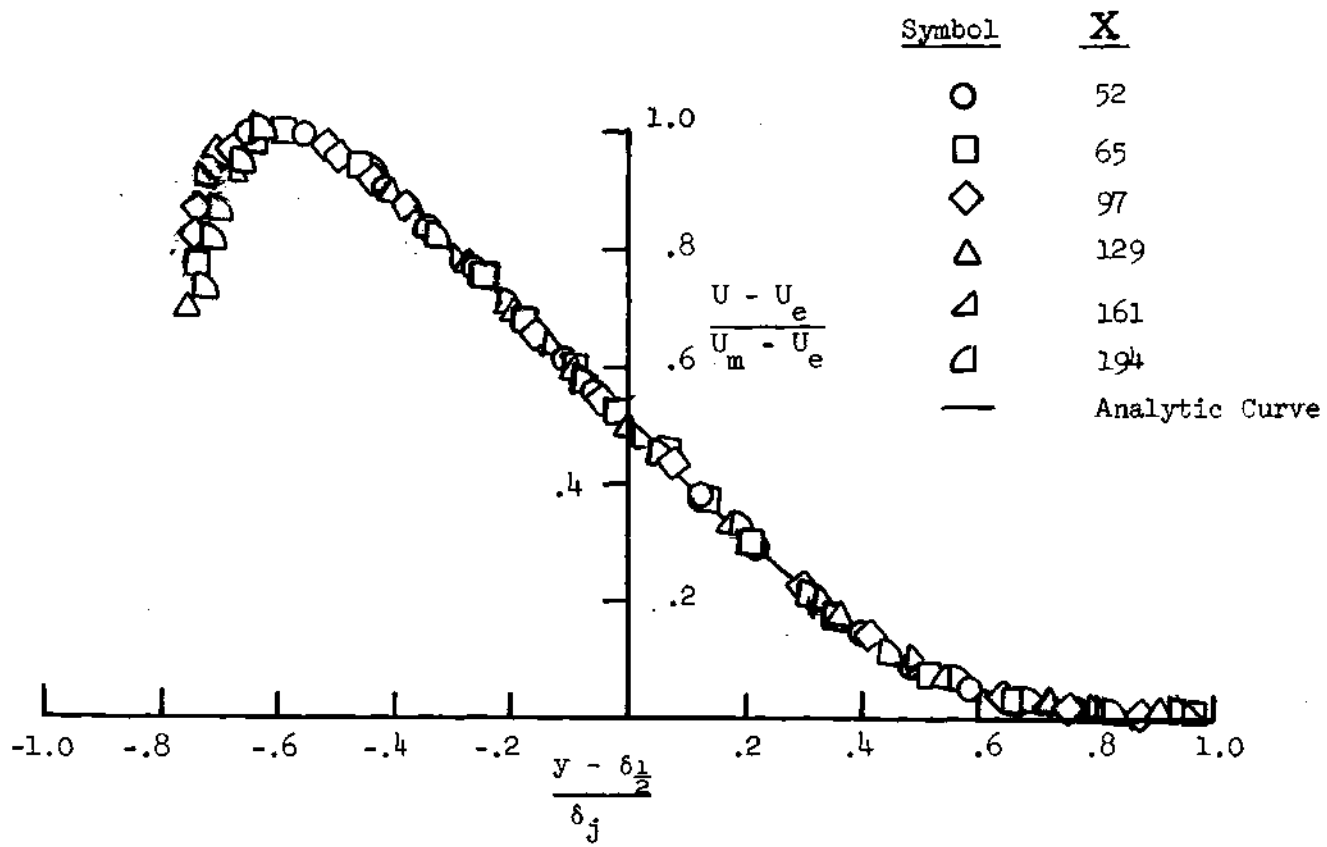

(c) Series II, VR = 4.0

Figure 3. (Continued)

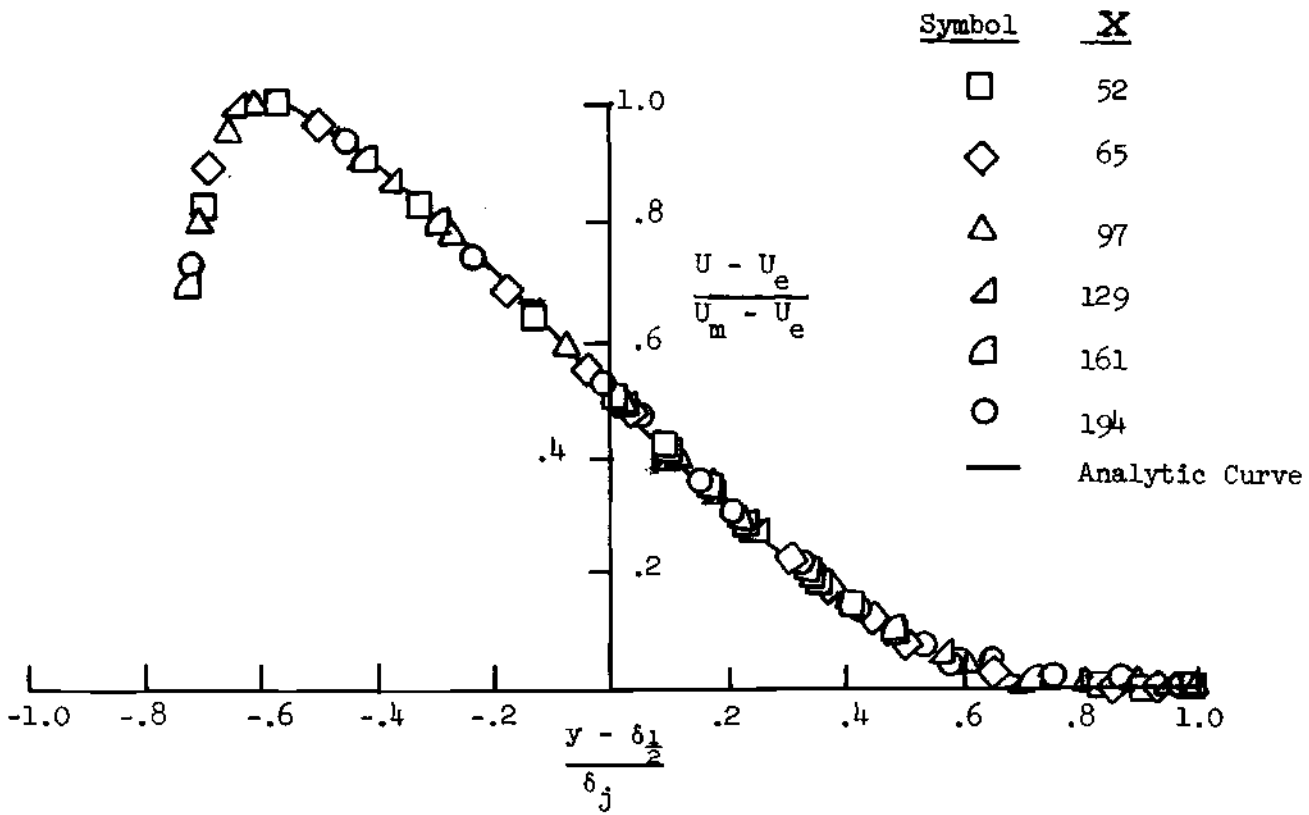

(d) Series II, VR = 6.0

Figure 3. (Continued)

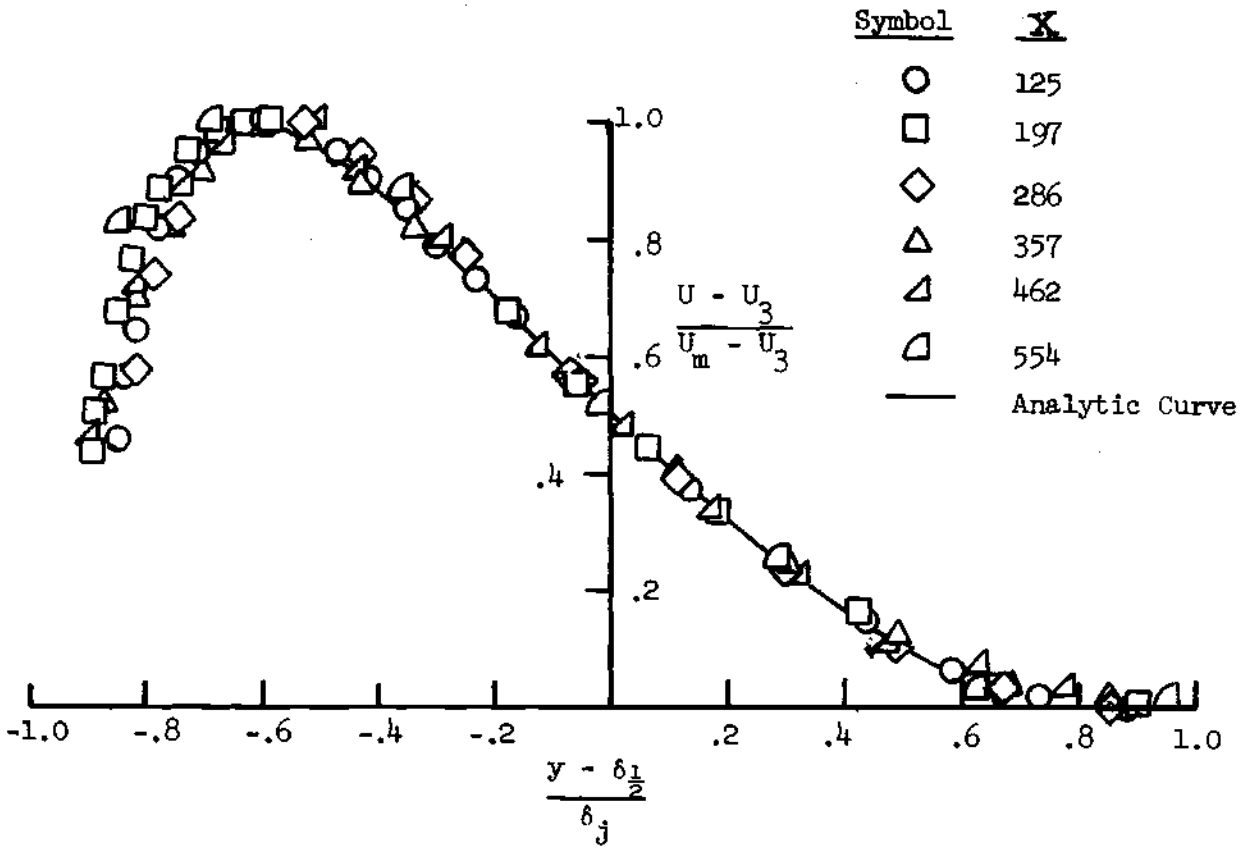

(e) Series III, VR = 2.07

Figure 3. (Continued)

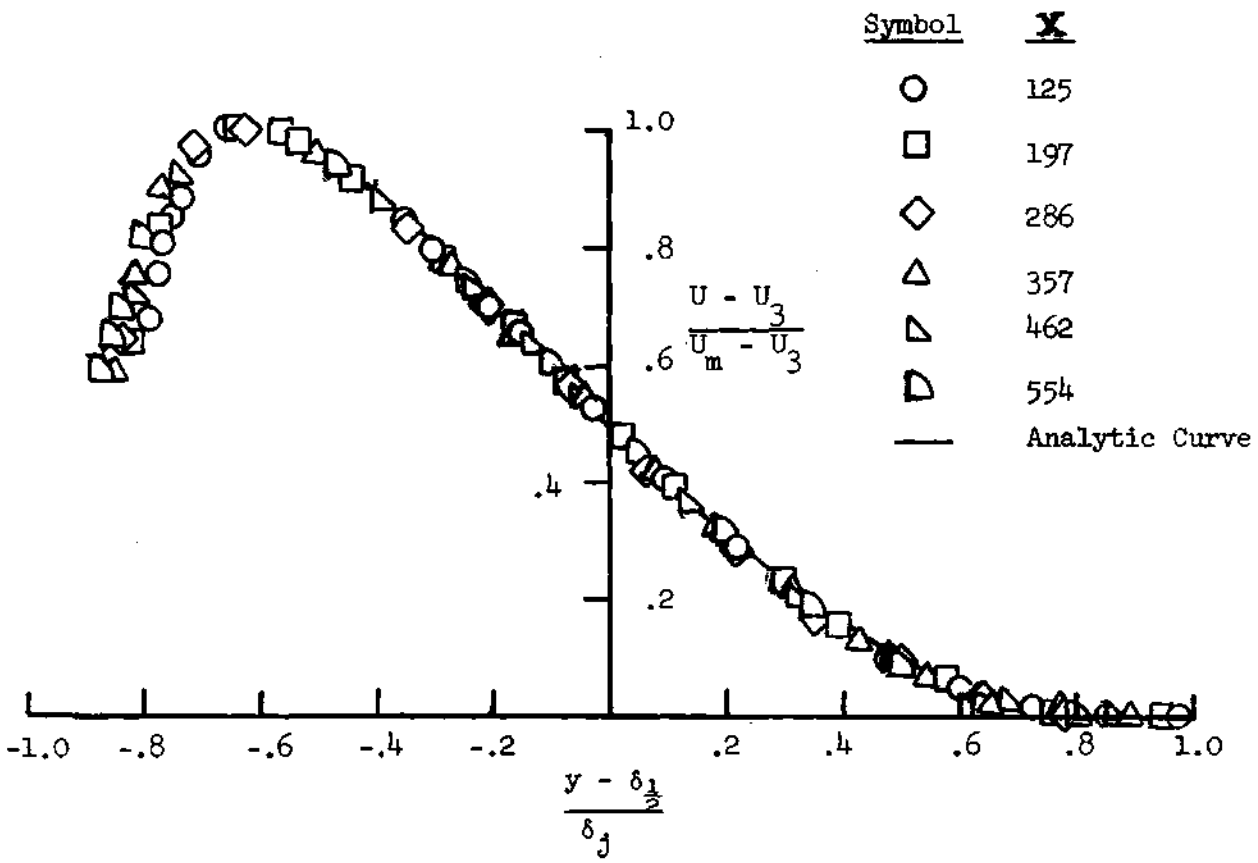

(f) Series III, VR = 2.92

Figure 3. (Continued)

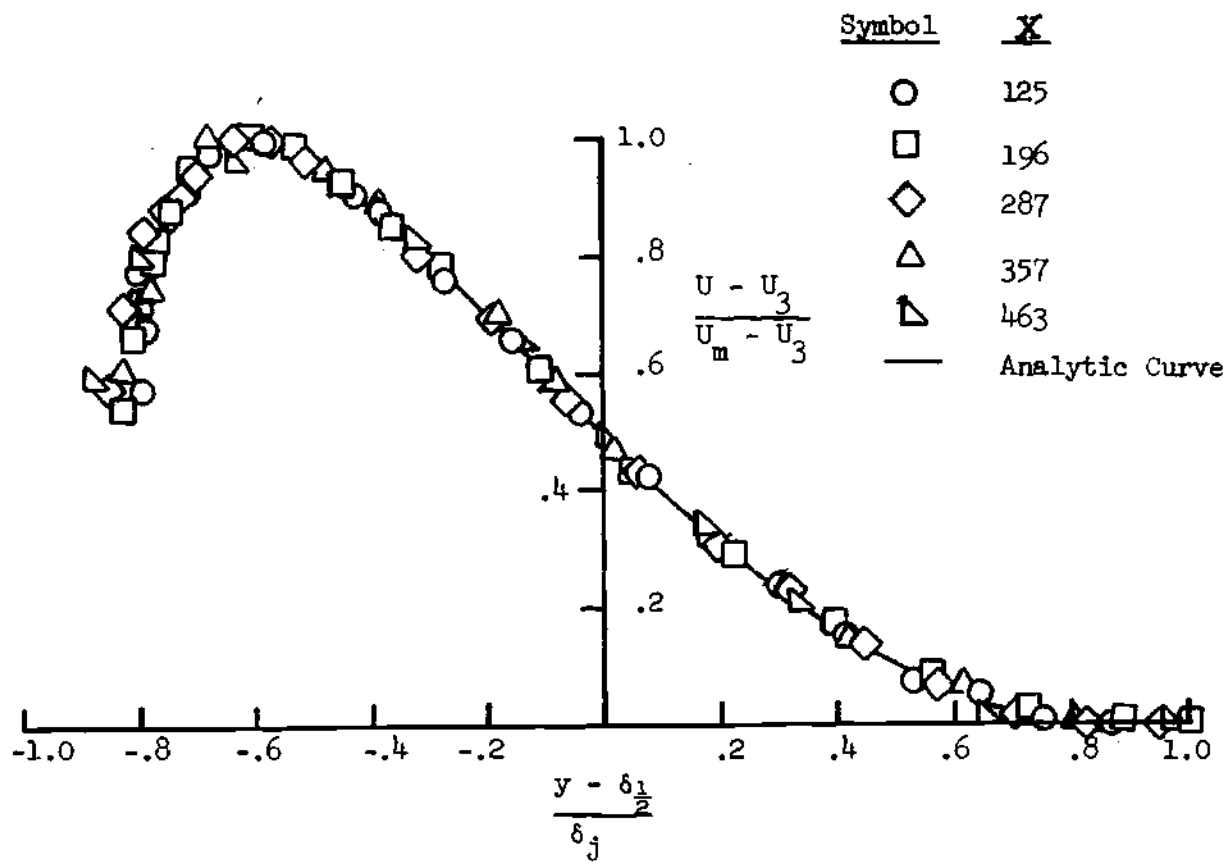

(g) Series IV, VR = 1.96

Figure 3. (Continued)

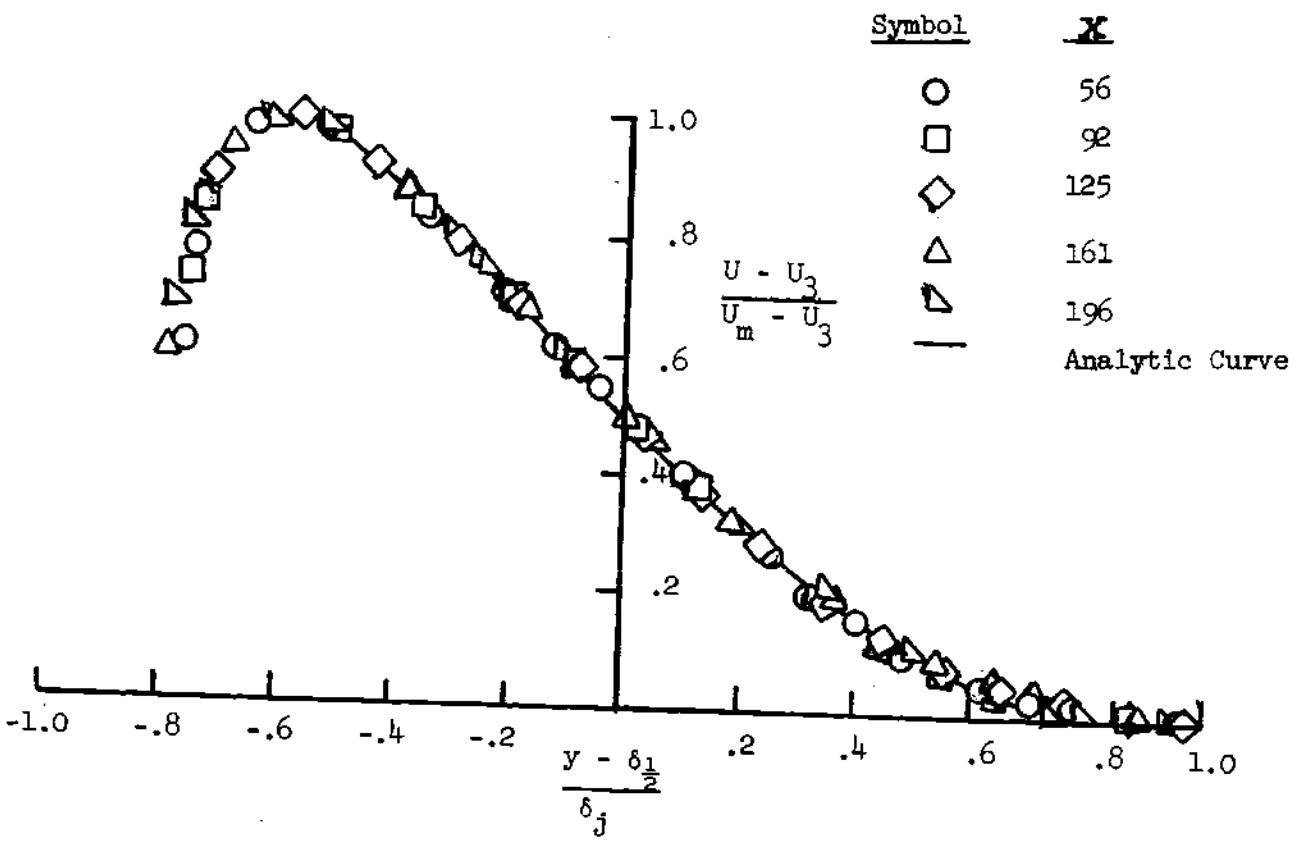

(h) Series IV, VR = 2.0

Figure 3. (Continued)

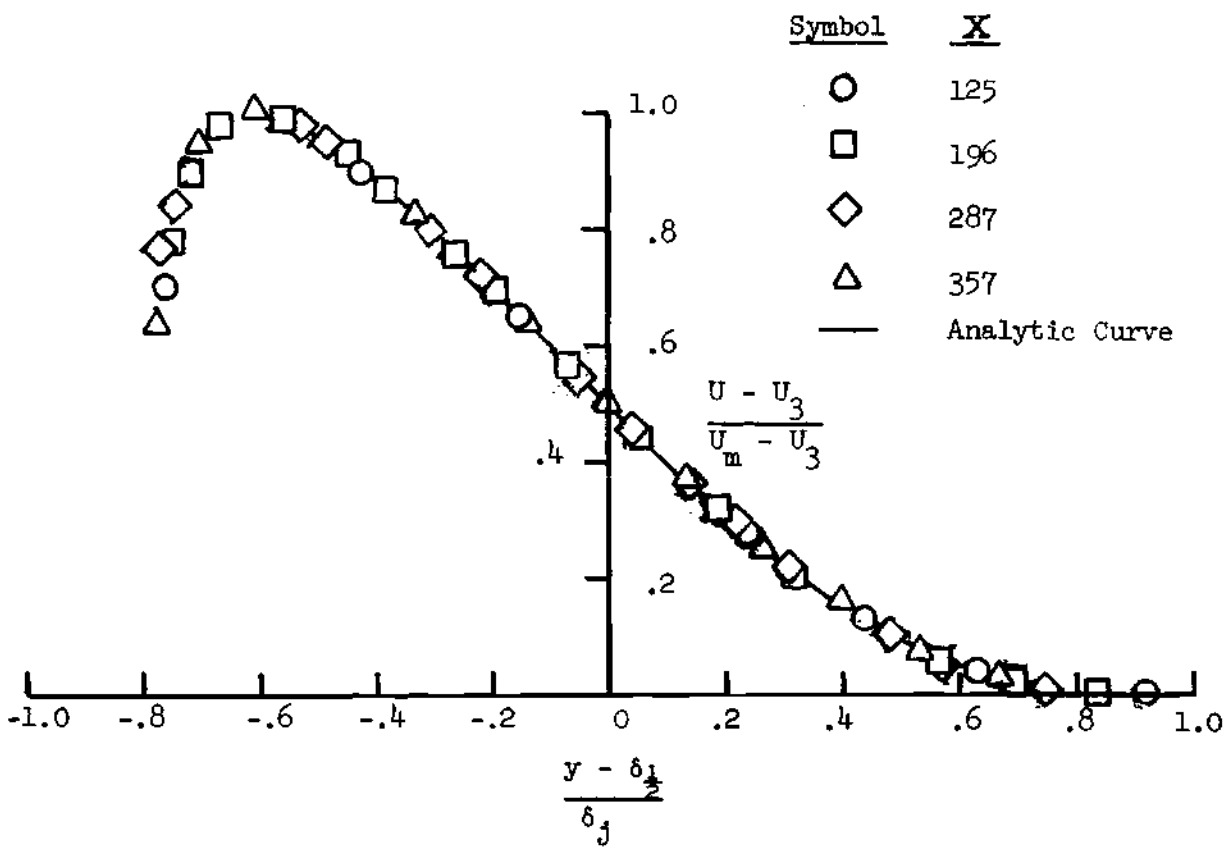

(i) Series IV, VR = 2.99

Figure 3. (Continued)

and δ_j is the jet layer length scale. Physically, δ_j represents the jet-layer length scale for a linear velocity profile with the same values of U_m and U_3 and with a velocity gradient equal to the maximum velocity gradient (see Figure 2(b)). It has been selected since it can be evaluated most accurately from experimental data. To determine δ_j the experimental data (U, y), in the region around the point of maximum velocity gradient, were represented by the polynomial function

$$U = \sum_{j=1}^{m} A_j \, y^{(j-1)} \tag{13}$$

where m is the degree of the polynomial function. The least square technique was then employed to determine the coefficients A_j. That is, expressing the error by

$$\epsilon = \left[\sum_{i=1}^{n} \left(U_i - \sum_{j=1}^{m} A_j \, y^{(j-1)} \right) \right]^2 \tag{14}$$

the values of A_j were obtained by setting $\partial\epsilon/\partial A_j = 0$ for $j = 1, 2, \ldots m$. This yields m simultaneous linear algebraic equations. The Gauss reduction technique was employed to solve the simultaneous linear equations governing the polynomial coefficients A_j. The jet layer scale, defined as

$$\delta_j = - \frac{U_m - U_3}{\left. \frac{\partial U}{\partial y} \right/ y = \delta_{\frac{1}{2}}} \tag{15}$$

was then evaluated using the velocity profile as represented by Eq. (13).

Once the jet layer length scale δ_j was established for each jet-layer velocity profile, all the jet layer velocity profiles were expressible in a similarity form with velocity scale $U_m - U_3$ and length scale δ_j. A similarity expression of the form

$$\frac{U - U_3}{U_m - U_3} = f_j(\eta) \tag{16}$$

where $\eta = (y - \delta_{\frac{1}{2}})/\delta_j$ was then sought. This jet layer was subdivided into four regions to eliminate any ill behavior due to the two extrema and the inflection. Each region was represented by a fourteenth degree polynomial. These polynomials were then least square fitted (using an equation similar to Eq. (14) to all the experimental velocity profile data for the jet layer. Typical results are shown in Figures 3(a) - (i). The single analytical curve accurately represents all of the experimental data. The root-mean-square error (RMS = $\sqrt{\epsilon}$) is 0.00303 for all data. The velocity profile derived from the least square fitting to the data (i.e., the analytical curve of Figures 3(a) - (i)) is tabulated in Table 2. This analytic representation of the experimental data for the jet layer is used in all subsequent analyses of the data. Comparison of the analytic expression with the exponential and hyperbolic tangent profiles commonly used for jets are shown on Figure 4.

Wake Layer Velocity Profile

The velocity profile in the wake layer is expressed as

Table 2. Tabulation of Velocity Profile for Jet Layer

η	f_j	η	f_j
-.6	.993	-.075	.5755
-.575	.9959	-.05	.5508
-.55	.9875	-.025	.5257
-.525	.9752	.0	.5000
-.5	.9604	.015	.4862
-.475	.9437	.04	.4616
-.45	.9257	.065	.4369
-.425	.9065	.09	.4119
-.4	.8860	.115	.3869
-.375	.8644	.14	.3622
-.35	.8416	.165	.3382
-.325	.8179	.19	.3149
-.3	.7950	.215	.2925
-.275	.7719	.24	.2707
-.25	.7490	.265	.2496
-.225	.7251	.29	.2290
-.2	.6999	.315	.2087
-.175	.6742	.34	.1887
-.15	.6489	.375	.1630
-.125	.6241	.4	.1440

Table 2. (Continued)

η	f_j	η	f_j
-.1	.5998	.425	.1261
.45	.1094		
.475	.0942		
.5	.0807		
.525	.0689		
.55	.0586		
.575	.0498		
.6	.0418		
.625	.0349		
.65	.0288		
.675	.0234		
.7	.0186		
.725	.0145		
.75	.0110		
.775	.0083		
.8	.0062		
.825	.0048		
.85	.0039		
.875	.0031		
.9	.0023		
.95	.0001		
.975	.0		

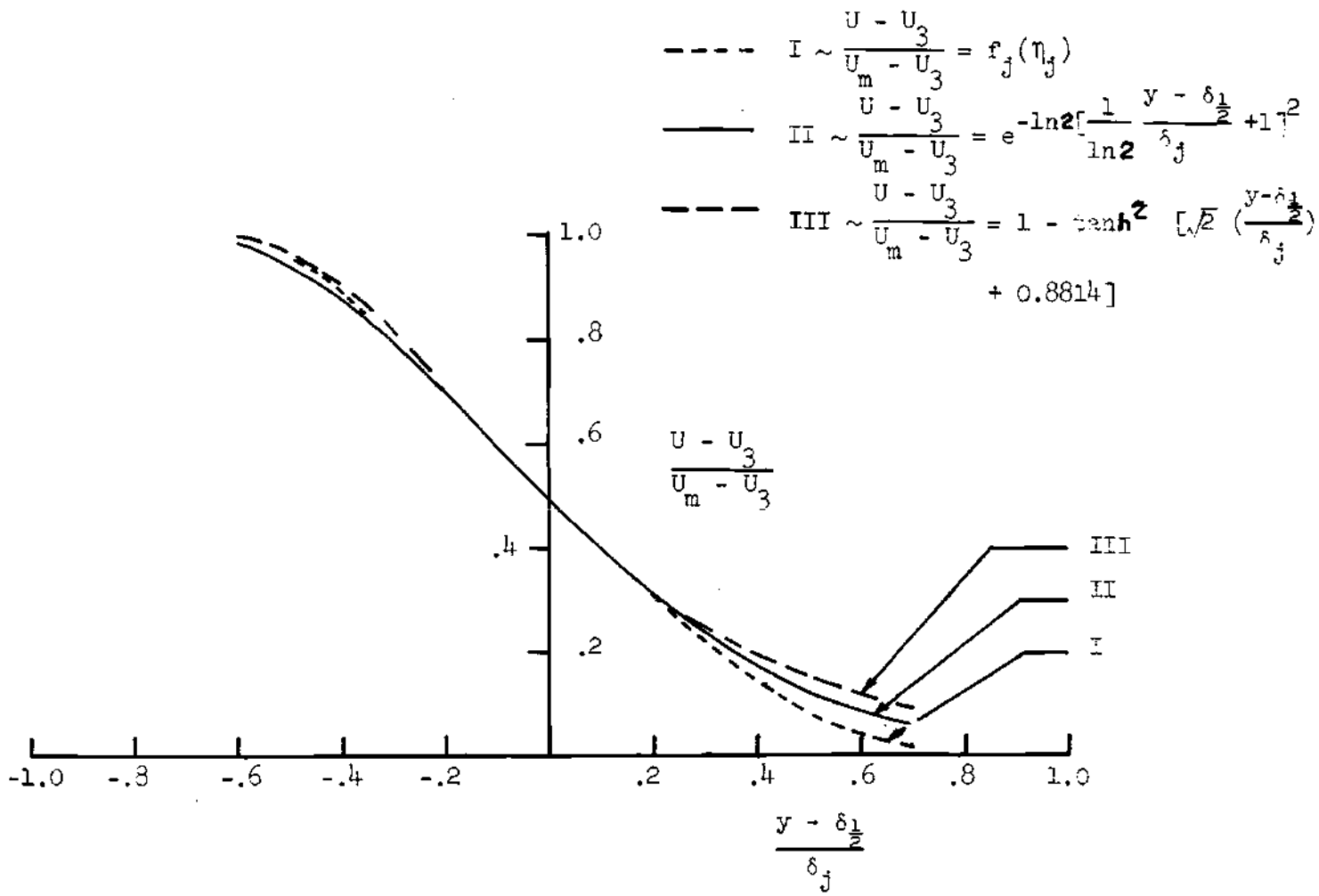

Figure 4. Comparison of Analytical Curve with Clasic Curves

$$\frac{U - U_3}{U_e - U_3} = f_w(\eta_w) \tag{17}$$

where $\eta_w = y - \delta_4/\delta w$, δ_4 is the wall jet thickness for $U = (U_e + U_3)/2$, and δw is the wake layer length scale which can be most accurately evaluated. The determination and physical significance of δw is identical to that of δ_j (see Figure 2(c)). Once the wake layer scale δw was established by a least square fit for each wake layer velocity profile, all the wake layer velocity profile were expressible in a similarity form with velocity scale $U_e - U_3$ and length scale δw. A similarity expression of the form

$$\frac{U - U_3}{U_e - U_3} = f_w(\eta_w) \tag{18}$$

where $\eta_w = (y - \delta_4)/\delta_w$ was sought. Typical results are shown in Figures 5(a) - (e).

The similarity results for the wake and jet layers were found to be similar to each other and, in fact, the analytical expression for the wake layer can be expressed as

$$f_w(\eta_w) = 1. - f_j(-\eta_w) \tag{19}$$

This single analytical curve accurately represents all of the experimental data. The actual differences between the experimental data and the least square fit is very small for the wake layer when it is recognized

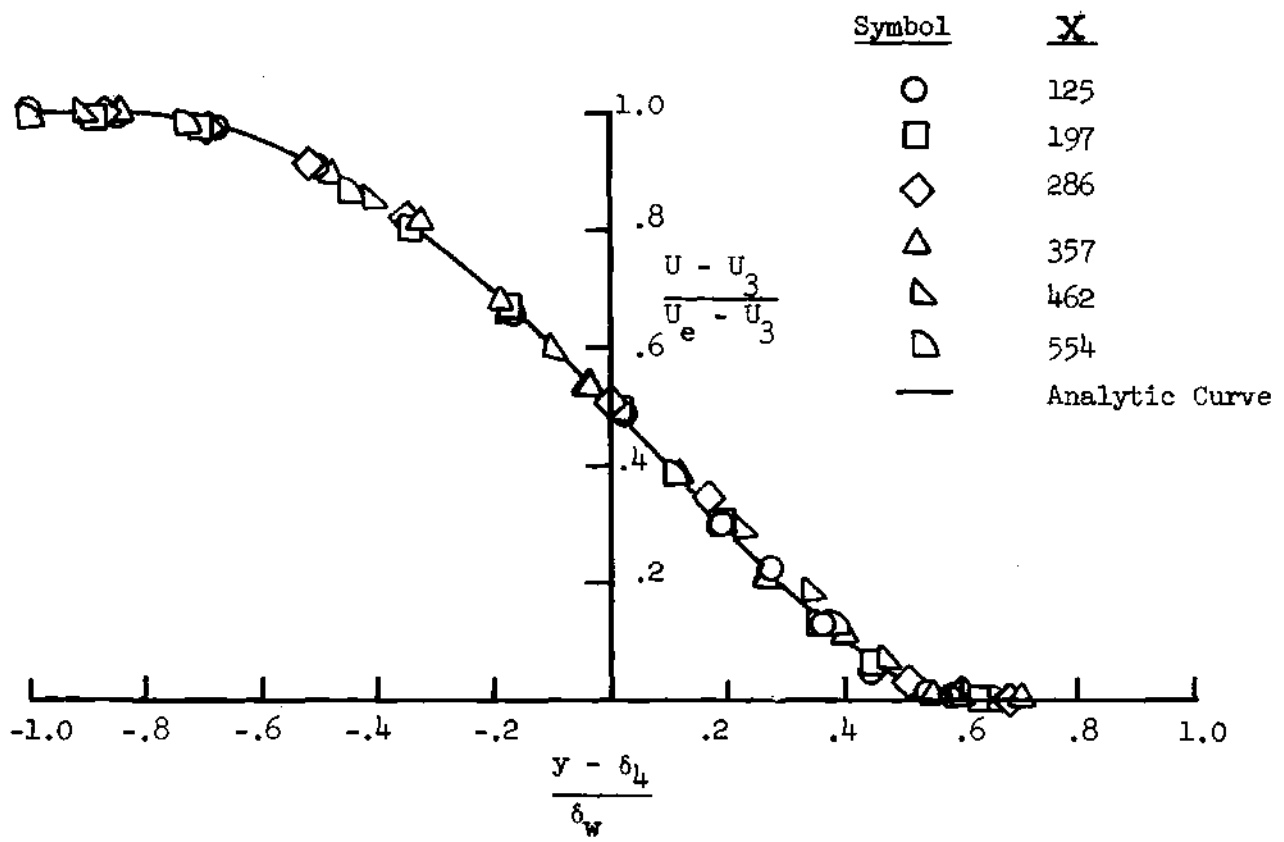

(a) Series III, VR = 2.07

Figure 5. Wake Layer Velocity Profile

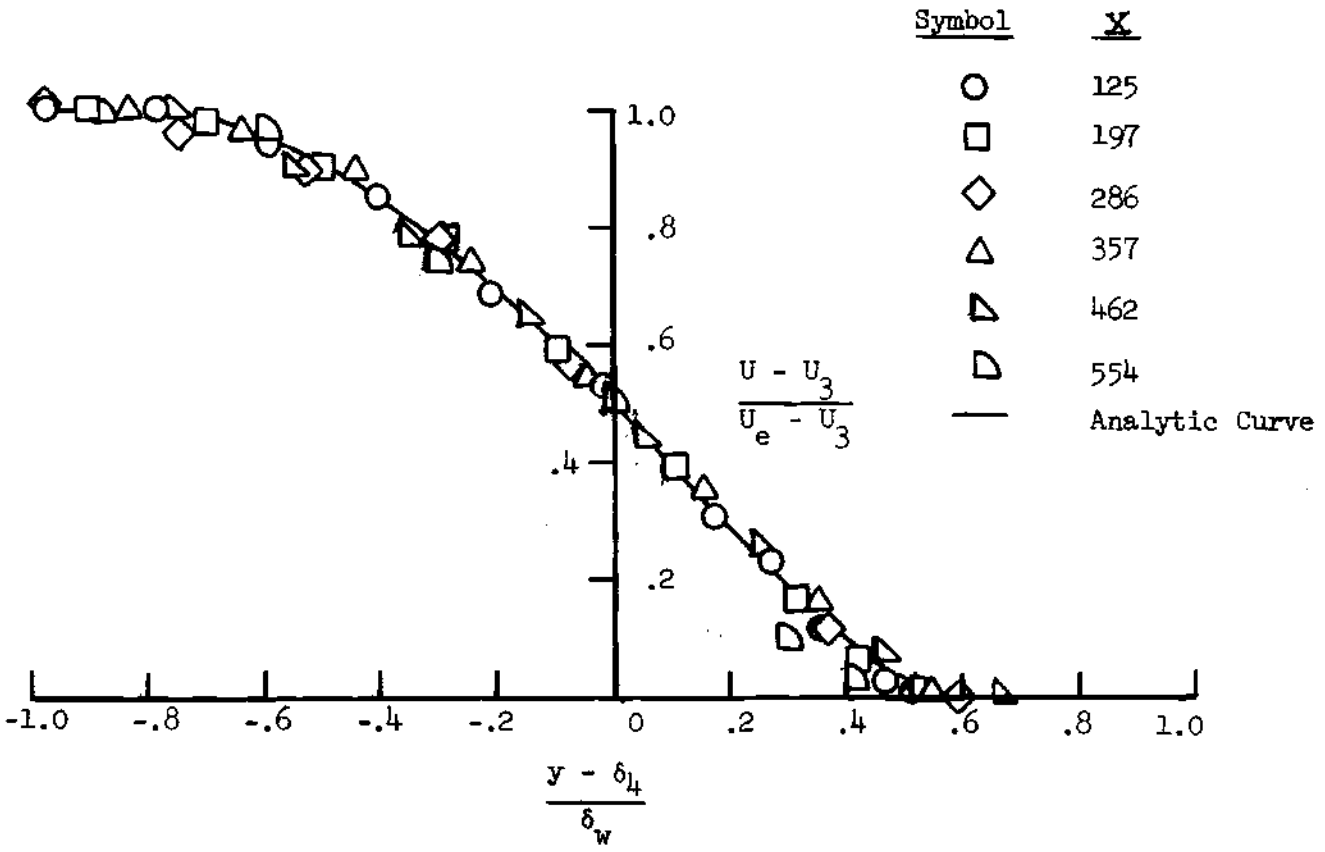

(b) Series III, VR = 2.92

Figure 5. (Continued)

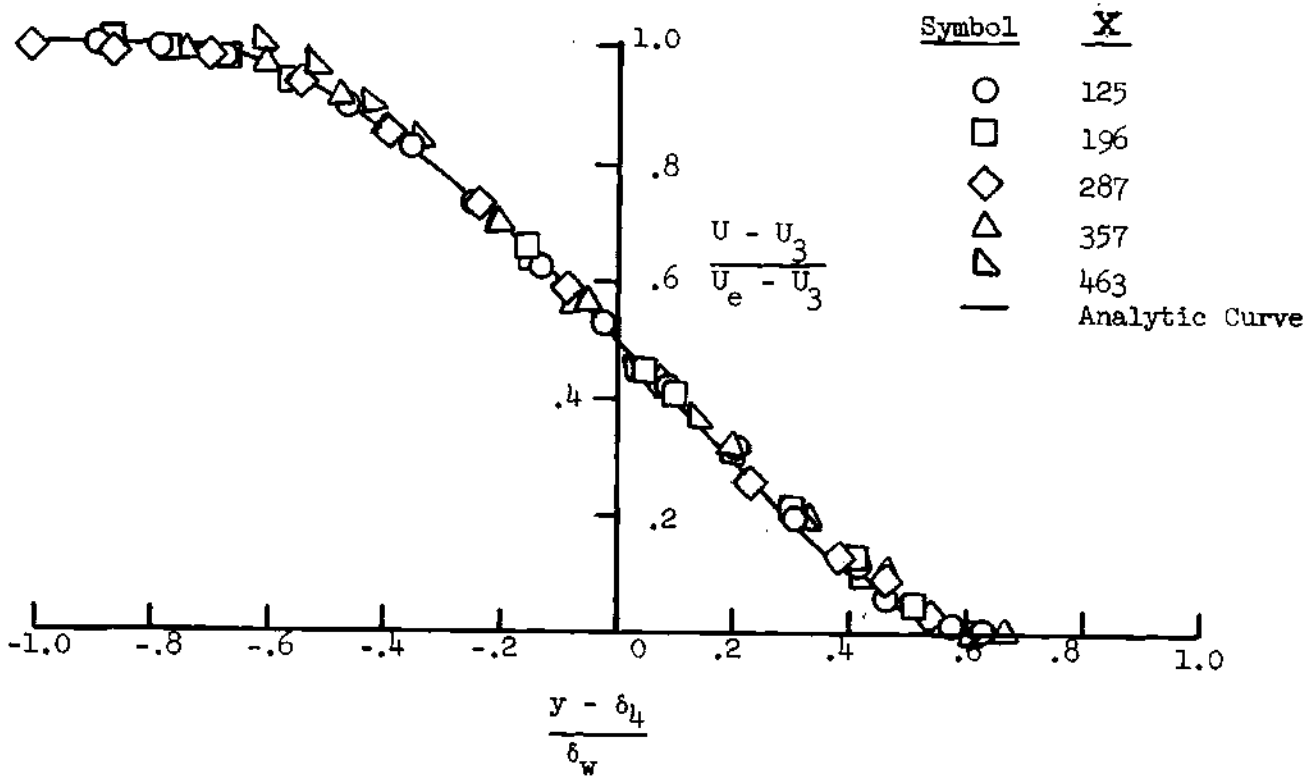

(c) Series IV, VR = 1.96

Figure 5. (Continued)

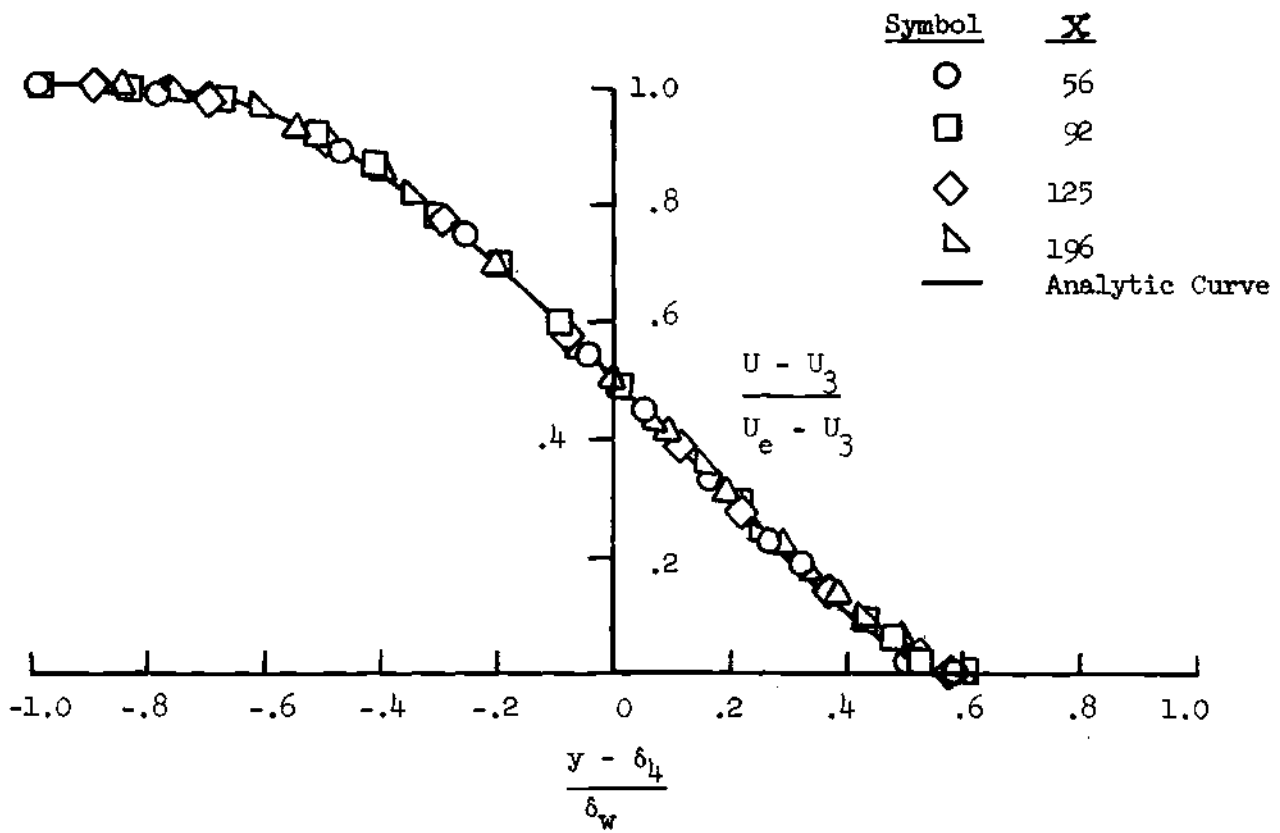

(d) Series IV, VR = 2.0

Figure 5. (Continued)

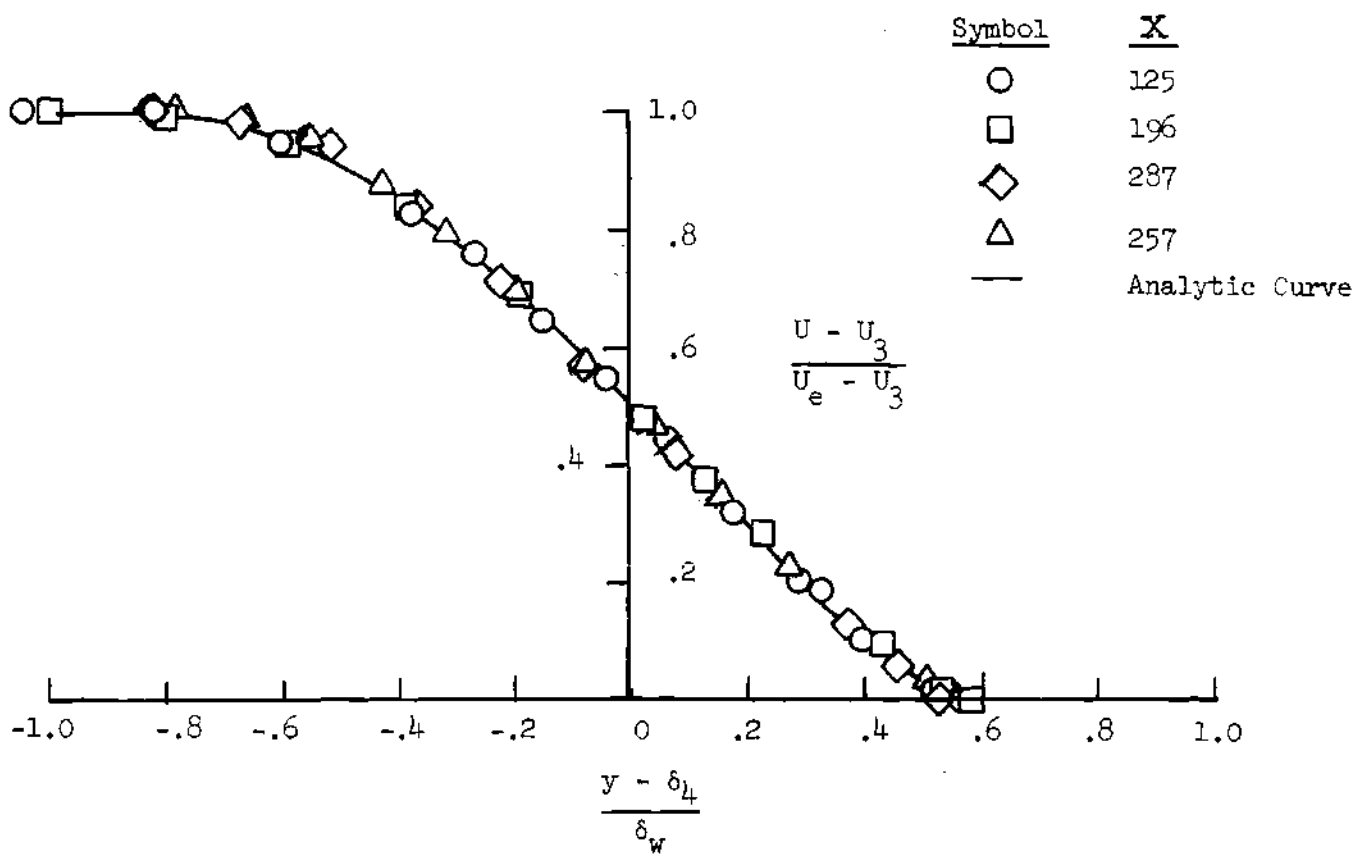

(e) Series IV, VR = 2.98

Figure 5 (Continued)

that $U_e - U_3$ in many cases was less than 20 percent of the edge velocity.

This analytical curve (Table 2) was used in place of the experimental data for all subsequent data analyses. It is felt that this is the most accurate representation possible.

Velocity Decay

The decay in the maximum velocity for Series II, III and IV are shown on Figures 6(a) - (3) (reproduced from Reference 12). The data is very consistent and the scatter is small. The combined influence of slot Reynolds number and initial velocity ratio is shown for Series II in Figure 6(a). The Reynolds number effect for these results is emphasized in Figure 6(b) by plotting jet peak velocity decay referenced from the mainstream velocity. Representative free-stream velocity retardation and jet peak velocity decay results for Series III and IV are given in Figure 6(c) for nominal initial velocity ratios of 2 and 3. Figures 6(d) and 6(e) show the corresponding variations in the minimum to edge velocity ratios and in the minimum to maximum velocity ratios.

For the present study a least square technique was employed to obtain polynomial functions for U_m, U_e, and U_3 which had been smoothly faired through the experimental data. These polynomial expressions were used in all subsequent analyses of the data.

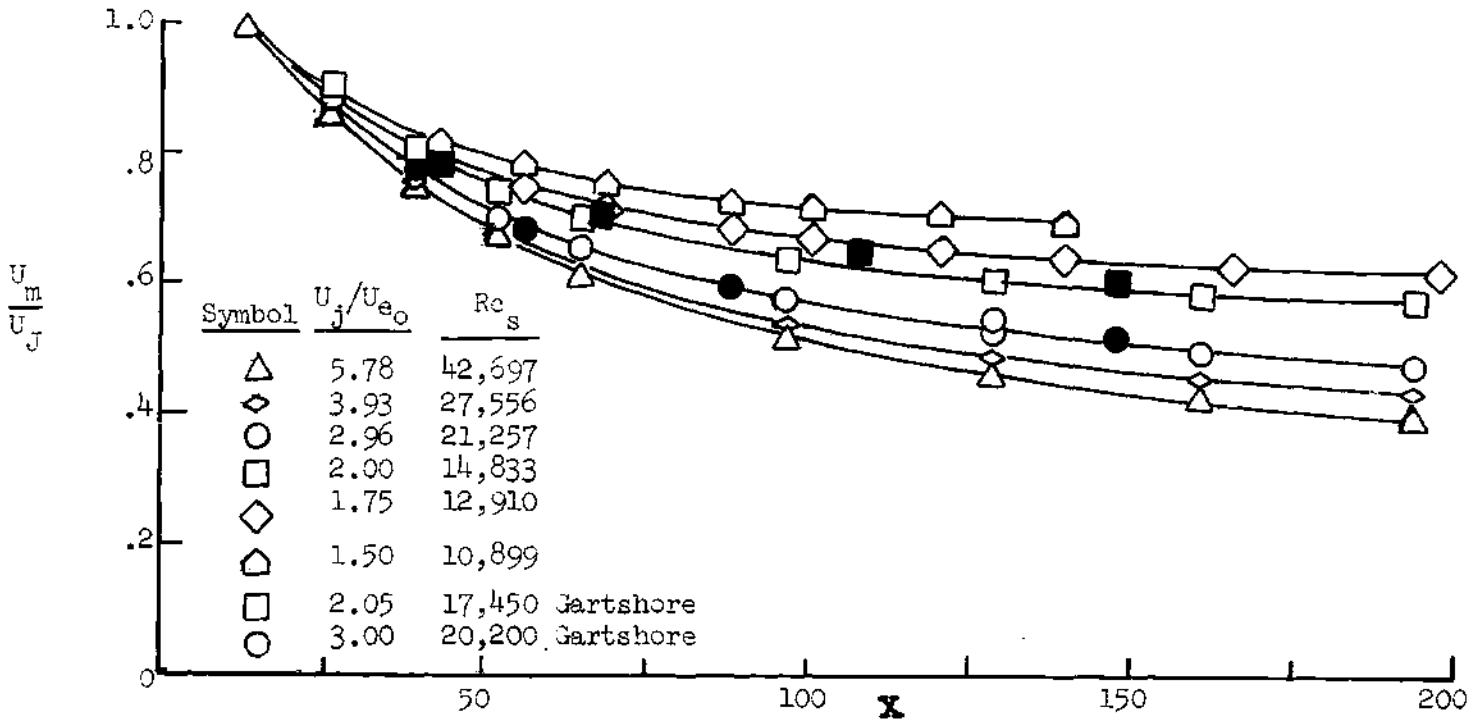

(a) Series II. Effect of Reynolds Number and Velocity Ratio

Figure 6. Wall-Jet Velocity Decay

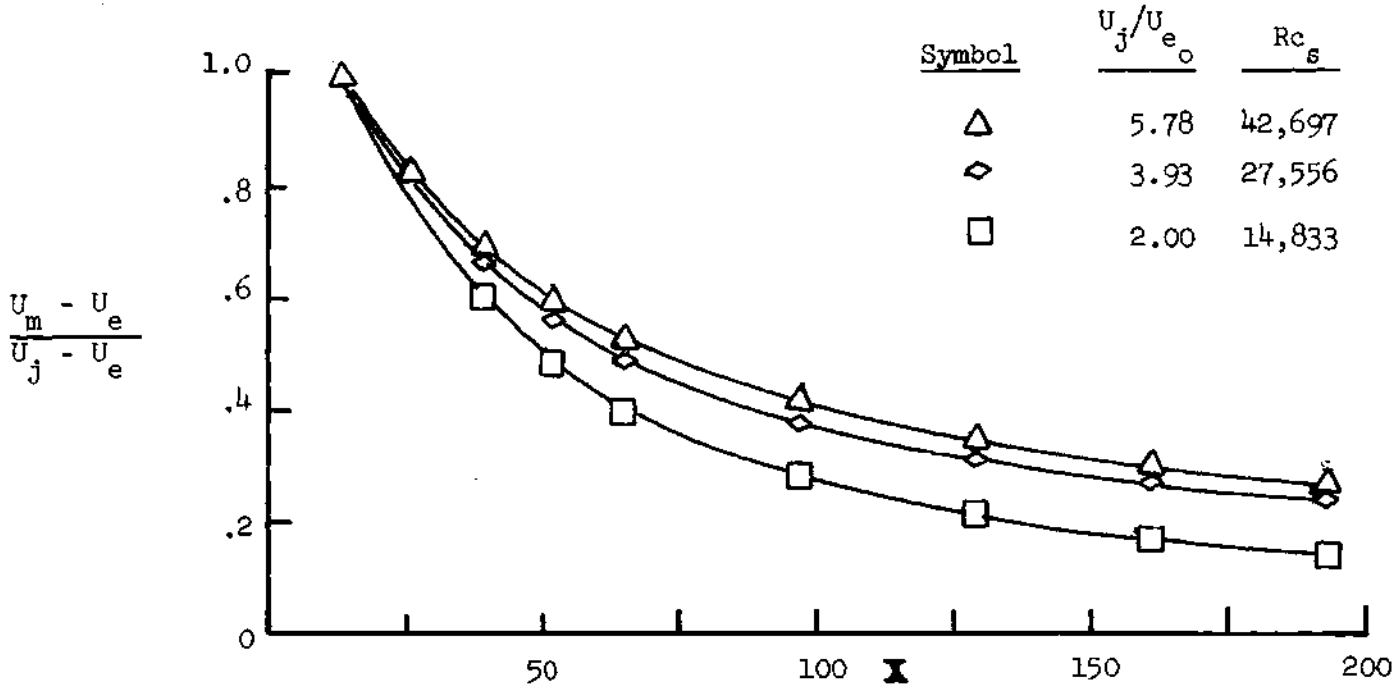

(b) Series II. Effect of Reynolds Number

Figure 6. (Continued)

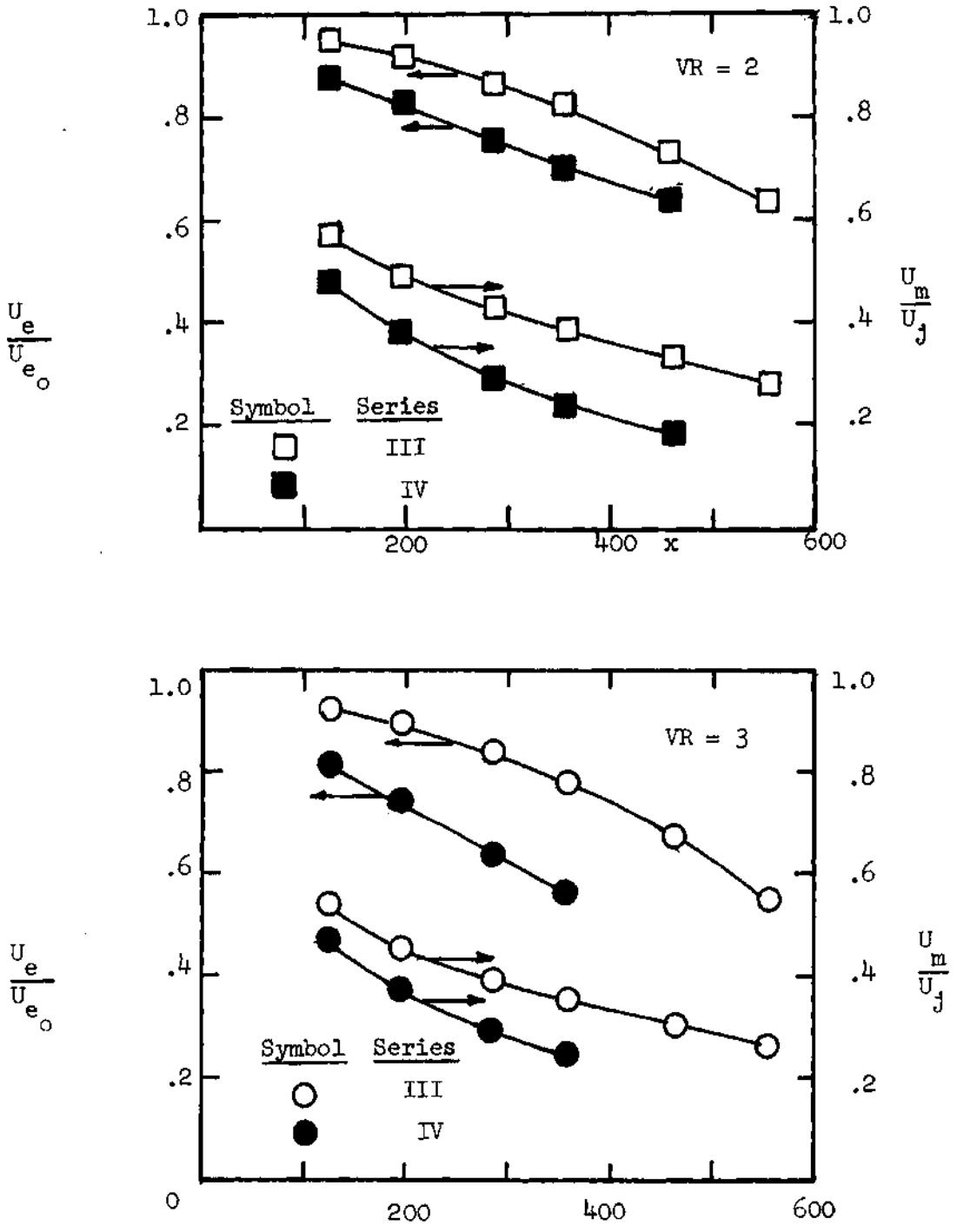

(c) Series III, and IV. Edge Velocity Distribution

Figure 6. (Continued)

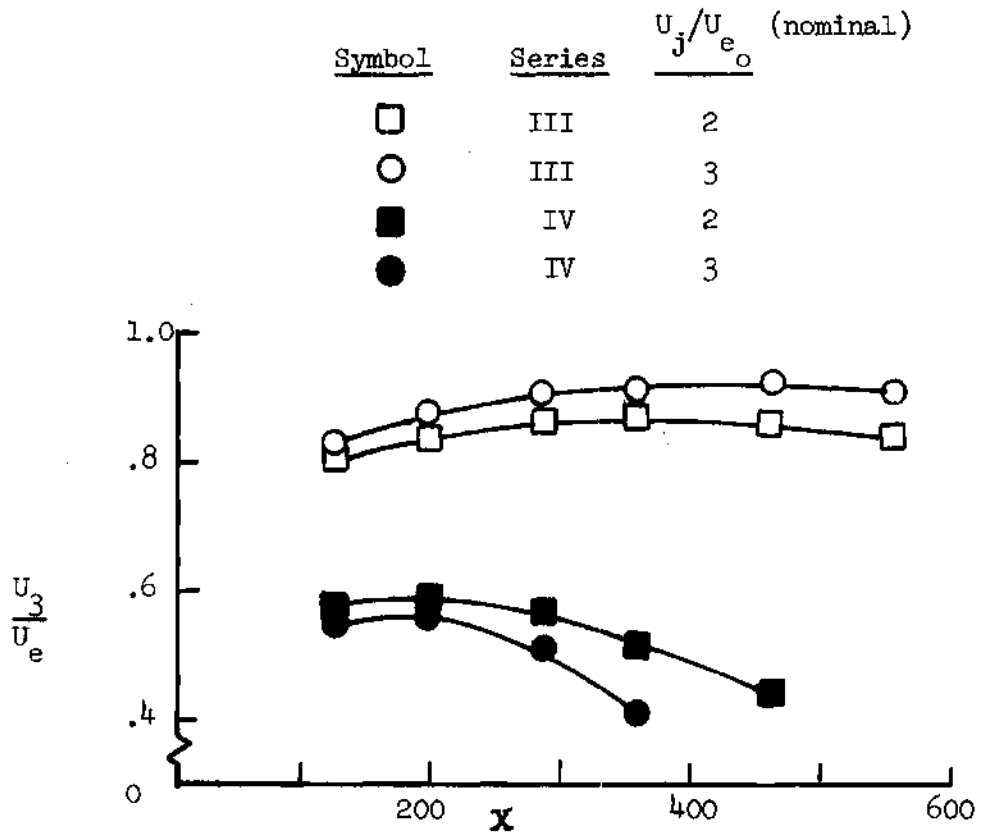

(d) Series III, and IV. Variation in Minimum to Edge Velocity Ratio

Figure 6. (Continued)

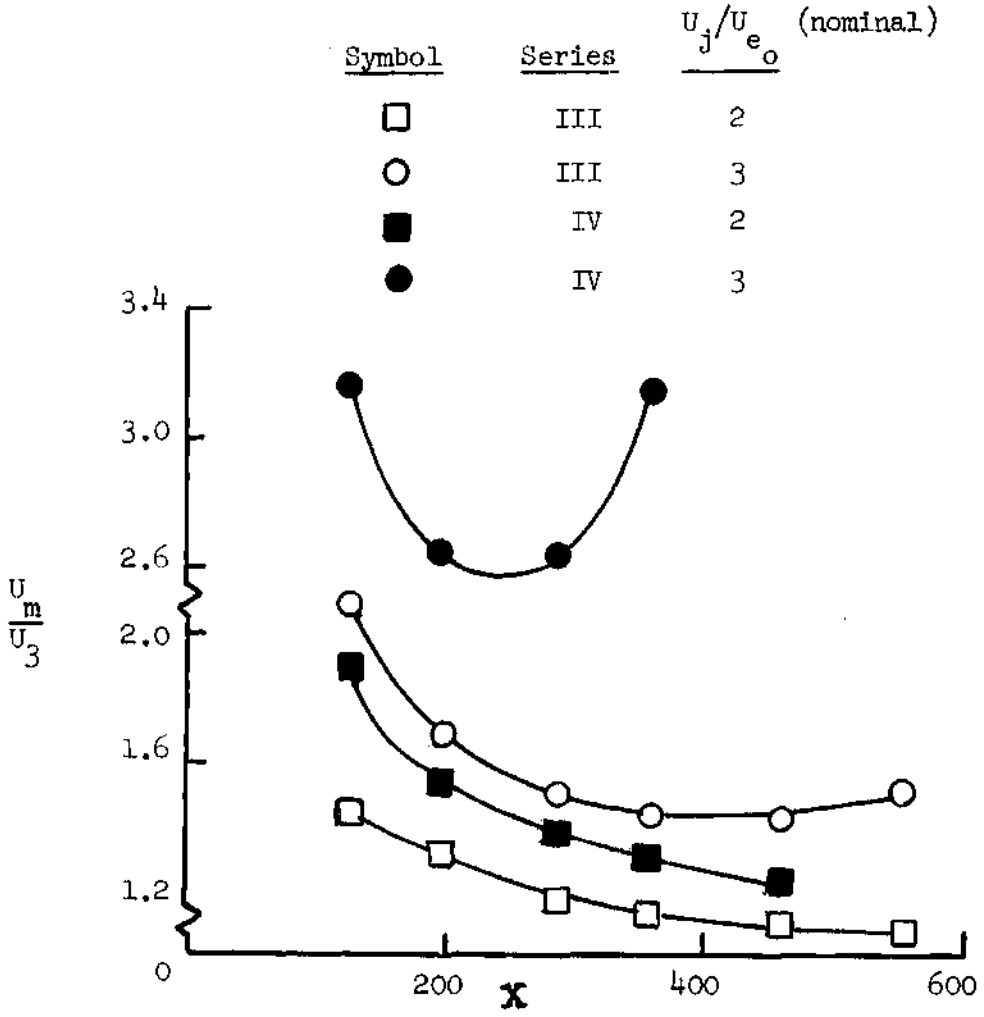

(e) Series III, and IV. Variation in Minimum to Maximum Velocity Ratio

Figure 6. (Continued)

Temperature Data

Temperature Profile

Figure 7 (reproduced from Reference 12) shows typical results for the nondimensional temperature profile through the wall jet for each of the major areas of investigation. A review of the tabulated data in Reference (12) reveals that for these experiments the total temperature remains essentially constant from the wall to the jet peak velocity. Near the jet peak the temperature begins to decay linearly with distance. The linear equation

$$\frac{T - Ty}{T_1 - Ty} = - 0.588\ y/\delta_j + 1.12 \qquad (20)$$

where Ty ≡ Te for Series II and Ty ≡ T_3 for Series III and IV, is a good representation of this decay for all three sets of measurements (see Reference 12).

In the present analyses, the temperature was considered constant from the wall to the jet peak and Eq. (20) was used from the jet peak to the shear layer edge for Series II and to U = U_3 for Series III and IV. The temperature was taken as constant from the point U = U_3 to edge for Series III and IV. Since the temperature differences were small, these assumptions were well within the accuracy of the study. A typical comparison between the analytical representation and the experimental data for Series III is shown in Figure 8.

Temperature Decay

Typical decays of the experimental jet peak temperature with

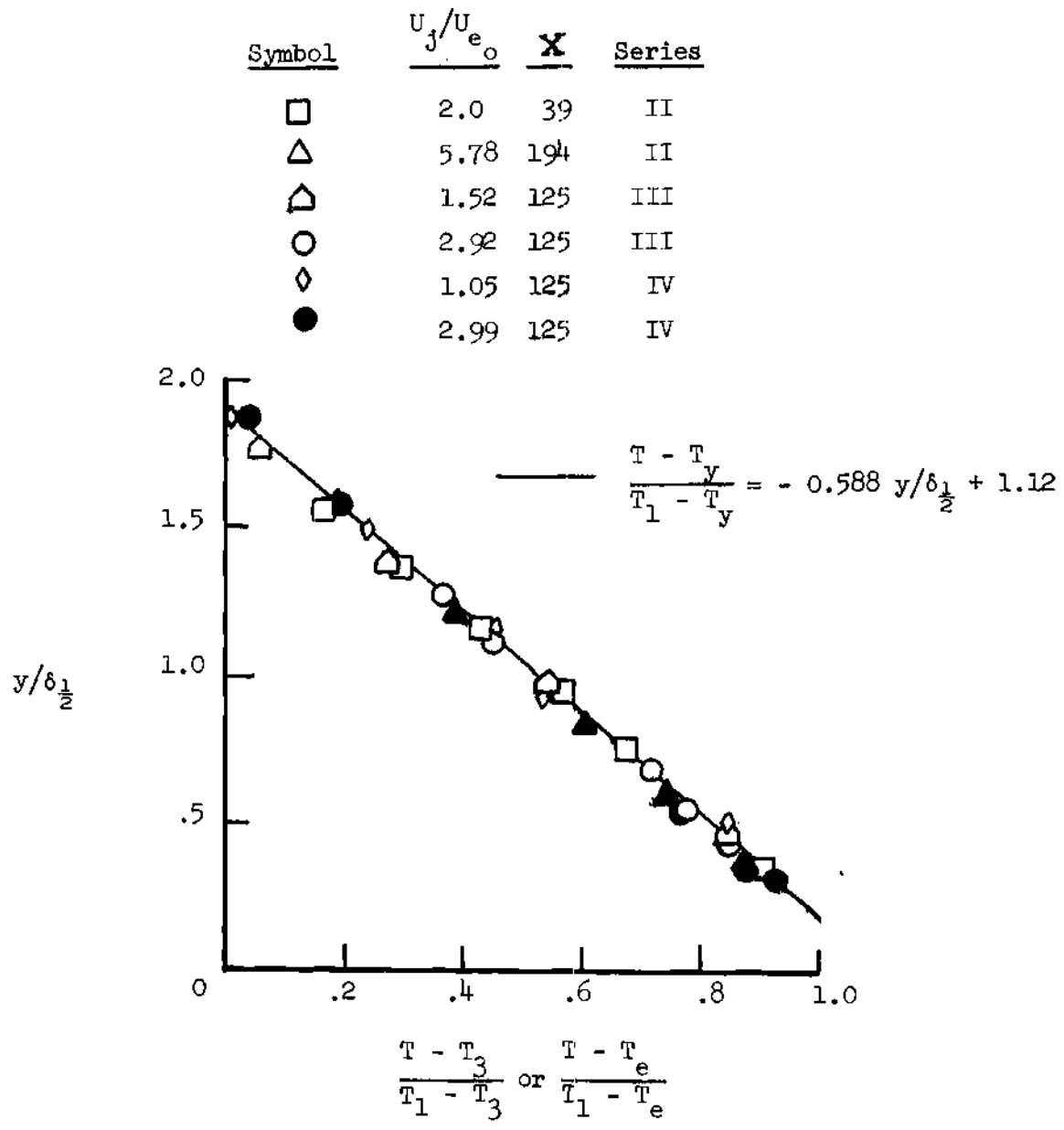

Figure 7. Wall Jet Temperature Profile

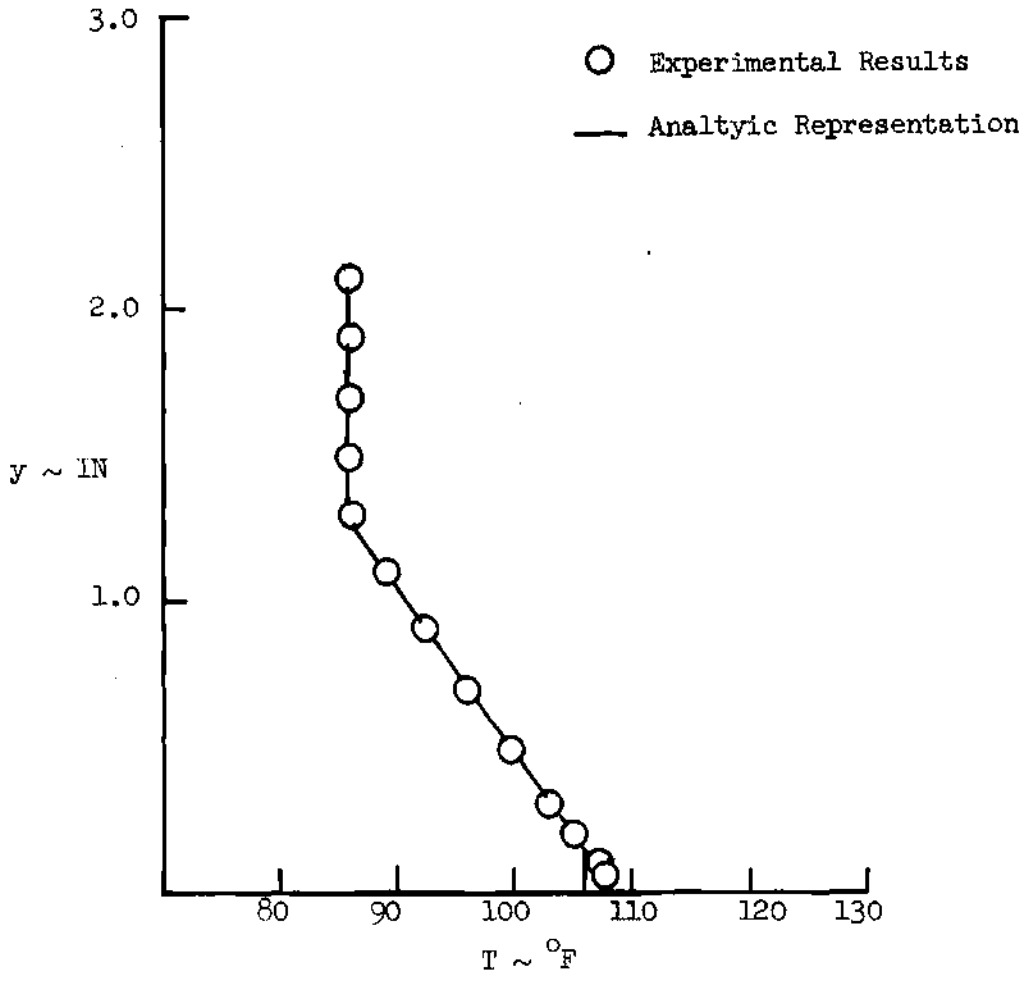

Figure 8. Temperature Profile for Series III VR = 2.92; X = 286

distance from the slot are illustrated in Figure 9 (reproduced from Reference 12). A least square technique was employed to obtain 4th-degree polynomial functions for T_1, Te, and T_3 which had been smoothly faired through the experimental data. These polynomial functions were then used in all subsequent analyses of the data.

Shear Stress

Shear stress similarities were sought to represent the shear stress terms which appeared in the momentum equation. Application of such a shear similarity approach could not only simplify the partial differential equation (i.e., reduced the order of the partial differential equation) but also avoid the singularity (at $\tau = 0$) which appears in the eddy viscosity approach and minimize the requirements for fundamental turbulence data and/or turbulence equations. The shear stresses were first calculated from the integrated momentum and continuity equations using the least square curve fits for the experimental velocity and temperature data. These shear stress results were then analyzed for similarities. As in the case of the previously described velocity profile similarities, the similarities for the shear stress profiles were obtained in the three subregions rather than for the complete shear stress profiles.

Shear Stress Profiles

An integral equation for evaluating shear stress was developed by integrating the momentum equation along with the continuity equation. Combining these equations and integrating gives

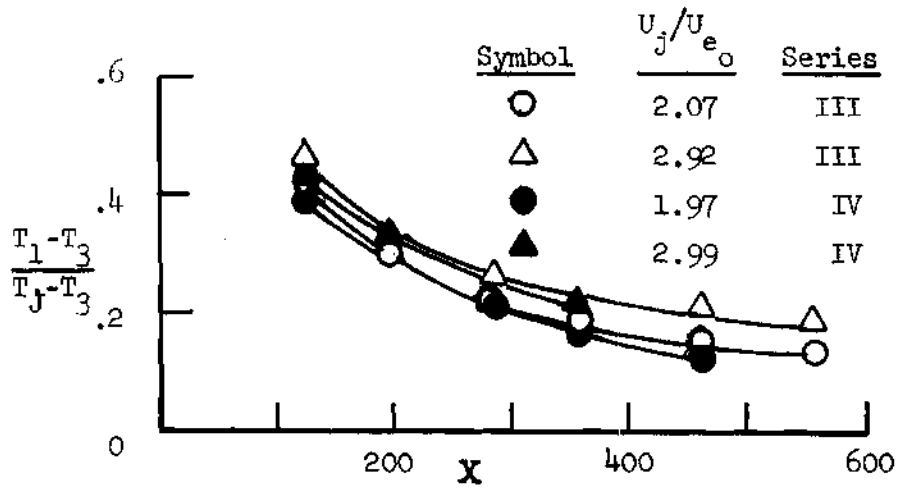

(b) Series III and IV

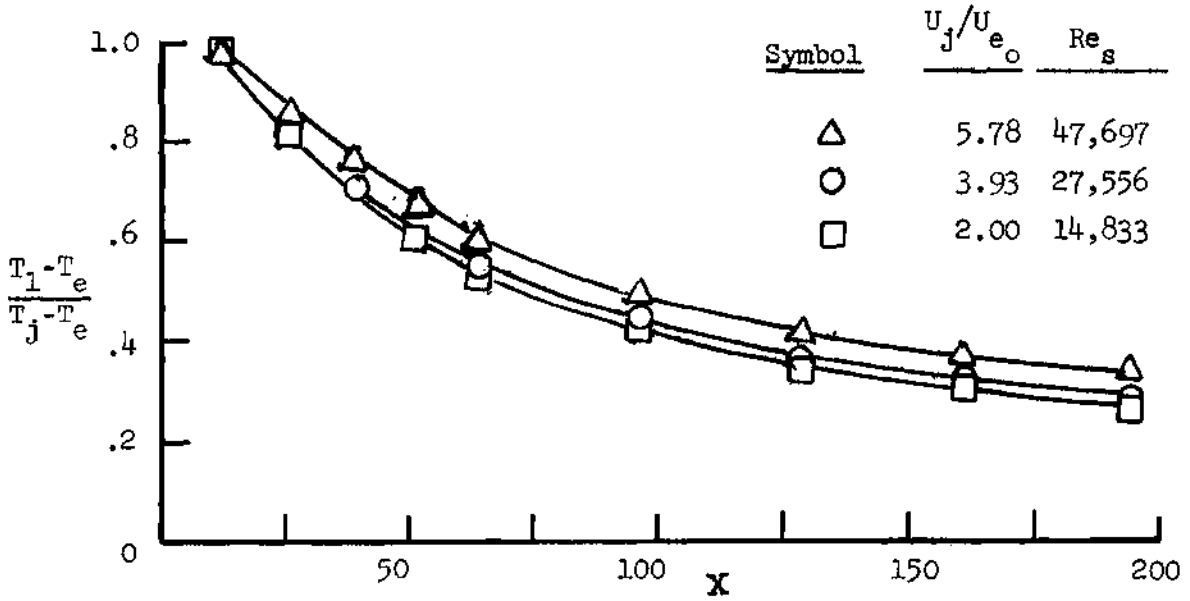

(a) Series II

Figure 9. Wall Jet Temperature Decay

$$\tau(y) = \tau w + \frac{dP}{dx} y + \frac{\partial}{\partial x} \int_o^y \rho u^2 dy - u \frac{\partial}{\partial x} \int_o^y \rho u dy \qquad (21)$$

Equation (21) is solved using the velocity and the temperature (required for evaluating the density ρ) profiles as discussed in previous paragraphs, the experimental values of the skin friction τw, and the pressure P as determined from the edge velocity. The partial derivatives for the mass flow rate and the momentum were solved by a finite difference technique. In order to satisfy the integral momentum equation (i.e., to force $\tau = 0$ at the shear-layer outer edge), an iteration technique for correcting U_m was used. This correction was made to adjust for errors in the velocity decay and the shear layer thicknesses obtained from the experimental data. The correction for U_m was both positive and negative, was generally about .4 percent, and was never greater than 0.75 percent. This is believed to be well within the accuracy of the experimental data.

The shear stress distribution through the entire shear layer for a typical case is shown in Figure 10. An evaluation of many shear stress distributions such as the one shown in this figure revealed that the entire shear stress profile could be subdivided into an "inner shear layer", a "submerged shear layer", and an "outer shear layer" as depicted in Figure 10. With this subdivision, shear stress similarities were evident. Typical results from analyzing these three shear layers are presented in Figures 11, 12 and 13. The method of analyzing and generalizing the results are presented in the following section.

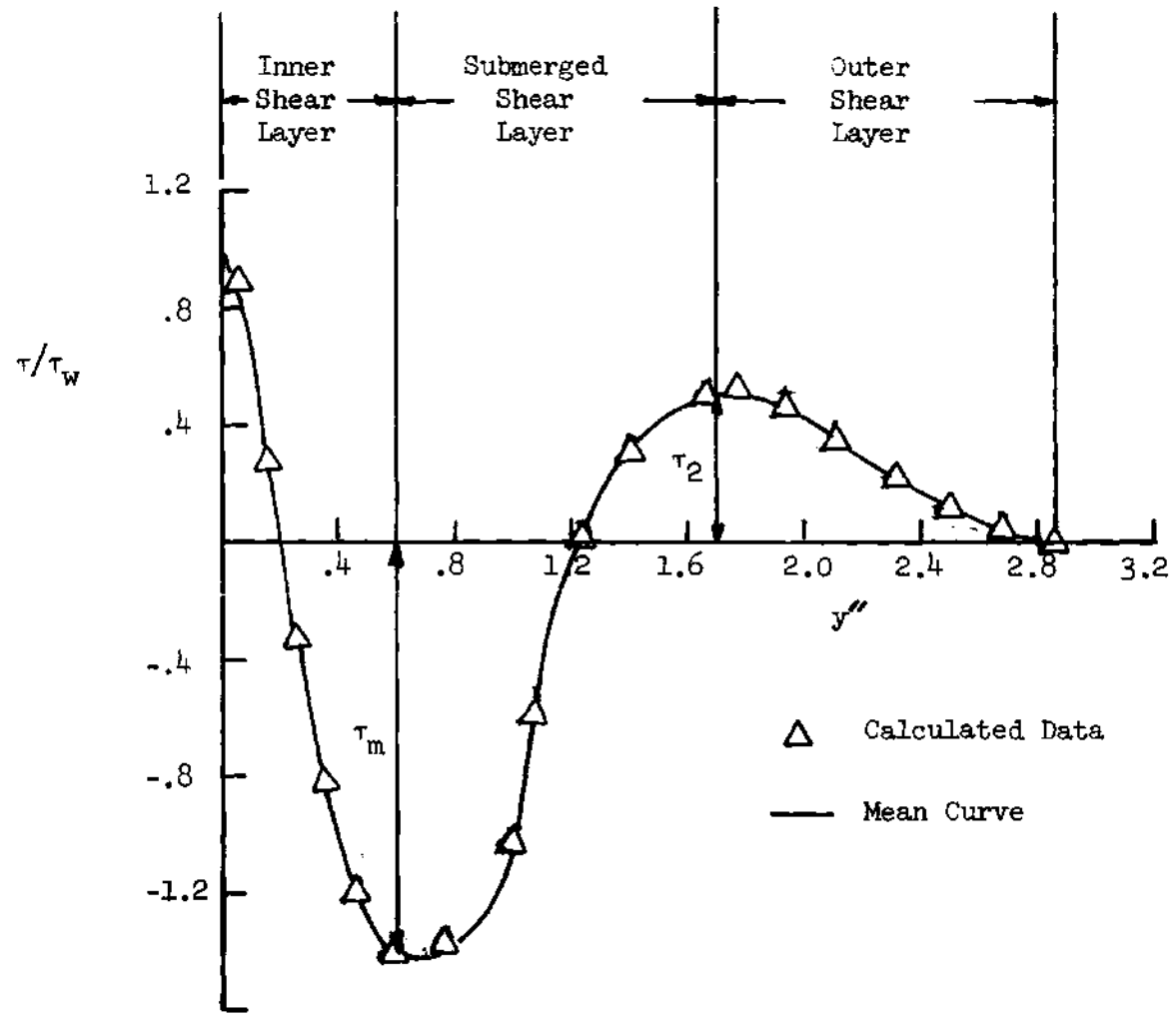

Figure 10. Shear Stress Distribution Series III, VR = 2.92, X = 341

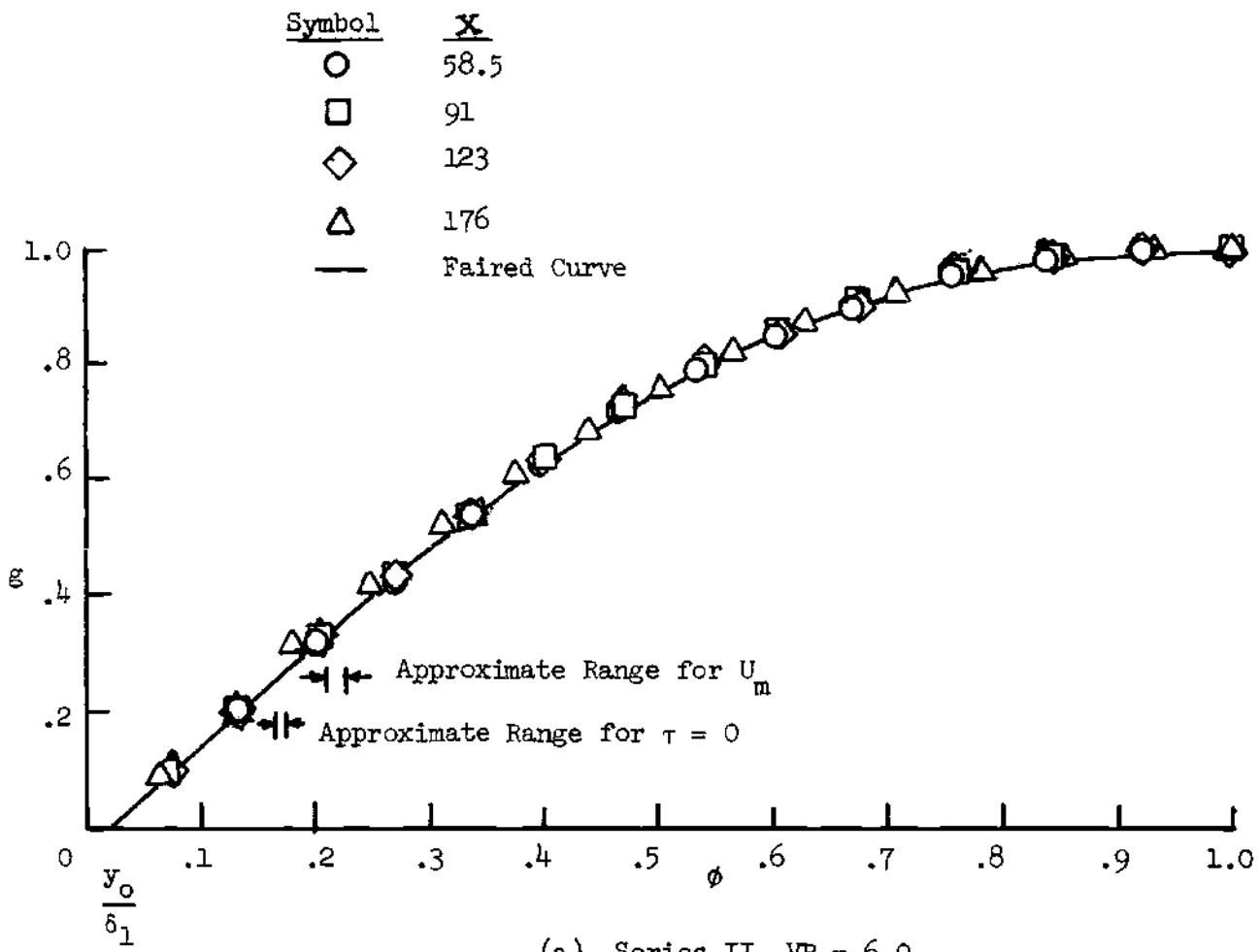

(a) Series II, VR = 6.0

Figure 11. Inner Shear Layer Profile

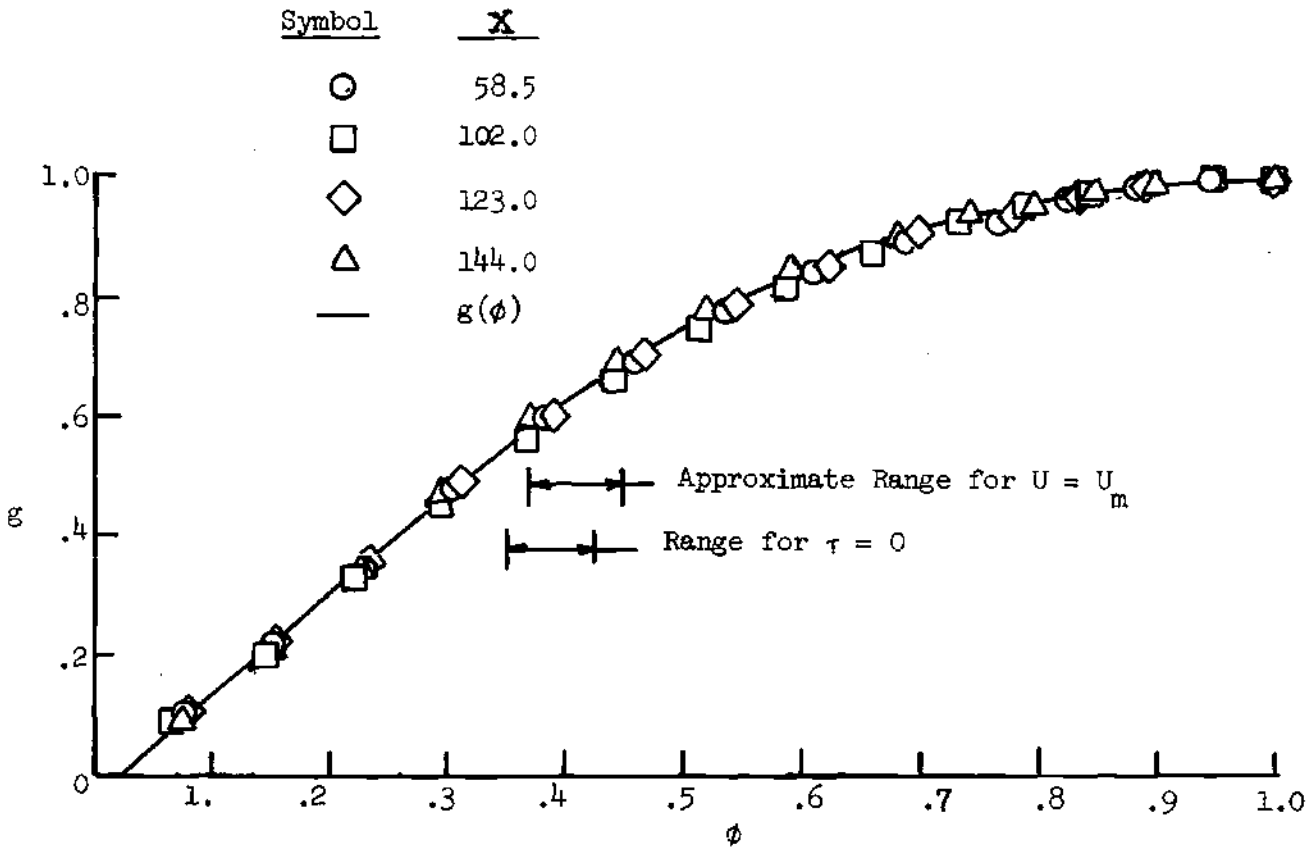

(b) Series II, VR = 2.0

Figure 11. (Continued)

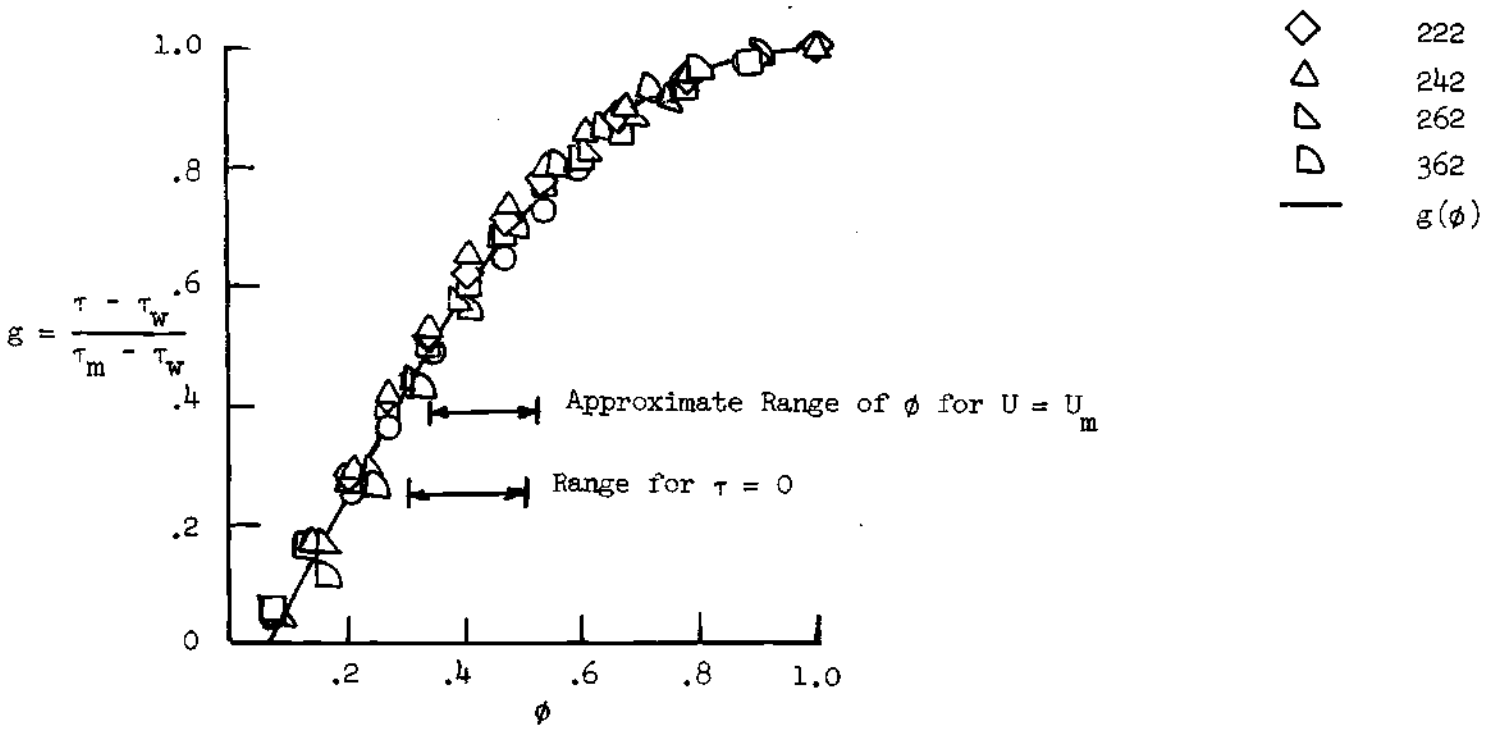

(c) Series III, VR = 2.07

Figure 11. (Continued)

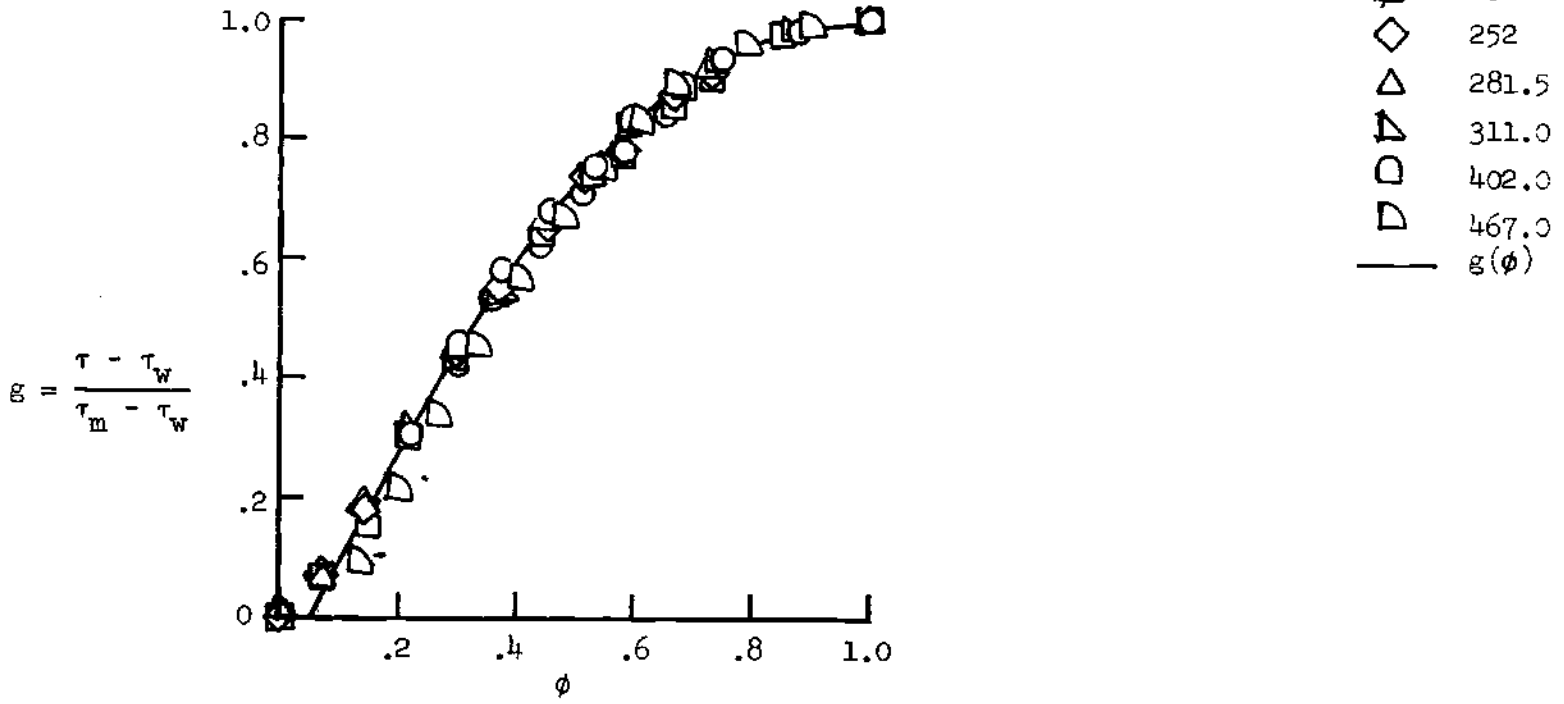

(d) Series III, VR = 2.92

Figure 11. (Continued)

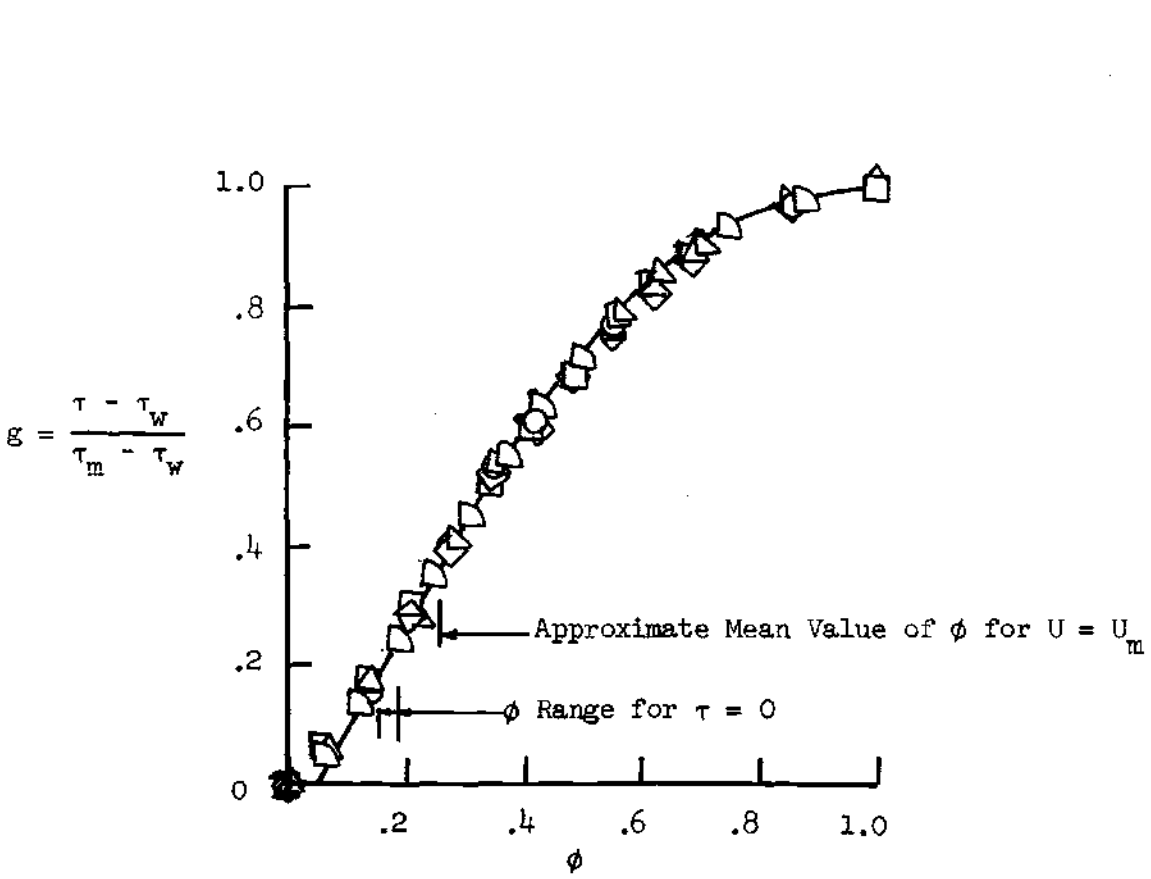

Symbol	X
○	160
□	180
◇	201
△	231
▷	251
▷	342
—	g(ϕ)

(e) Series IV, VR = 2.99

Figure 11, (Continued)

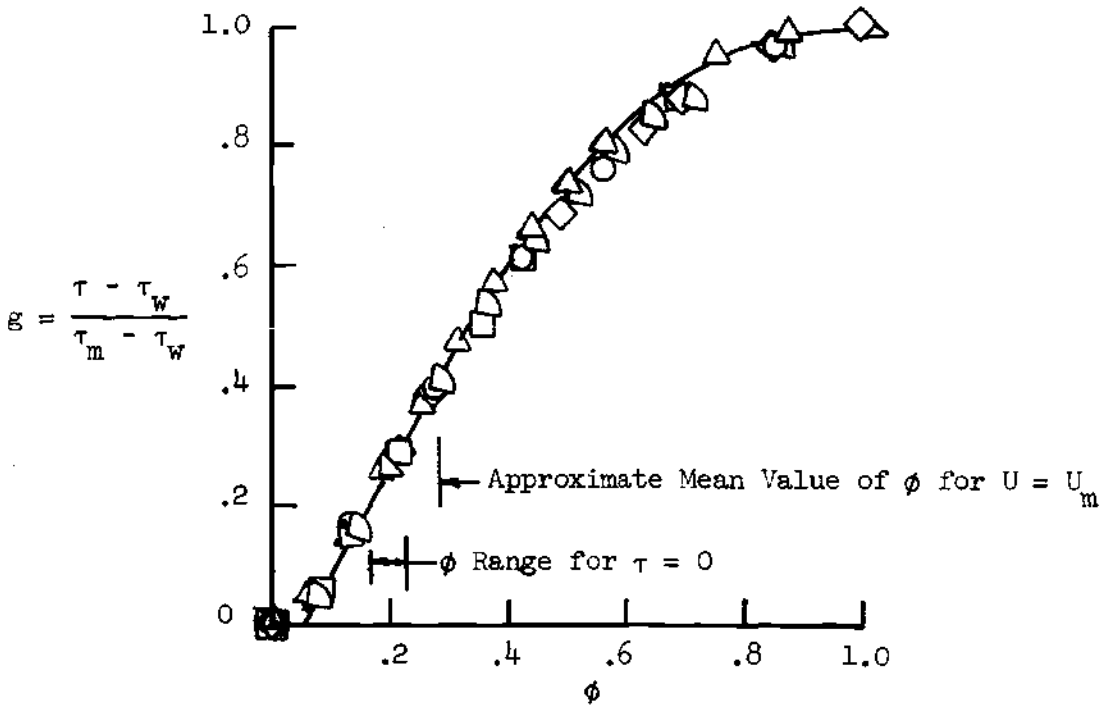

(f) Series IV, VR = 2.0

Figure 11. (Continued)

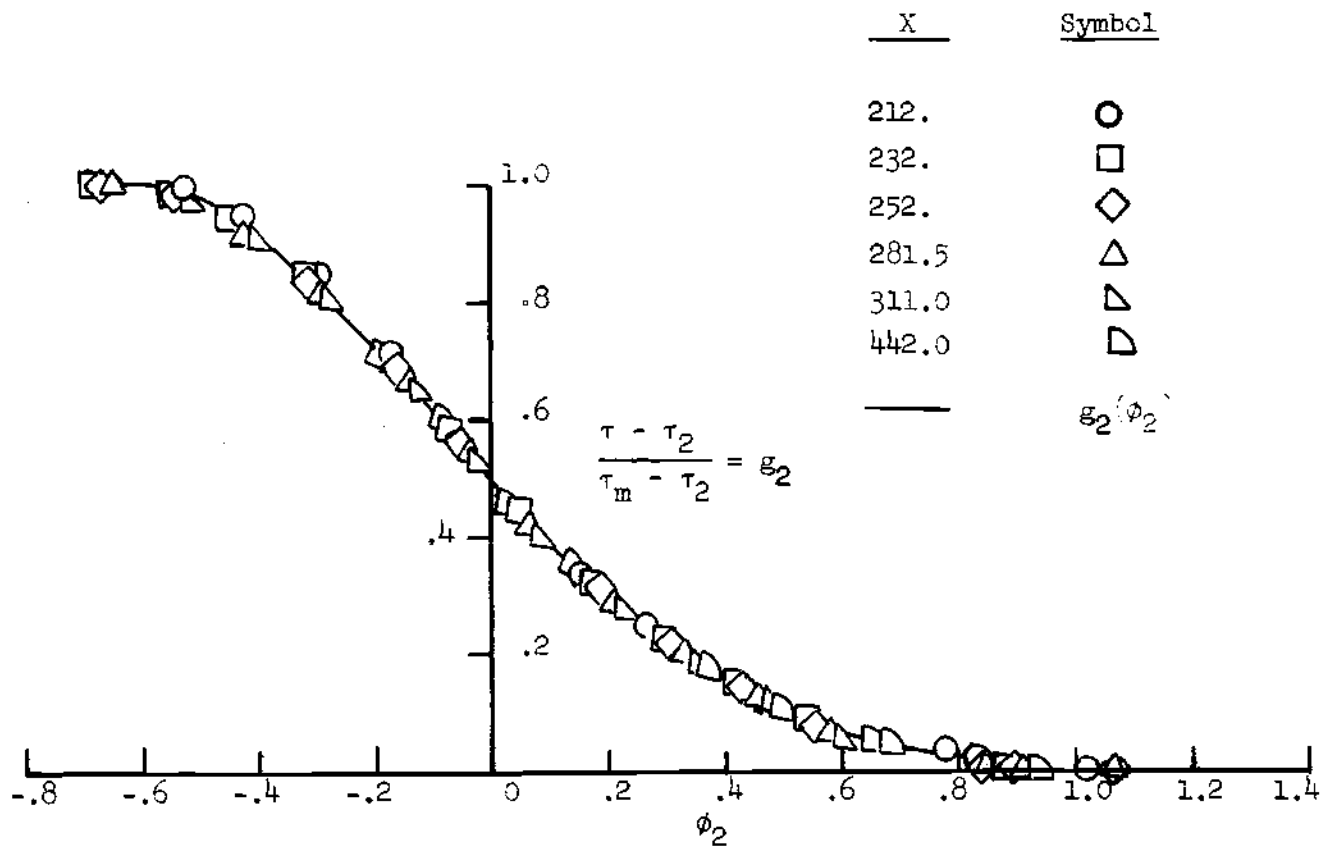

Figure 12. Submerged Shear Layer Profile

(a) Series III, VR = 2.92

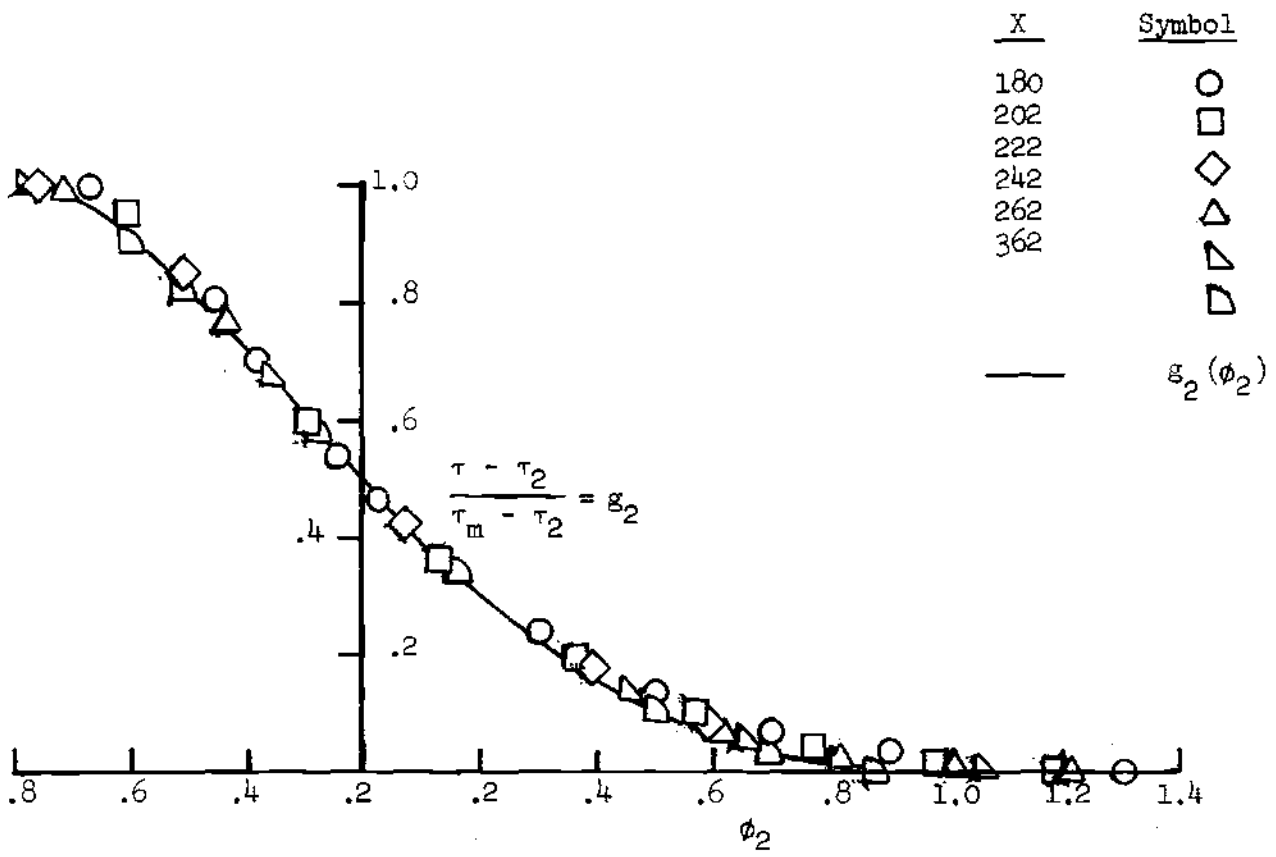

Figure 12. (Continued)

(b) Series III, VR = 2.07

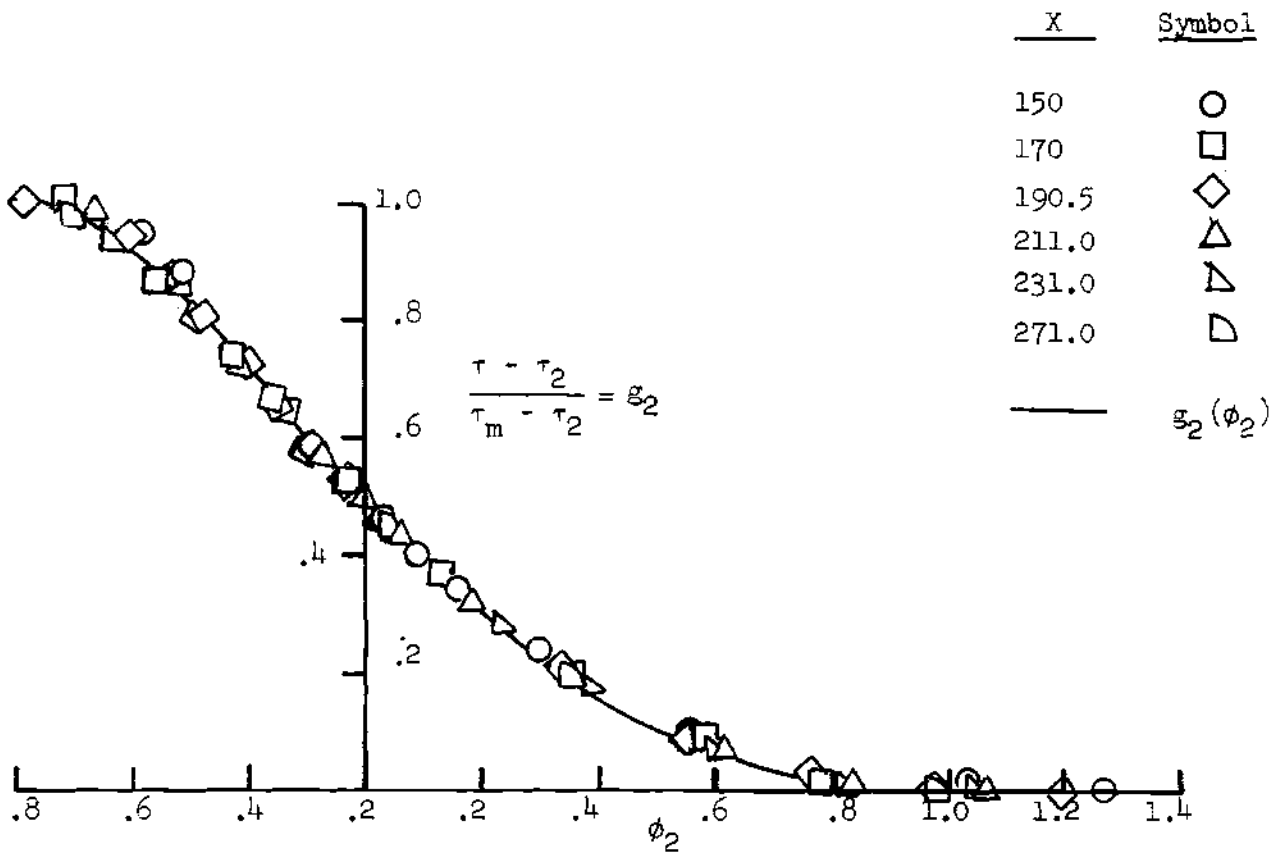

Figure 12. (Continued)

(c) Series IV, VR = 1.97

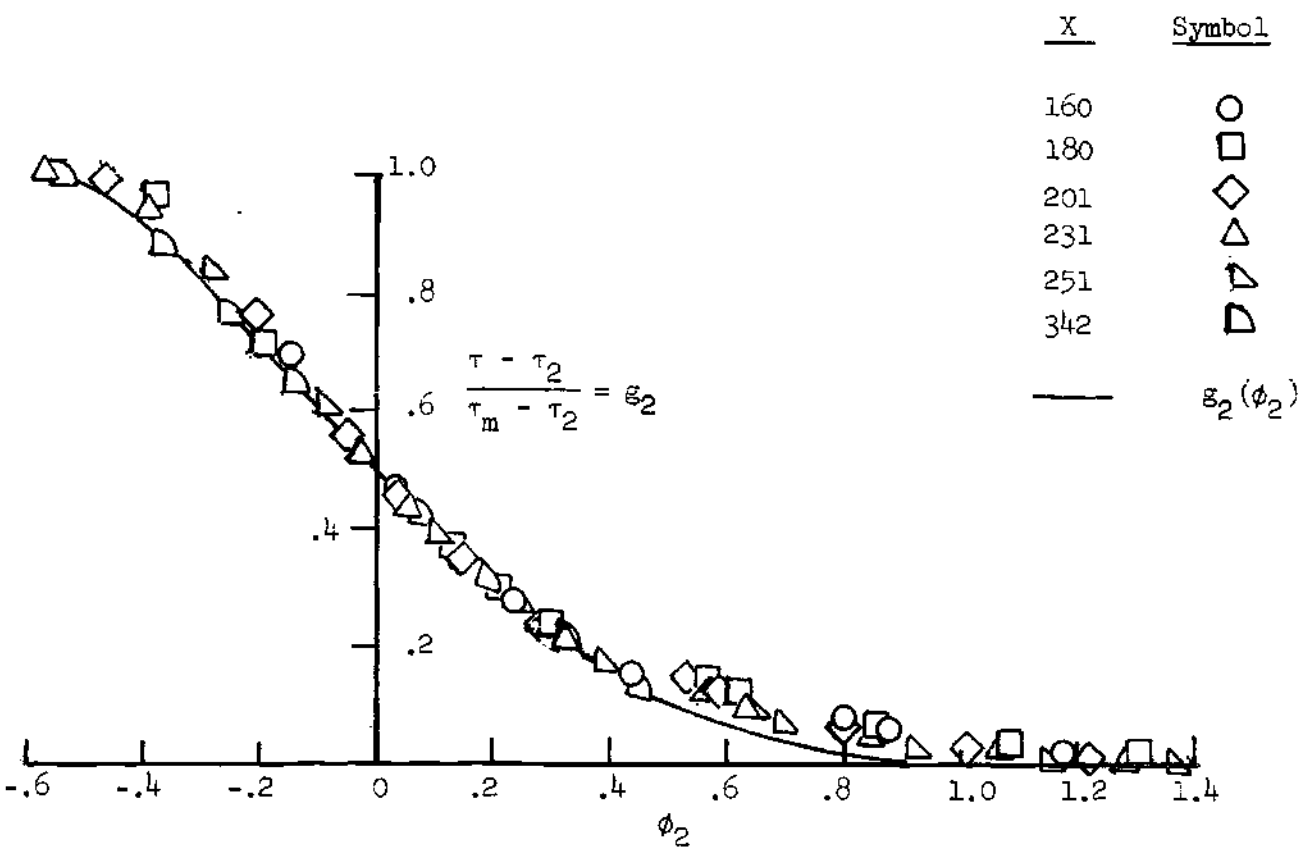

Figure 12. (Continued)
(d) Series IV, VR = 2.99

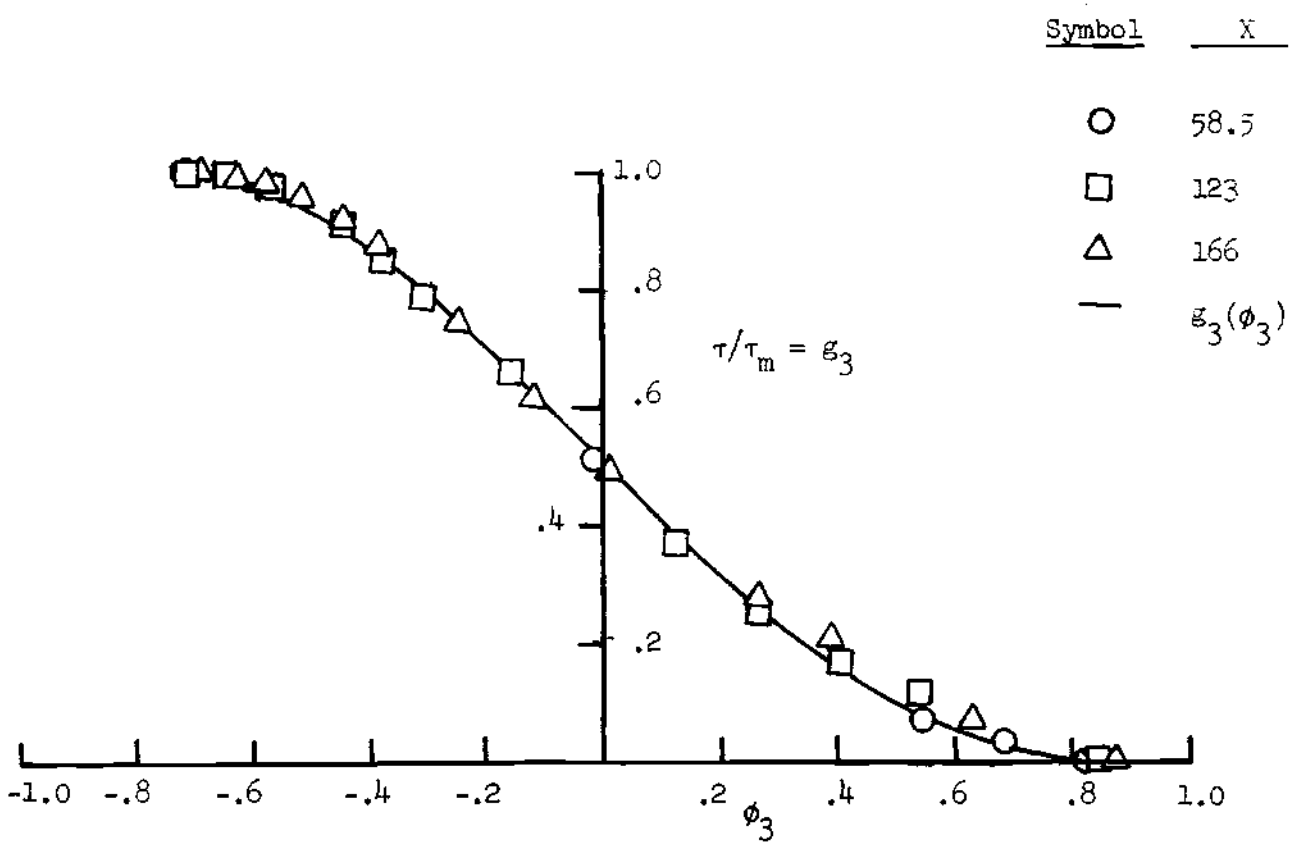

Figure 13. Outer Shear Layer Profile

(a) Series II, VR = 2.0

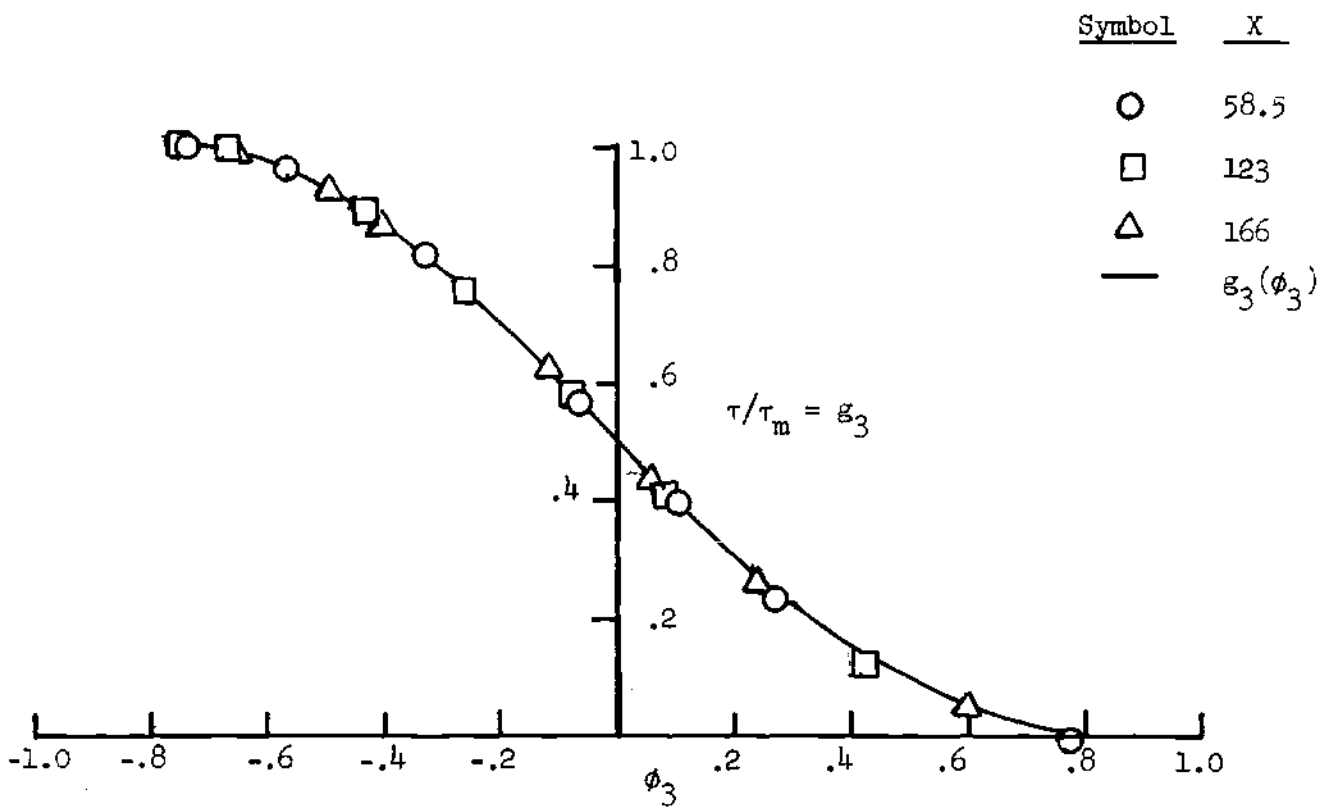

Figure 13. (Continued)

(b) Series II, VR = 6.0

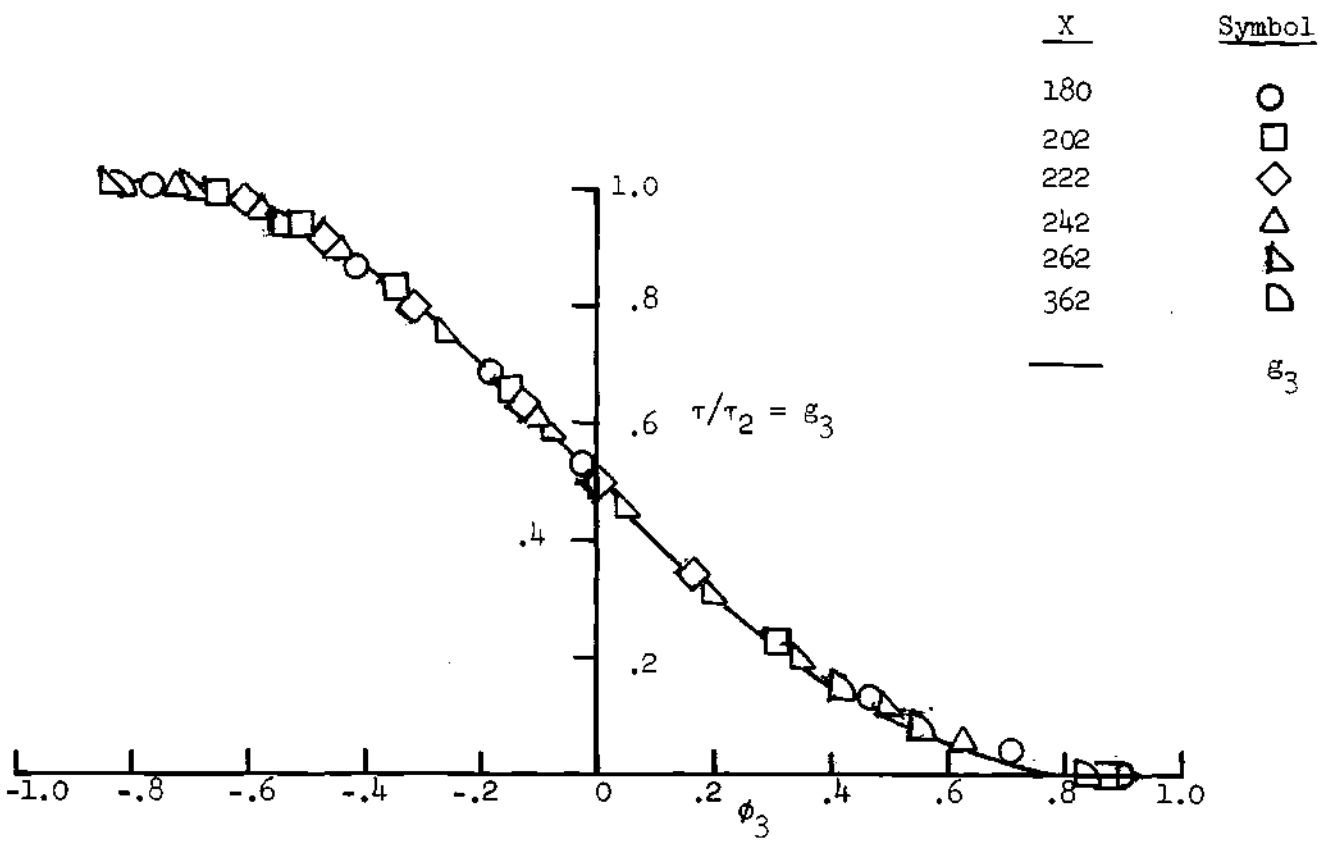

Figure 13. (Continued)

(c) Series III, VR = 2.07

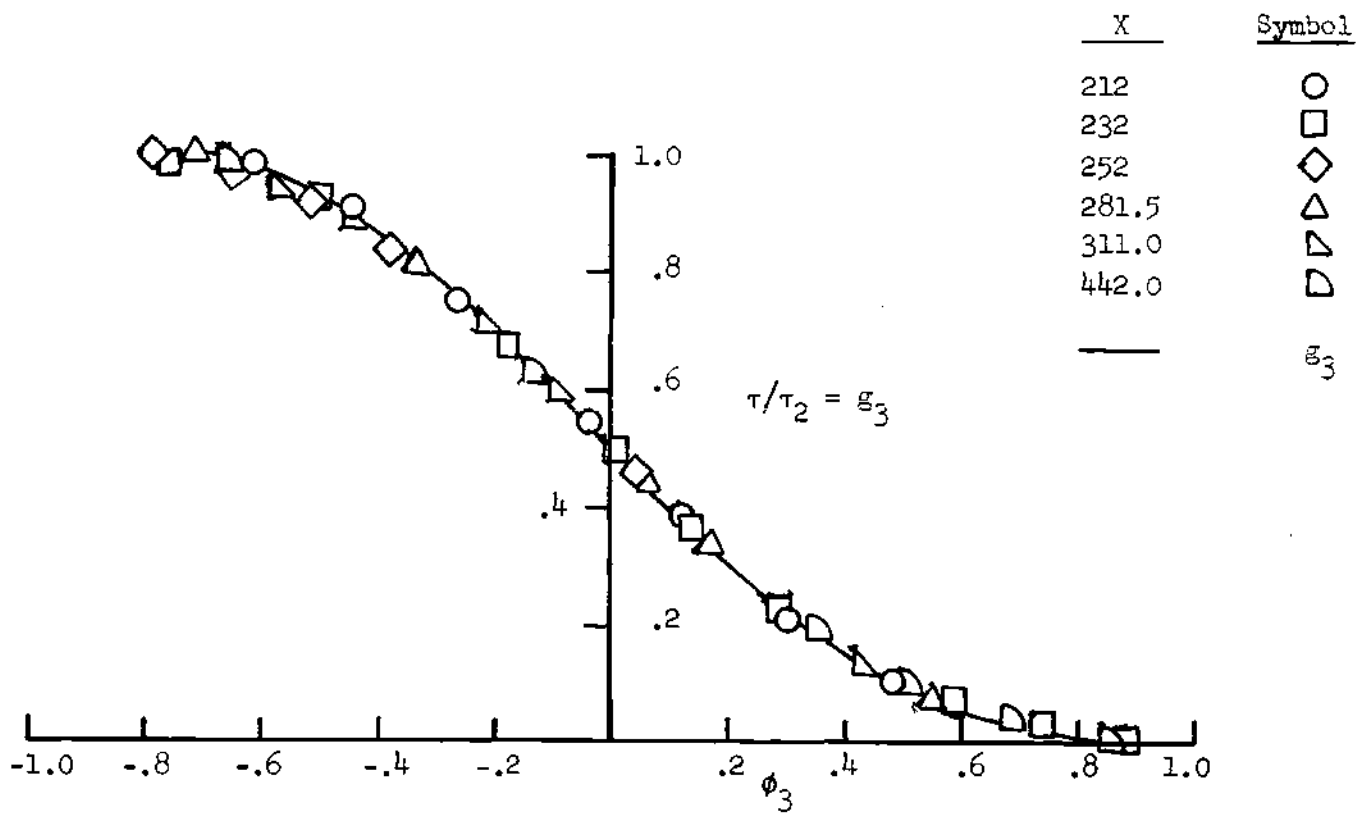

Figure 13. (Continued)

(d) Series III, VR = 2.92

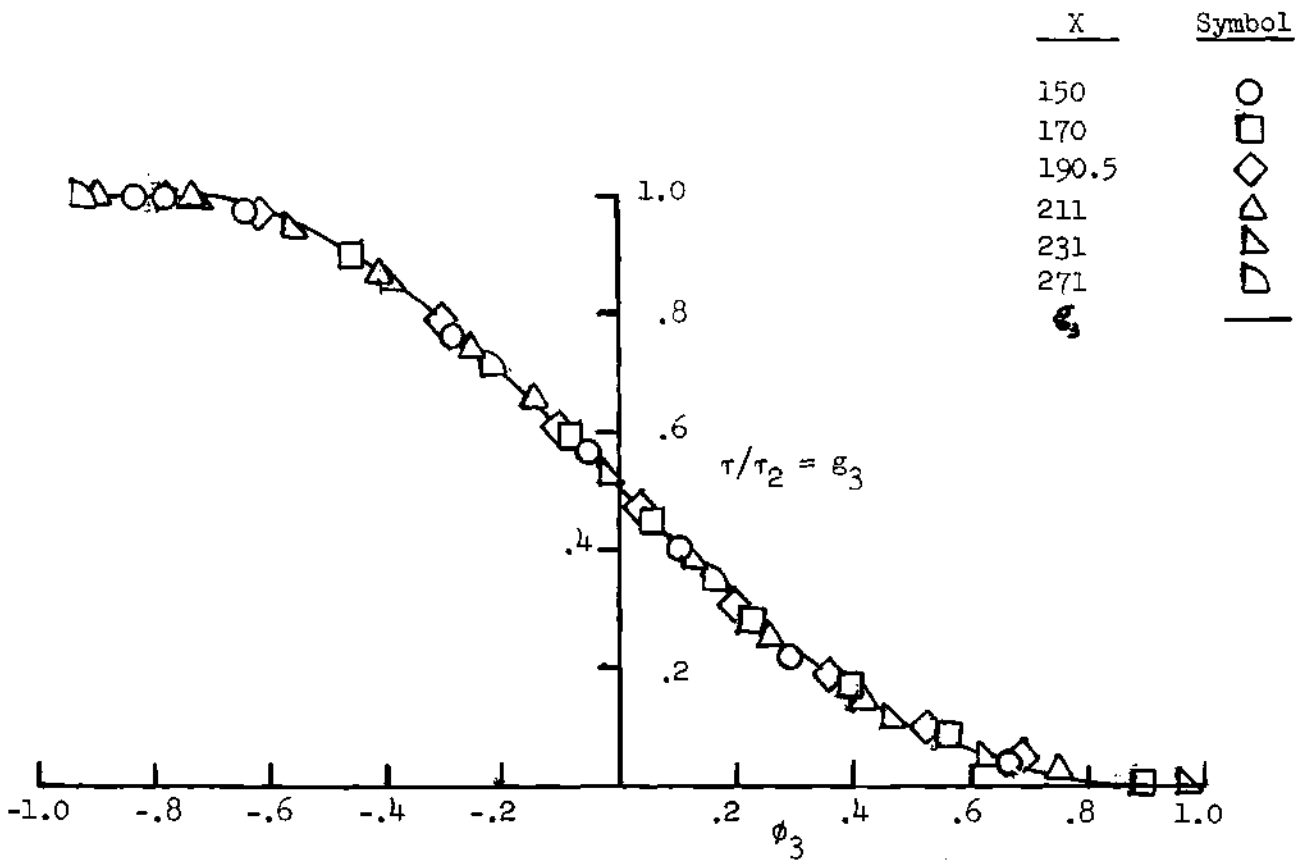

Figure 13. Continued

(e) Series IV, VR = 1.97

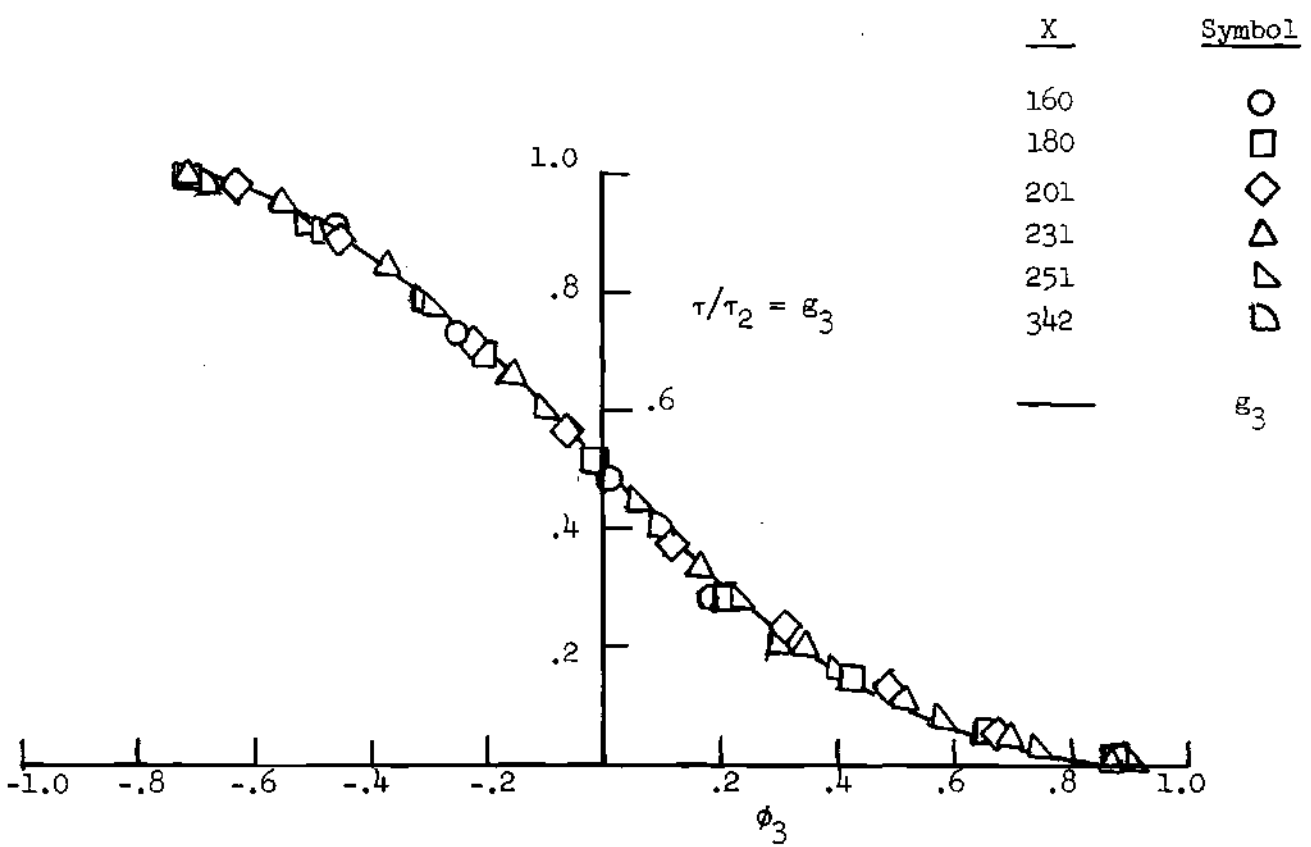

Figure 13. (Continued)

(f) Series IV, VR = 2.99

Shear Stress Similarities

Inner Shear Layer. Shear stress distributions in the inner shear layer are plotted in Figures 11. The normalized shear stress parameter g, defined as

$$g \equiv \frac{\tau - \tau_W}{\tau_m - \tau_W} \tag{22}$$

is plotted against the normalized distance ϕ, defined as y/δ_1 where τ_m and δ_1 are the shear stress and thickness at the inflection point of the velocity profile in the jet layer. An inspection of these results reveals that shear stress similarity appears to exist except in the narrow region close to the wall where the stress gradients become smaller as U_m/U_e becomes smaller. (This region near the wall is later identified as the wall sublayer and then analyzed separately.) To explore the degree of similarity outside this narrow region close to the wall, a curve is faired through the data of Figure 11(a), (i.e., the data for the highest velocity ratio and without pressure gradients) and linearly extrapolated to g = 0 (the linear portion of the curve extends over 25 percent of the entire layer) as shown in Figure 11(a). Identifying a new normalized length scale (to exclude the region near the wall) as

$$\phi_1 \equiv \frac{y - y_o}{\delta_1 - y_o} \tag{23}$$

where y_o is the intercept for g = 0. This faired curve can be expressed as

$$g = g(\phi_1) \tag{24}$$

This function is tabulated in Table 3. The function g can now be tested as a possible similarity function for all of the data. $g(\phi_1)$ is shown on the remaining plots of Figures 11(a) - (f). In each case, the intercept y_o is determined by linearly extrapolating the data to $g = 0$.

The function $g(\phi_1)$ accurately represents all of the shear stress results for the protion of the inner shear layer outside of the narrow region near the wall. An improved matching of a similarity parameter with the data could undoubtedly be achieved by employing a two parameter function (rahter than the single parameter y_o) but this is viewed as impractical and unnecessary considering the accuracy of the results and the sensitivity of theorectical analyses to slight changes in the shear stress distribution.

In summary, it is concluded that stress similarity does exist in the inner shear layer and this similarity can be represented by the function $g(\phi_1)$.

The approximate locations for which $U = U_m$ and $\tau = 0$ are also indicated on Figures 11(a) - (f). For the higher velocity ratios the location for which $\tau = 0$ is substantially closer to the wall than the location for which $U = U_m$ and, correspondingly, the location for which $dU/dy = 0$. As expected the two locations move closer together as the velocity ratio decreases. The relative location of the maximum velocity in this layer also varies substantially with velocity ratio. This location varies from $\phi_1 \approx 0.5$ as a maximum to about $\phi_1 \approx 0.15$ as a

Table 3. Tabulation of Shear-Stress Similarity Functions

Inner Shear Layer		Submerged Shear Layer		Outer Shear Layer	
ϕ_1	g	ϕ_2	g_2	ϕ_3	g_3
0	0	-0.6	1.0	-.7	1.0
.1	.169	-0.50	0.981	-.6	.978
.2	.338	-0.40	0.914	-.5	.930
.3	.502	-0.30	0.824	-.4	.866
.4	.645	-0.20	0.720	-.3	.788
.45	.707	-0.10	0.610	-.2	.700
.5	.762	0	0.50	-.1	.602
.55	.812	0.10	0.397	0	.5
.6	.857	0.2	0.305	.1	.400
.65	.890	0.3	0.224	.2	.308
.70	.923	0.4	0.157	.3	.227
.75	.950	0.5	0.104	.4	.157
.80	.969	0.6	0.063	.5	.100
.90	.990	0.7	0.034	.6	.055
1.0	1.0	0.8	0.016	.7	.022
		0.9	0.006	.8	.003
		1.0	0	.85	0

minimum. It is surprising that stress similarity is apparently maintained over such a wide range of conditions.

Submerged Shear Layer. The shear profile in the submerged shear layer is expressed as

$$\frac{\tau - \tau_2}{\tau_m - \tau_2} = g_2(\phi_2) \tag{25}$$

where $\phi_2 = y - \xi_{\frac{1}{2}}/\xi_j$, $\xi_{\frac{1}{2}}$ is the thickness to $\tau = \frac{1}{2}(\tau_m + \tau_2)$ and ξ_j is the submerged shear layer length scale. ξ_j is defined by

$$\xi_j = \frac{\tau_m - \tau_2}{-\frac{\partial \tau}{\partial y}/y = \xi_{\frac{1}{2}}} \tag{26}$$

The determination of ξ_j is identical to that of δ_j in velocity profile. Once the submerged shear layer length scale ξ_j was established for each submerged shear layer profile, all the submerged shear layer profiles were expressible in a common form with shear scale $\tau_m - \tau_2$ and length scale ξ_j. Typical results are shown in Figures 12(a) - (d).

A similarity function $g_2(\phi_2)$ was obtained from all of the results for the submerged shear layer. The values of $g_2(\phi_2)$ are also tabulated in Table 3. In addition, the function is shown on each plot of Figures 12(a) - (d). The function $g_2(\phi_2)$ accurately represents all of the data.

Outer Shear Layer. The shear profile in the outer shear layer is expressed as

$$\frac{\tau}{\tau_2} = g_3(\phi_3) \tag{27}$$

where $\phi_3 = y - \xi_4/\xi_w$, ξ_4 is the thickness to $\tau = \tau_2/2$ ($\tau_2 = \tau_m$ for Series II), and ξ_w is the outer shear layer length scale. The determination of ξ_w is similar to that of ξ_j, that is $\xi_w = \tau_2/\partial\tau/\partial y)y = \xi_4$. Once the outer shear layer length scale ξ_w was established for each outer shear layer profiles, all the outer shear layer profile were expressible in a common form with shear scale τ_2 for Series III and IV and τ_m for Series II and length scale ξ_w. Typical results are shown in Figures 13(a) - (f).

A similarity function $g_3(\phi_3)$ was also obtained from all of the results for the outer shear layer. The values are tabulated in Table 3 and the function is shown on each plot of Figures 13(a) - (f). Again, the agreement between the similarity function and the data is excellent.

Eddy Viscosity and Mixing Length

The eddy viscosity and the mixing length distribution through the jet and wake layers are illustrated in Figures 14(a) - (b) for two extremes in the flow conditions. These results were evaluated from the computed shear stress and velocity gradient distributions. Both the eddy viscosities and the mixing lengths are normalized by their respective value at the point of maximum stress in the jet layer. The eddy viscosity and the mixing length are singular at the points of maximum and minimum velocity where the shear stresses are not zero. In a relatively broad region around these singularities both the eddy viscosity and mixing length vary markedly. In the regions of high velocity gradients the mixing length is essentially constant where as the eddy viscosity varies significantly.

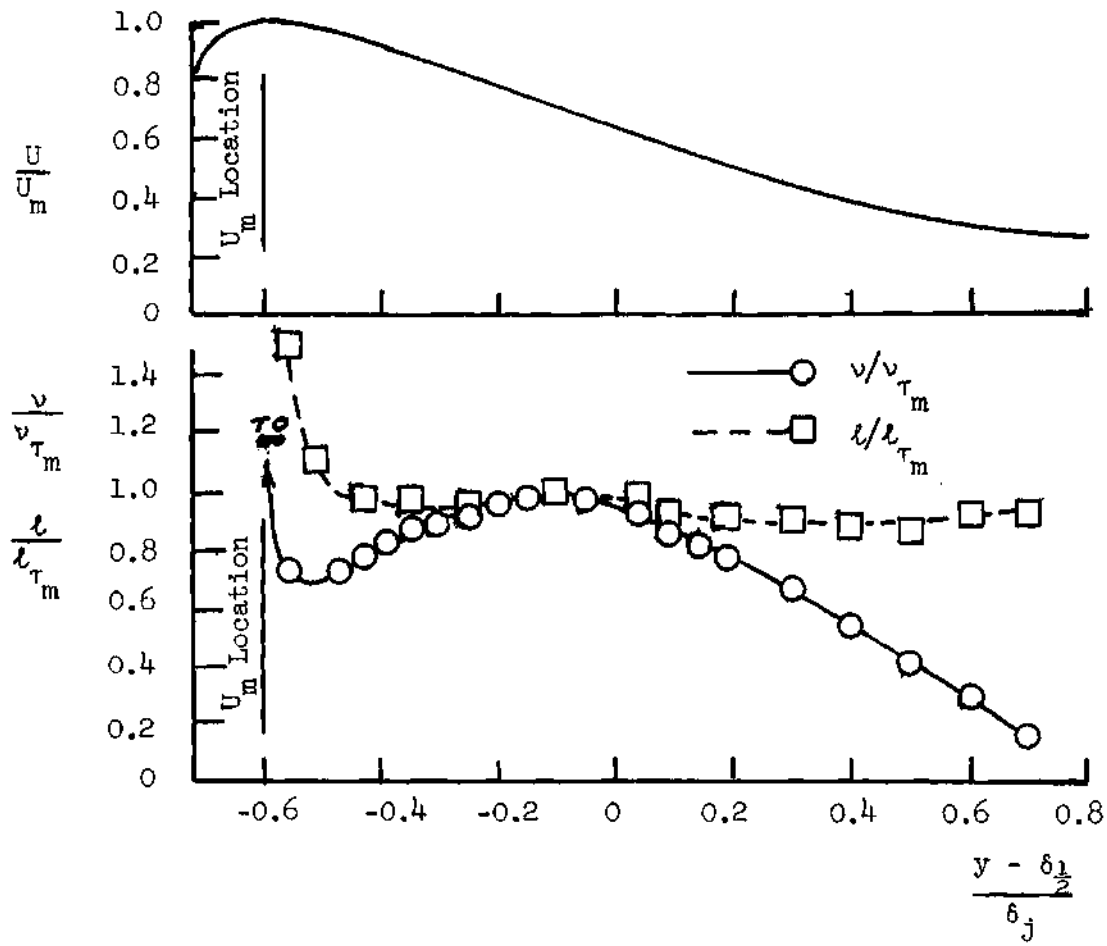

Figure 14. Eddy Viscosity Profile

(a) Series II; VR = 6; $\boldsymbol{X}$ = 58.5

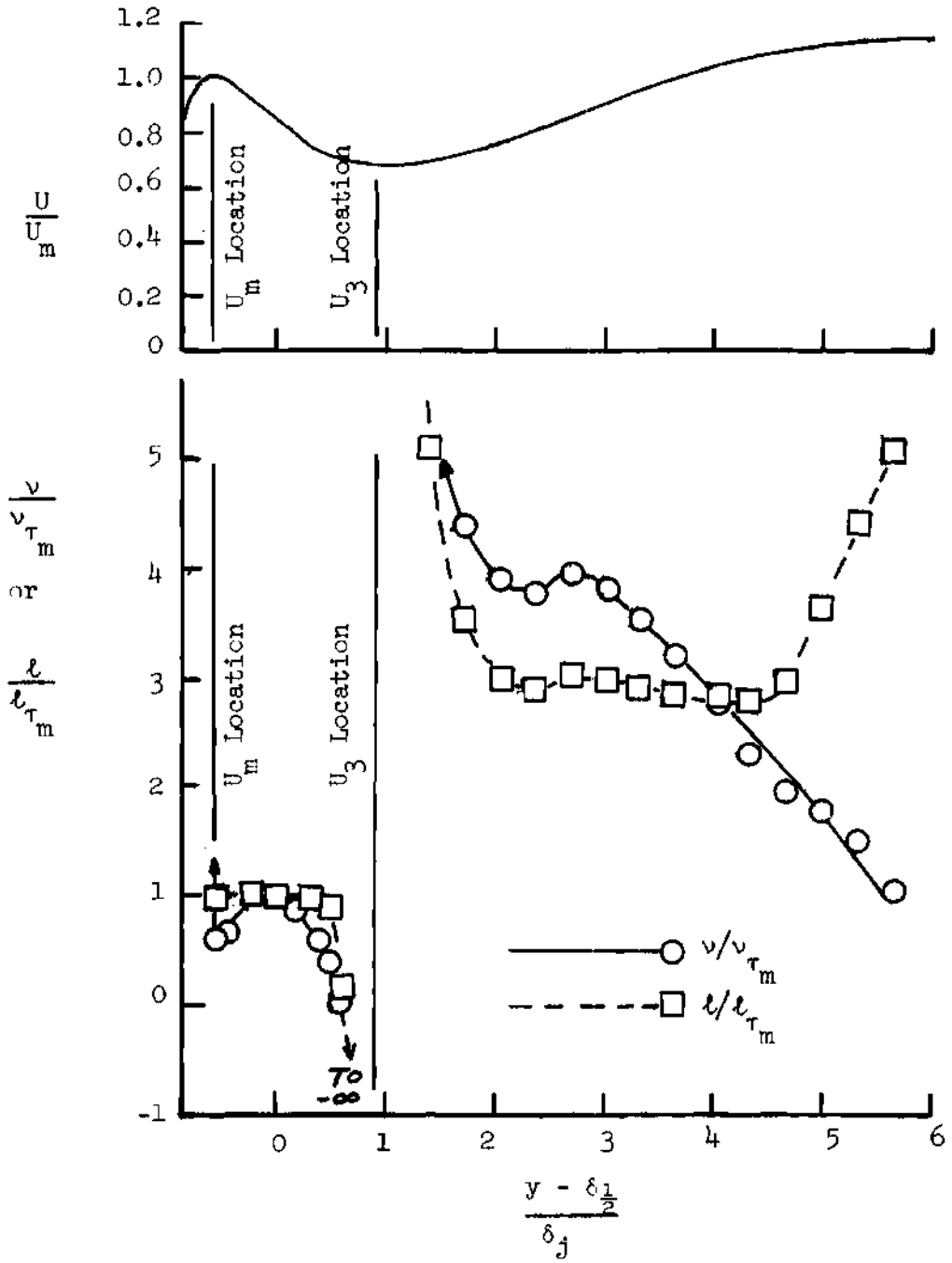

Figure 14. (Continued) (b) Series IV; VR = 1.97; $\mathbf{X}$ = 211

The use or evaluation of eddy viscosities or mixing lengths will not be persuaded any further because they vary substantially, they have singularities, and it appears prohibitively difficult to establish useful analytical representations for them. Instead, the use of shear stress similarities seems to offer a more promosing approach.

Maximum Shear Stresses

The shear stress distributions presented in Figures 11, 12, and 13 were normalized using the maximum values of the shear stresses within the jet and wake layers. Therefore, in order to explicitly define the shear stress distributions it is necessary to specify these maximum shear stresses.

The hypothesis of an eddy viscosity which connects the turbulent shear stresses to the local mean velocity gradient has proven to be useful for analyzing many practical turbulent shear flows particularly in the regions of high velocity gradients. Furthermore, the concept of an eddy Reynolds number for relating the eddy viscosity to the mean flow properties has received wide usage. Although there is no general relationship for the eddy Reynolds number even for simple shear flows, it has been useful, primarily because it varies over a relatively narrow range. Therefore, the maximum shear stresses in the jet and wake layers from the results of the present study have been reflected into an eddy viscosity defined as

$$\nu_{T_j} = \frac{1}{\rho_m} \frac{\tau_m}{\frac{\partial u}{\partial y}/m} \tag{28}$$

for the jet layer and

$$\nu_{T_w} = \frac{1}{\rho_2} \frac{\tau_2}{\frac{\partial u}{\partial y}/2} \tag{29}$$

for the wake layer. These eddy viscosities have then been used to evaluate the corresponding turbulent Reynolds numbers defined as

$$R_{T_j} = \frac{(U_m - U_3)\ \delta_j}{\nu_{T_j}} \tag{30}$$

for the jet layer and

$$R_{T_w} = \frac{(U_e - U_3)\ \delta_w}{\nu_{T_w}} \tag{31}$$

for the wake layer.

The values of the reciprocal of the turbulent Reynolds numbers (the reciprocal is directly proportional to ν_T) as computed from the experimental data are presented in Figures 15(a) - (c), and 16(a) - (b). Only those results which the author considered to be significant are included on these figures. Results which scattered or varied rapidly due to small shear stresses or due to data smoothing near the upstream and downstreams extremes have ben omitted. The results of Figures 15 and 16 show that the turbulent Reynolds number varies substantially with both streamwise location for all three series and velocity ratio. The reciprocal of the turbulent Reynolds numbers for a two-dimensional jet exhausting into still air and a small deficit, two-dimensional wake (26) converted to the present definition) are 0.021 and 0.049, respectively.

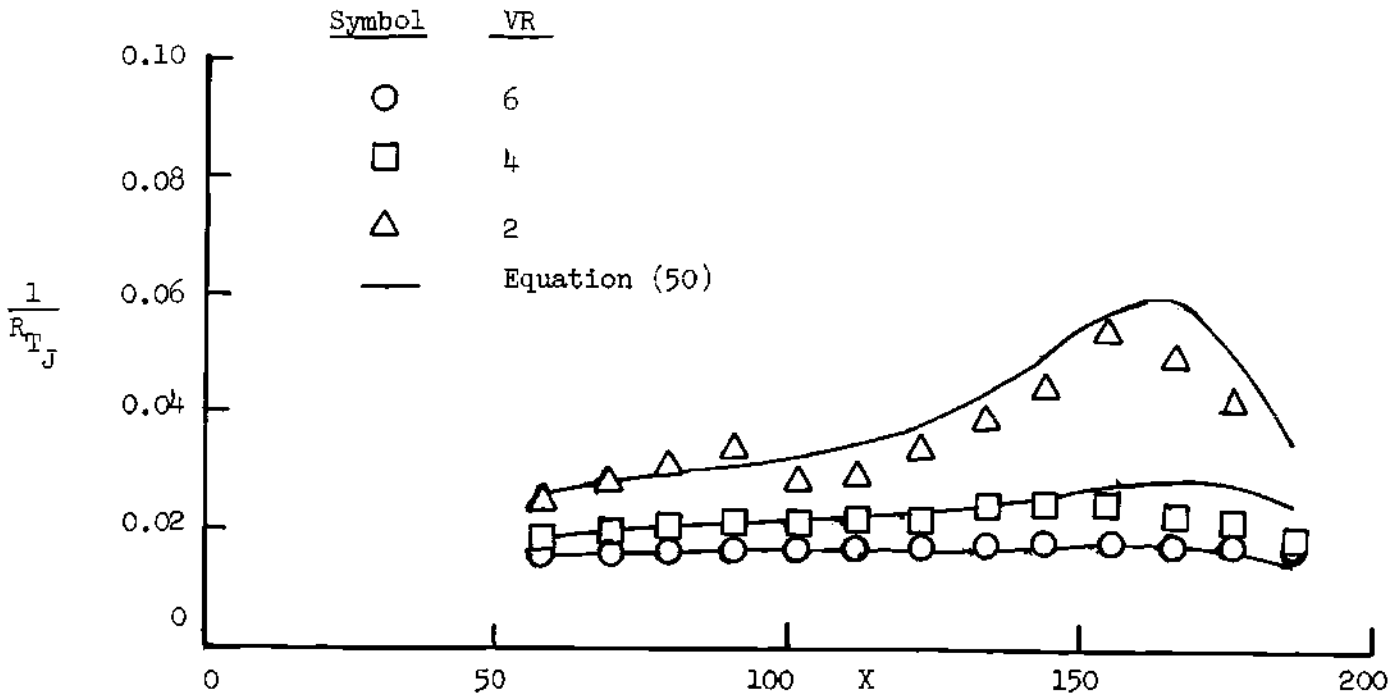

Figure 15. Turbulent Reynolds Number Variation with x - Jet Layer

(a) Series II

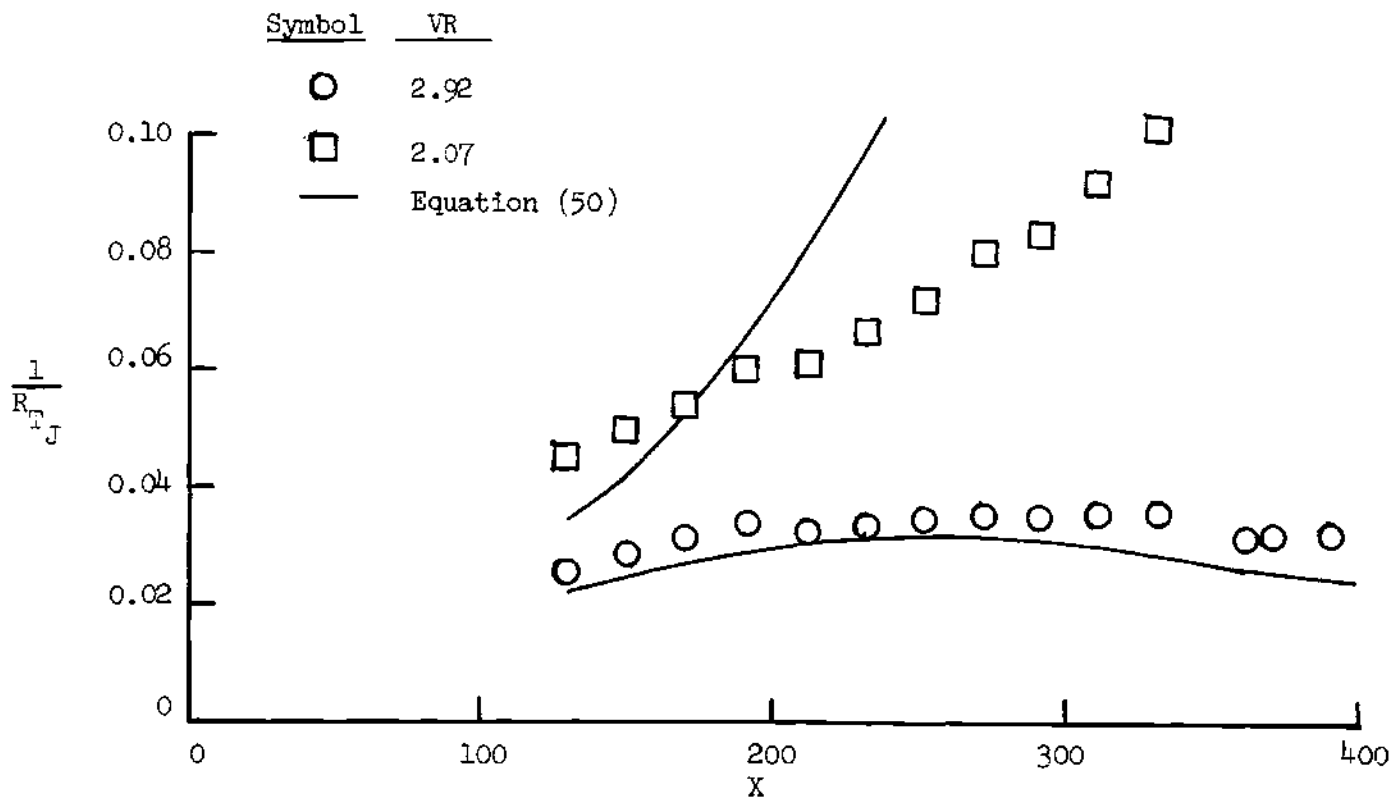

Figure 15. (Continued)

(b) Series III

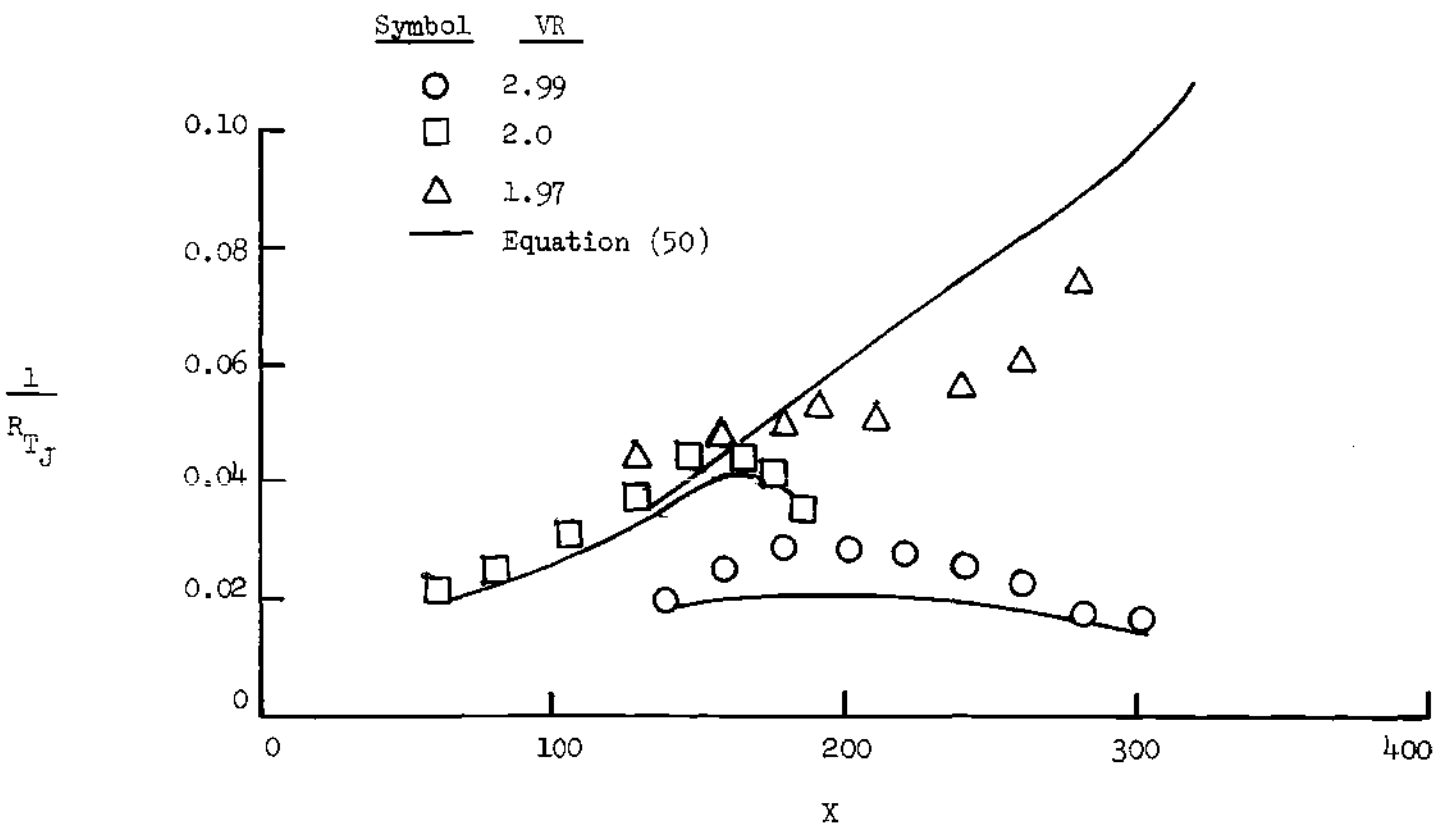

Figure 15. (Continued)

(c) Series IV

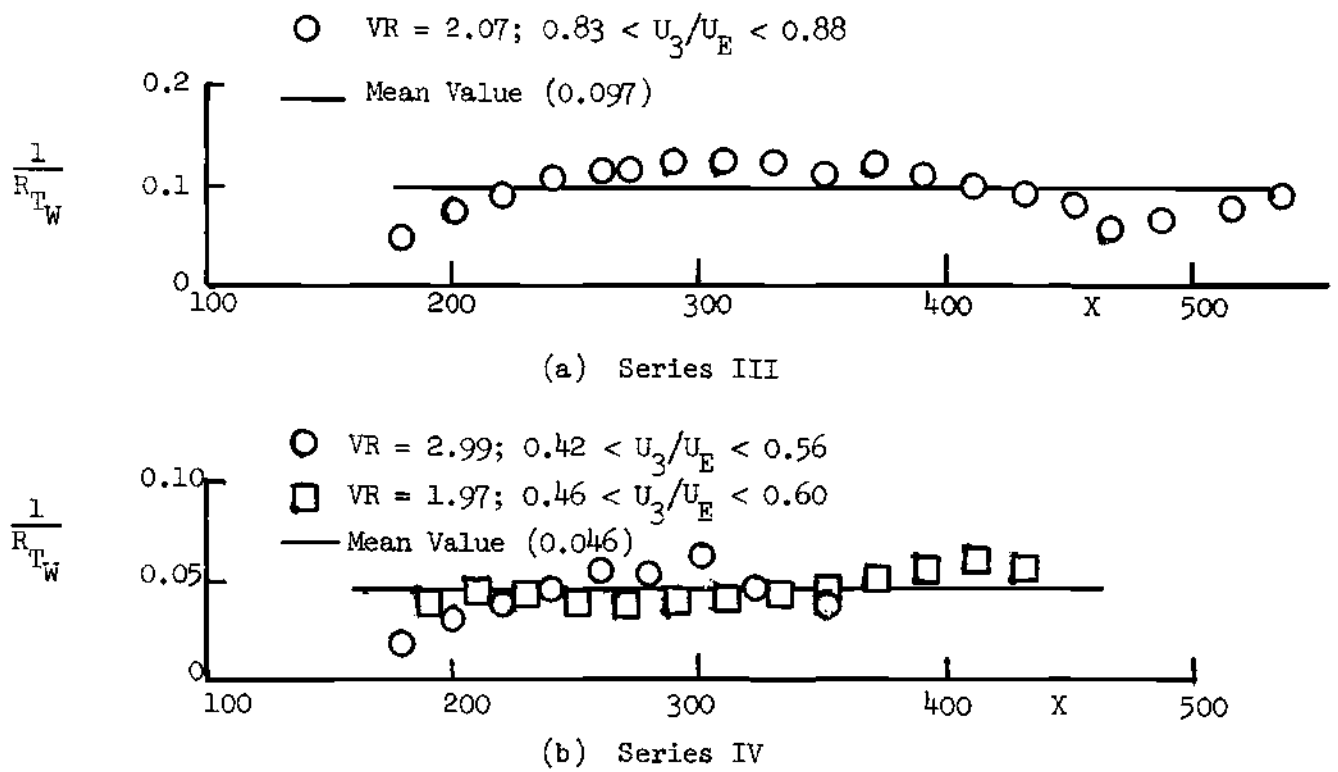

Figure 16. Turbulent Reynolds Number Variation with x - Wake Layer

The lowest value for the wall jet, about 0.016, occurs at the highest velocity ratio (Figure 15(a); VR = 6). This is consistent with conclusions reported in the literature (26), (27), and (33) where it is argued that the eddy viscosity in the jet layer of a high velocity ratio wall jet is lower than that in a two-dimensional jet because of a damping effect due to the wall. The highest value for the reciprocal of the turbulent Reynolds number for the jet and wake layers of the wall jet exceeds that for the small deficit wake. Generally, however, most of the results fall between the extremes of a jet and a wake.

As previously mentioned, there is to date no general relationships between the turbulent Reynolds number and the mean flow properties. For the present case, in which only the turbulent Reynolds number corresponding to the maximum shear stress is of concern, it is possible to develop such a relationship from the turbulent energy equation following the approach used by Bradshaw (27) for the turbulent wall boundary layer. This relationship is derived in the subsequent paragraphs. Following Bradshaw, various turbulence quantities are related in order to reduce the turbulent energy equation. Additional assumptions are then made to finally obtain an explicit relationship for the turbulent Reynolds number. This expression is then matched to and compared with the results of Figures 15.

The turbulent energy equation for an incompressible mean flow, outside the viscous sublayer is

$$\frac{D\,\frac{\overline{q^2}}{2}}{Dt} = \frac{\tau}{\rho}\frac{\partial u}{\partial y} - \frac{\partial}{\partial y}\left[\frac{\overline{pv}}{\rho} + \frac{\overline{q^2 v}}{\rho}\right] - \varepsilon \qquad (32)$$

where $\epsilon \simeq \nu \overline{(\partial u_i/\partial x_j)^2}$. Equation (32) can be regarded as an equation for the advection or rate of change of turbulent kinetic energy along a mean streamline through a point if all the other terms are known at that point, just as the boundary layer momentum equation,

$$\rho \left[u \frac{\partial u}{\partial x} + v \frac{\partial u}{\partial y} \right] = \rho u_1 \frac{du_1}{dx} + \frac{\partial \tau}{\partial y} \tag{33}$$

can be regarded as an equation for the rate of change of mean flow momentum ρu. Following Bradshaw, it is assumed that the various turbulent quantities are related to the turbulent shear stress as follows:

$$\frac{\tau}{\rho} = - \overline{uv} = aq^2 \tag{34}$$

$$\frac{\tau}{\rho} \left(\left|\frac{\tau}{\rho}\right| \right)^{3/2} = \frac{1}{G} \left(\frac{\overline{Pv}}{\rho} + \frac{\overline{q^2 v}}{\rho} \right) \tag{35}$$

$$\left(\left|\frac{\tau}{\rho}\right| \right)^{3/2} = L\epsilon \tag{36}$$

where a, L and G are functions of y/δ which depend on the shape of the shear stress profile. a and G are dimensionless. L is a dissipation length scale and is usually the most important of the three functions because over most of the boundary layer the dissipation is much larger than the advection or diffusion.

Substitution of Equations (34), (35) and (36) into Eq. (32), gives

$$\frac{U}{2}\frac{\partial \frac{\tau}{\rho a}}{\partial x} + \frac{V}{2}\frac{\partial \frac{\tau}{\rho a}}{\partial y} = \frac{\tau}{\rho}\frac{\partial U}{\partial y} - \frac{\partial G}{\partial y}\left(\frac{\tau}{\rho}\right)\left(\left|\frac{\tau}{\rho}\right|\right)^{3/2} - \frac{\left(\left|\frac{\tau}{\rho}\right|\right)^{3/2}}{L} \tag{37}$$

Equation (37) is now applied at the maximum value of $|\tau/\rho|$ where

$$\frac{\partial \frac{\tau}{\rho}}{\partial y} = 0 \tag{38}$$

In addition, it is assumed that a is constant and G is negligible (or constant) in the region where $|\tau/\rho|$ is a maximum and that local similarity exists in the sense that at most

$$a = a(y/\delta) \tag{39}$$

or

$$\left.\frac{\partial a}{\partial x}\right) = 0 \qquad \begin{matrix} \\ y = \text{value for which } |\tau/\rho| \text{ is max} \end{matrix} \tag{40}$$

Hence, at the location for which $|\tau/\rho|$ is a maximum Equation (37) becomes

$$\frac{U}{2a}\frac{\partial \frac{\tau}{\rho}}{\partial x} = \frac{\tau}{\rho}\frac{\partial U}{\partial y} - \frac{\left(\left|\frac{\tau}{\rho}\right|\right)^{3/2}}{L} \tag{41}$$

Employing

1. $$\left(\frac{U - U_e}{U_m - U_e} \right) = f(\eta) , \quad \eta = y/\delta_j \tag{42}$$

2. y_o to represent the location for which $|\tau/\rho|$ is a maximum

3. $$\delta_j \equiv - \frac{U_m - U_e}{\left(\frac{\partial U}{\partial y} \right)_{max}} \tag{43}$$

4. $$\left(\frac{\partial U}{\partial y} \right)_{y=y_o} = - \frac{U_m - U_e}{\delta_j} \tag{44}$$

5. $$U = U_e + (U_m - U_e) f(\eta_o) \tag{45}$$

and assuming that $L = 1/C \ \delta_j$, Equation (41) gives

$$\frac{U_e + (U_m - U_e) f(\eta_o)}{2a} \frac{\partial \frac{\tau}{\rho}}{\partial x} = - \frac{\tau}{\rho} \frac{(U_m - U_e)}{\delta_j} \left[1 + \frac{C \left(\left| \frac{\tau}{\rho} \right| \right)^{3/2}}{\frac{\tau}{\rho} (U_m - U_e)} \right] \tag{46}$$

The shear stress can now be written in terms of the turbulent Reynolds number. Introducing the eddy viscosity as

$$\epsilon = \frac{(U_m - U_e) \delta_j}{R_T} \tag{47}$$

the shear stress becomes

$$\frac{\tau}{\rho} = \epsilon \frac{\partial U}{\partial y} = - \frac{(U_m - U_e)^2}{R_T} \tag{48}$$

Thus Eq. (46) finally becomes

$$\frac{dR_T}{dx} = R_T \left[\frac{2}{U_m - U_e} \frac{d(U_m - U_e)}{dx} + \frac{2a(U_m - U_e)}{\delta_j [U_e + U_m - U_e) f(\eta_o)]} \left(1 - \frac{C}{\sqrt{R_T}} \right) \right] \tag{49}$$

Equation (49) relates the advection, production, and dissipation of turbulent shear stresses. If one assumes local self-preservation then $dR_T/dx = 0$ and Eq. (49) becomes an algebraic expression for R_T. Calculations using Eq. (49) show that $1/(U_m - U_e)^2 \times d(U_m - U_e)^2/dx$ is more than an order of magnitude greater than $1/R_T \times dR_T/dx$ and, therefore, the latter may be neglected. In this case, Eq. (49) becomes

$$\sqrt{R_T} = \frac{\dfrac{a(U_m - U_e)\, C}{\delta_j [U_e + (U_m - U_e) f(\eta_o)]}}{\dfrac{1}{U_m - U_e} \dfrac{d(U_m - U_e)}{dx} + \dfrac{}{\delta_j [U_e + (U_m - U_e) f(\eta_o)]}} \tag{50}$$

where the constants a and c must be determined from experimental data. Equation (50) has been shown (28) to accurately express the turbulent Reynolds numbers for the following two-dimensional shear flows:

1. Jets exhausting into still air
2. Jets exhausting into a coflowing stream
3. Small deficit wakes

4. Shear layer between uniform coflowing streams with velocity ratios from 0 to ∞.

The constants a and c in Eq. (50) have been determined by a least square fit of Eq. (50) to the results of Series II for a velocity ratio of 6. The values of a and c are

$$a = 0.110$$

$$c = 10.98$$

These are reasonable values and are close to these obtained by Bradshaw for boundary layers (a = 0.15 and c ≈ 11). The corresponding results from Eq. (50) are shown on Figure 15(a). In spite of the simplifications, this semiempirical equation accurately predicts the results from the data of Series I.

The predictions of Eq. (50) for the jet layer results from the data of Series III and IV are shown on Figures 15(b) and 15(c). The predictions are reasonably good (especially for the higher velocity ratios) except for the cases in which the velocity differences are relatively small (i.e., $x > 200$ with velocity ratios near 2.0). Even in these cases the trends are properly predicted.

The comparison of Eq. (50) with the data of Figures 16(a) - (b) was less satisfactory and conclusive. Therefore, the best values that can be recommended at the present are the mean values included on these figures.

The fact that the theory (Eq. (50)) accurately predicts the

trends of the computed data is better illustrated in Figure 17 where a single, consolidated plot with less of the data is presented. These results indicated the large differences in $1/R_{T_J}$ for the three Series and the large variation in $1/R_{T_j}$ with velocity ratio. This plot is not intended to imply however, that U_e/U_m is the significant parameter since clearly the initial B. L. and pressure gradient have an effect.

Wall Sublayer

In this section it is shown that, if the well-known mixing-length formula is regarded simply as a relationship between the velocity and the stress distributions in the wall region of a turbulent flow, then a truly universal distribution of mixing length is sufficient to describe the experimentally observed departures of the velocity distribution from the usual law of the wall. Comparisons are made with a wide range of the experimental wall jet data to demonstrate the general validity of the modified mixing-length model in describing the flow close to the wall. A rapid streamwise decay in the wall shear stress (due to a rapid decay in the wall-jet peak velocity) uniquely distinguishes the wall jet sublayer from that of an ordinary boundary layer.

General Characteristics of Wall Sublayer

Coles (29) analyzed the bulk of available measurements of turbulent boundary layers for low Reynolds number and zero pressure gradients. He determined the surface shear stress from the velocity profile by assuming that the velocity in the inner layer ($y/\delta \lesssim 0.2$) but outside the viscous sublayer ($U_\tau y/\nu \gtrsim 40$) followed the usual logarithmic form

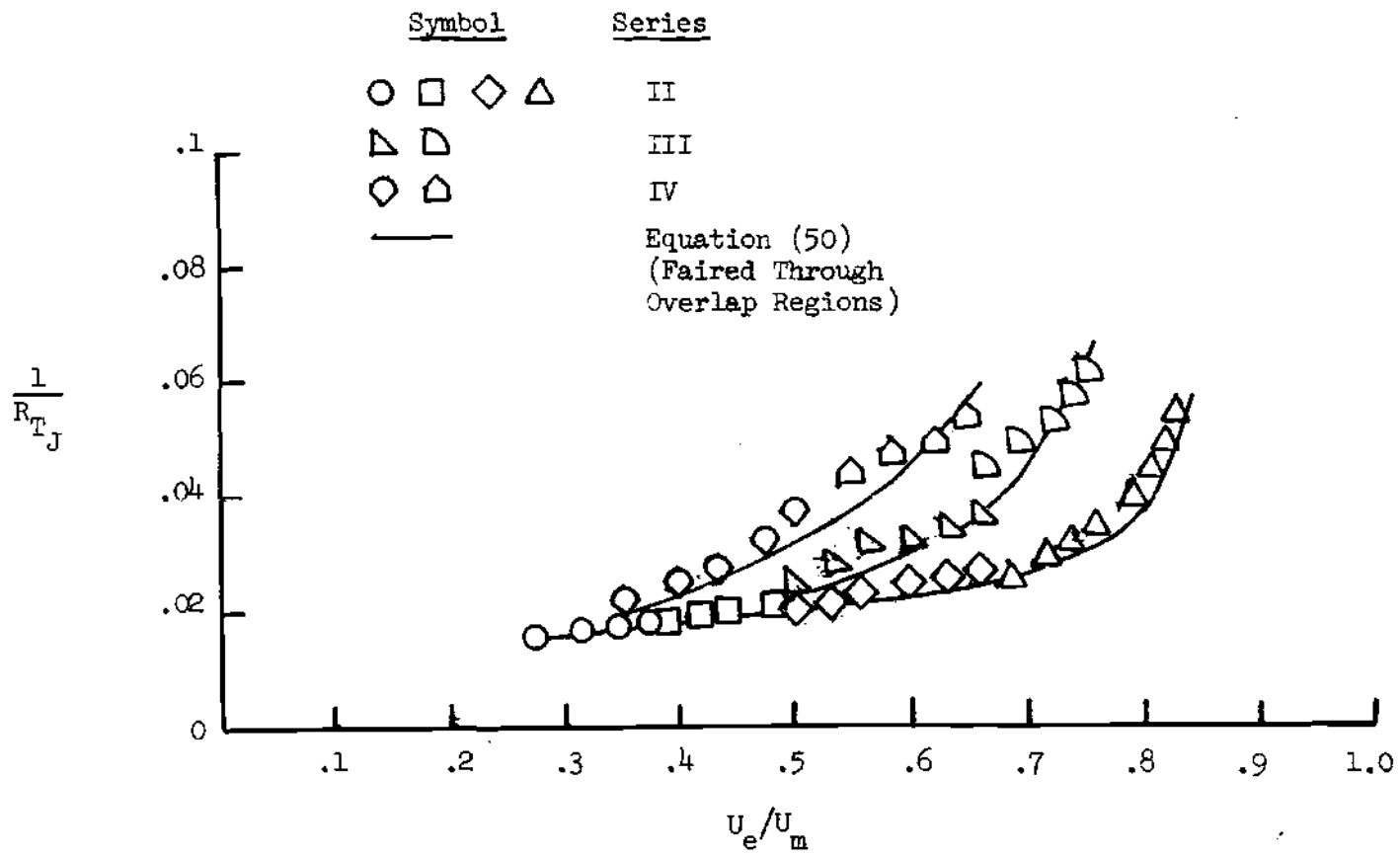

Figure 17. Turbulent Reynolds Number Variation with U_e/U_m - Jet Layer

$$U^+ \equiv \frac{U}{U_\tau} = \frac{1}{K} \log y^+ + c \qquad (51)$$

where $y^+ \equiv U_\tau y/\nu$, $K = 0.41$ and $c = 5.0$. Coles demonstrated that the surface shear stress deduced from Eq. (51) was within about 10 percent of that deduced from the momentum integral equation, at least in the case of the more reliable experiments. The modern derivation of the 'mixing-length' formula, from which Eq. (51) follows by integration when $\tau/\rho = U_\tau^2 = \tau_w/\rho$, uses the assumption that the turbulent structure of the flow near the surface is unaffected by the flow further from the surface. The outer layer and outer boundary conditions affect the inner layer primarily via the shear stress gradient $\partial\tau/\partial y$ in the inner layer, which is non-zero when the velocity and/or pressure are functions of x. In a constant-pressure boundary layer at Reo = 1000, the effect of $\partial\tau/\partial y$ is to reduce the velocity gradient at $y/\delta = 0.1$ by about 3 percent from that in a true constant-stress layer.

Simpson (30) suggested that much larger changes in the logarithmic law occurred at low Reynolds numbers. He showed that his own velocity profiles, and those of Wieghardt, for $1000 < \text{Reo} < 6000$ collapse together, except in the wall sublayer, when plotted as U/U_e versus y/δ. Since $U_\tau/U_e \equiv (\frac{1}{4}c_f)^{\frac{1}{2}} \propto \text{Reo}^{-1/8}$ approximately, it follows that K varies as $\text{Reo}^{-1/8}$, decreasing to 0.33 at Reo = 1000; c also varies. There is therefore a direct contradiction between the analyses of Wieghardt's data by Coles (constant K) and by Simpson (variable K). Recently Cebeci and Mosinskis (31), following Simpson, used values of K and c varying with Reo as part of the input to a method of calculating turbulent

boundary layers and showed improved agreement with experimental data. On the other hand Herring and Mellor (32), using a very similar calculation method, obtained improved agreement by letting the eddy viscosity in the outer layer depend on Reynolds number, leaving K and c unaltered. Huffman and Bradshaw (33) say that the boundary-layer data currently available are not accurate enough to check the validity of the logarithmic law at low Reynolds number. Nevertheless, the question is of some importance, if only because of the implications for the inner-layer analysis in other situations. They analyzed the data for flows in which Reynolds number effects on the inner layer are likely to be stronger than in a boundary layer, and thus easier to detect. The procedure adopted is to adjust K and the 'damping constant' A^+, which determines c, so as to optimize the agreement between the actual velocity profiles in the inner layer and those calculated from the mixing-length formula. The results show that c or its equivalent is Reynolds number dependent and that K appears to be a constant to good accuracy. It appears that even the variation of c is likely to be small in boundary layers unless the influence of the outer layer is extremely large. Cebeci (34) in a later and more detailed study also concluded that the Karman parameter K and the Van Driest parameter A^+ in the inner eddy-viscosity formula are universal constants.

Typical experimental wall-jet data matched to Eq. (51) at log y^+ = 2.0 are shown on the semi-logarithm plot in Figures 18(a) - (d). Deviations from Coles' semi-logarithm plot (of particular importance is the region of log y^+ from about 2 to 2.5) may be seen from these results. Both rapid decreases in the wall shear stresses and pressure gradient

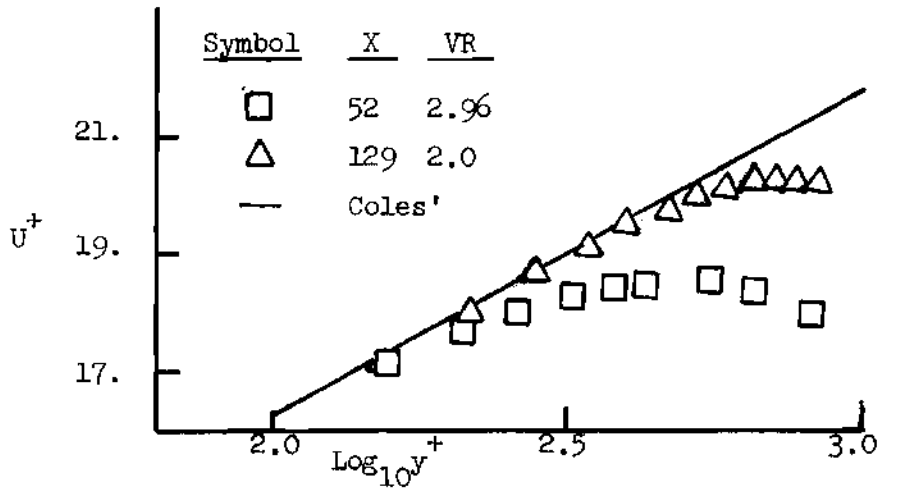

(b) Series II

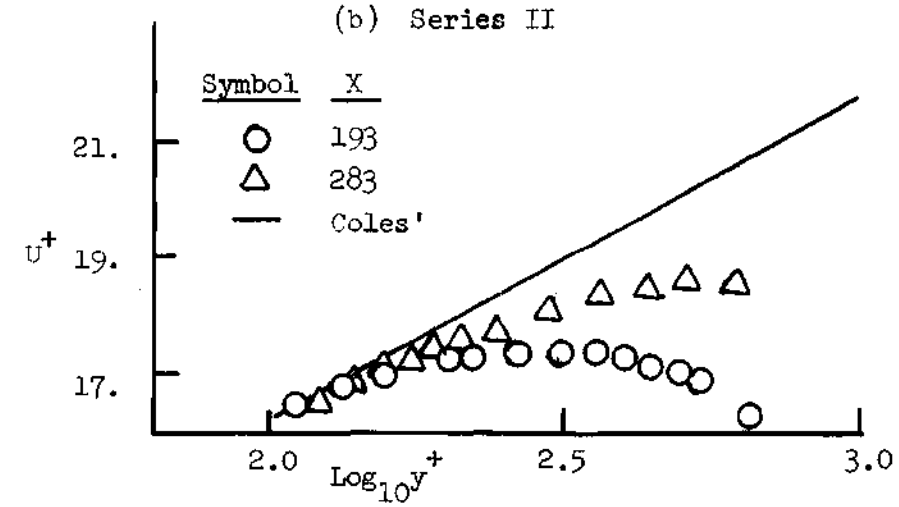

(a) Series I; VR = ∞

Figure 18. Wall Sublayer Velocity Profile

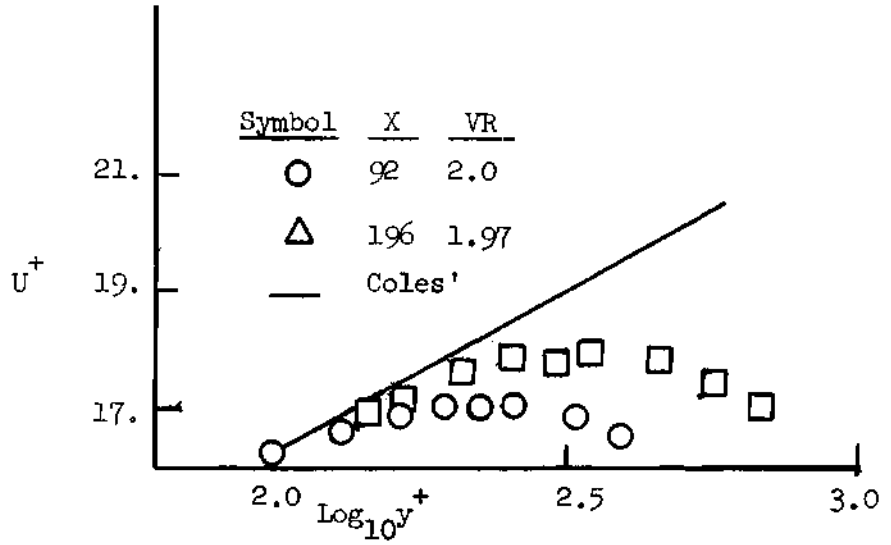

(c) Series IV

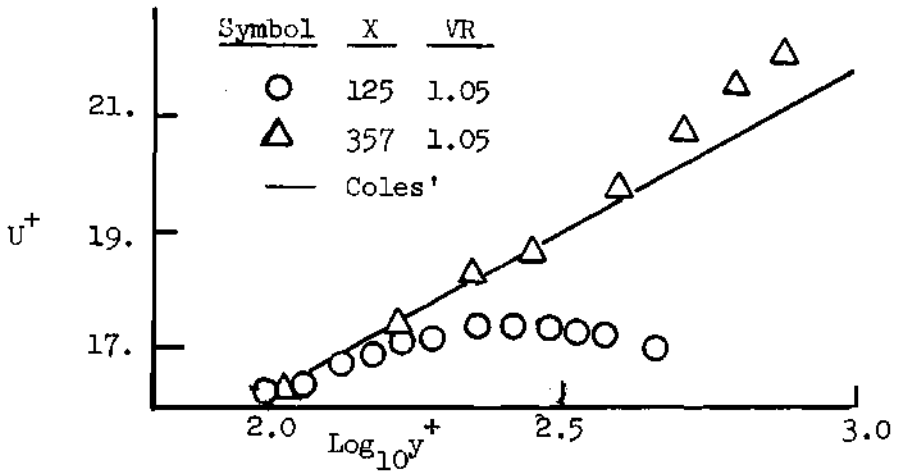

(d) Series IV

Figure 18. (Continued)

account for these deviations. In order to explain such deviations and establish a theoretical basis for the wall sublayer, further investigations are made in the next section using the modified mixing length formula along with the boundary layer equations. The results of this investigation agree quite well with the experimental data.

Development of Theoretical Equation

The assumption that the turbulent flow near a smooth solid surface ($y/\delta \lesssim 0.2$) depends only on U_τ, y ρ, ν, dP/dx and dU_τ/dx leads via similarity arguments and dimensional analysis to

$$U^+ = f_2 (y^+, \pi, \lambda) \tag{52}$$

where

$$\pi \equiv = \frac{\nu}{\rho U_\tau^3} \frac{dP}{dx} , \lambda \equiv \frac{\nu}{U_\tau^2} \frac{dU_\tau}{dx}$$

and f_2 is a universal function of y^+, π, and λ. Equation (52) in conjunction with the momentum and continuity relations

$$\rho U \frac{\partial U}{\partial x} + \rho V \frac{\partial U}{\partial y} = - \frac{dp}{dx} + \frac{\partial \tau}{\partial y} \tag{53}$$

and

$$\frac{\partial}{\partial x} (\rho U) + \frac{\partial}{\partial y} (\rho V) = 0 \tag{54}$$

yield an equation for the total (viscous plus turbulent) shear stress as a function of distance from the surface and a number of parameters. Using

Eqs. (52) and (54) to eliminate U and V in Eq. (53) and then integrating with respect to y gives after some manipulation

$$\tau^+ = 1 + \pi y^+ + \lambda \int_0^{y^+} U^{+2}\, dy^+ \tag{55}$$

where $\tau^+ = \tau/\tau_w$. The total shear stress can also be related to the velocity gradient by

$$\tau = \mu \frac{\partial U}{\partial y} - \rho \overline{u'v} \tag{56}$$

where the first term is the molecular stress and the second term is the Reynolds stress. The Reynolds stress is related to the mean velocity distribution by the mixing-length theory. Thus equation (56) becomes

$$\tau = \mu \frac{\partial U}{\partial y} + \rho \ell^2 \left(\frac{\partial U}{\partial y} \right)^2$$

or

$$\tau^+ = \frac{\partial U^+}{\partial y^+} + \left(\ell + \frac{\partial U^+}{\partial y^2} \right)^2 \tag{57}$$

where $\ell^+ \equiv U_\partial \ell/\nu$ and ℓ is the mixing length. This can be taken as a definition of the 'mixing length' ℓ. The common assumption that ℓ is proportional to y can be justified by local equilibrium arguments within the inner layer but outside the viscous sublayer Eq. (57) has also been used in the viscous sublayer (which is not a local equilibrium region because significant turbulent energy transport normal to the surface occurs) but its status is simply that of a means of correlating data.

Van Driest (1956) showed that, for the simple case τ^+ = constant = τ_w^+, experimental velocity profiles were well fitted throughout the inner layer by the semi-empirical form

$$\ell^+ = Ky^+\{1 - \exp\,[-\tau^{+\frac{1}{2}}\, y^+/A^+]\} \tag{58}$$

which tends to $\ell^+ = Ky^+$ for large y^+.

For the present analysis, Eq. (57) is solved for $\partial U^+/\partial y^+$ to give

$$\frac{\partial U^+}{\partial y^+} = \frac{(1 + 4\ell^{+2}\,\tau^+)^{\frac{1}{2}} - 1}{2\ell^{+2}} \tag{59}$$

Introducing Eqs. (52), (55) and (58) this becomes

$$\frac{du^+}{dy^+} = F(y^+, \int_o^{y^+} f_2^{\,2}\, dy^+, \pi, \lambda, k, A) \tag{60}$$

Equation (60) is an integral-differential equation for u^+. It can be solved numerically to obtain the velocity profile near the wall for given values of π, λ, k, and A. The wall shear stress profile can then be determined from Equation (55).

Considerable controversy, as discussed in the previous section, has existed concerning the effects of Reynolds number on the values of A and K. Authors have generally agreed that A and K are independent of Reynolds number for boundary layers at Reynolds numbers (based on the momentum thickness) in excess of 6000. However, many authors have argued that A and K must be variables for lower Reynolds numbers, as previously

pointed out. Recently Bradshaw (33) and Cebeci (34) have more conclusively established that A and K are independent of Reynolds number even at low Reynolds numbers. Consequently, A = 26 and K = 0.41 (the most commonly accepted values) have been used for the final results of this study. This assumption was also justified in the present study by comparisons with the experimental data. The values of A and K were adjusted in attempting to improve the matching between the experimental data and theory. It was concluded that within the accuracy of the data the matching could not be improved by changing A and K from the values of 26 and 0.41.

Typical theoretical results illustrating the effect of π and λ on the sublayer velocity profile are shown in Figures 19(a) - (b) for $\pi = \lambda = 0$; Coles' linear semilogarithm law of the wall is reproduced with $y^+ \gtrsim 40$. The linear semilogarithm law does not exist if π or λ are significantly different from zero.

Comparisons of Theory with Experimental Data

The boundary layer velocity profile measured in the wall jet facility (12) immediately upstream of the jet nozzle is compared with theoretical results computed from Equation (60) in Figure 20. This comparison of the theory with an ordinary boundary layer is included to illustrate the characteristics and quality of the experimental data for the classical case in which the linear semilogarithm region is expected to exist. As shown in Figure 20, the data is in excellent agreement with the linear portion of the theoretical curve for log y^+ between about 2 and 2.5. Above this range $y/\delta \lesssim 0.2$ and the data rises systematically

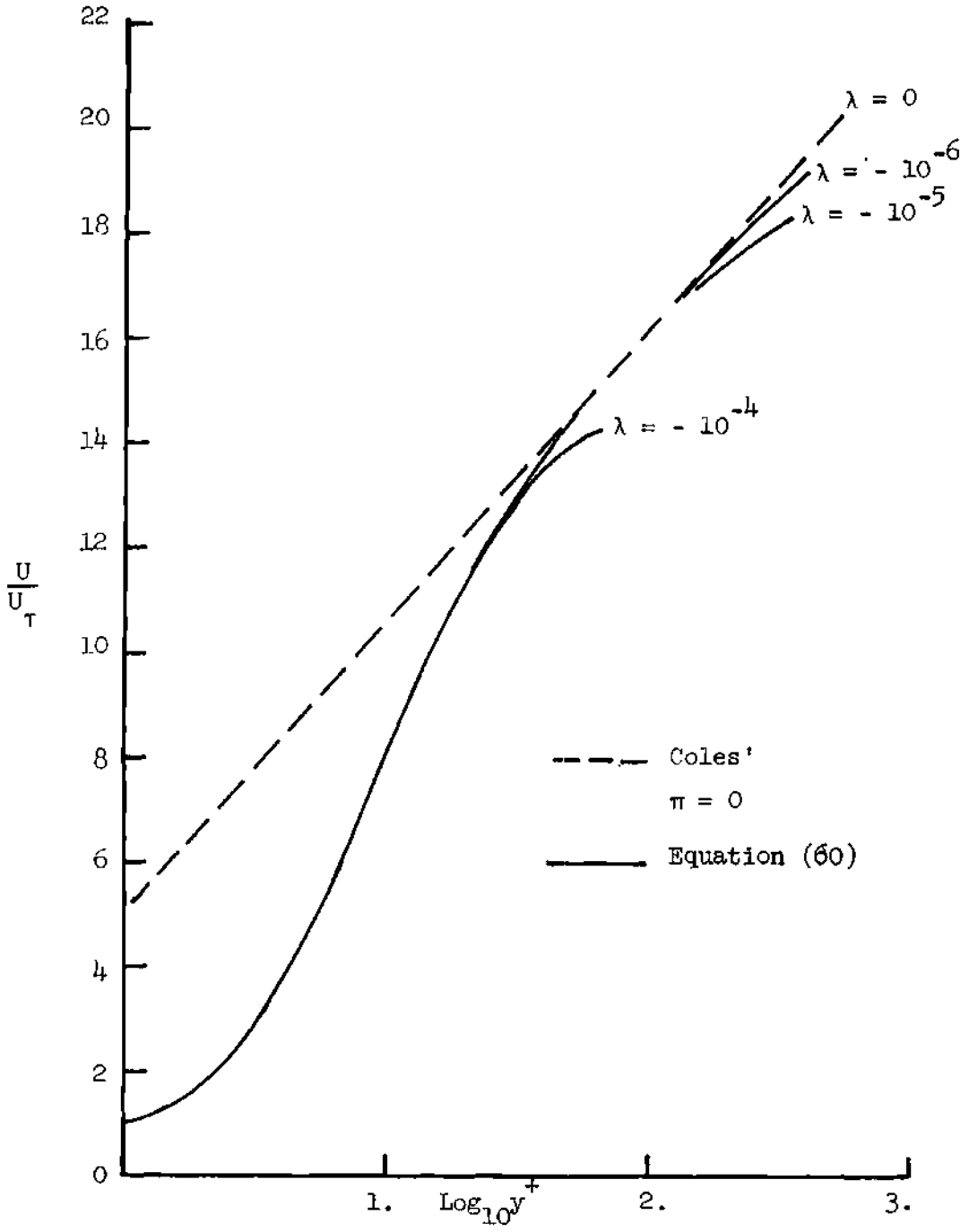

(a) Effect of λ; A = 26; K = .41

Figure 19. Wall Sublayer Velocity Profile

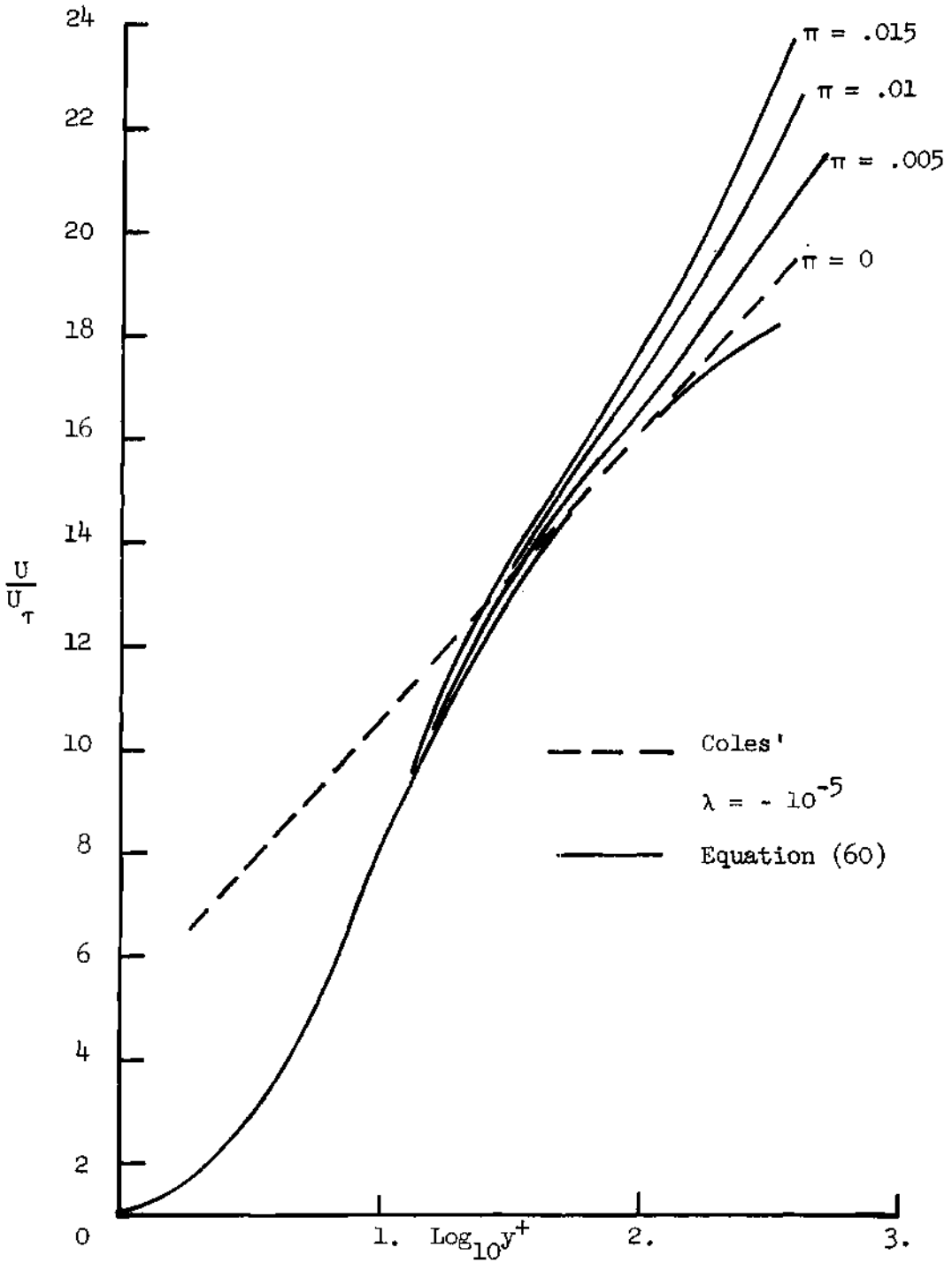

(b) Effect of π; A = 26; K = .41

Figure 19. (Continued)

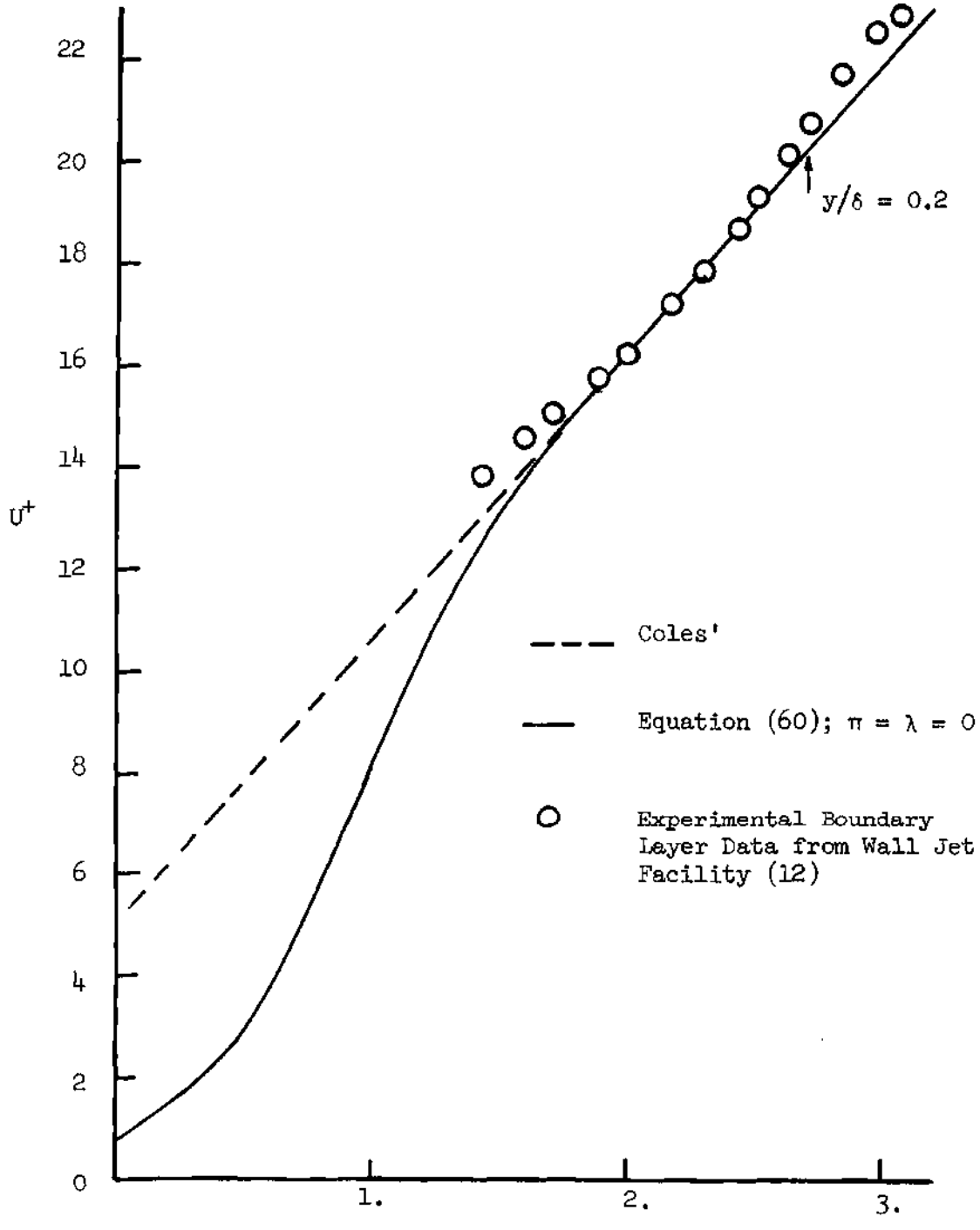

Figure 20. Wall Sublayer Velocity Profile

above the linear "law of the wall". This, of course, corresponds to the boundary layer "wake region". Below this range the data also is above the predictions of Eq. (60) and, in fact, above the linear semilogarithm plot. Unfortunately, attempts to explain these differences by making turbulence and probe displacement corrections have not been successful (although these corrections do reduce the differences). In fact, Reference 12 points out that three different probes yielded the same results. It is clear from the results presented in Reference 12 as well as those presented later that this is a characteristic of all the wall jet data of Reference 12. As shown in Figure 21, it also exists in the classical data of Wieghardt (35). Much, but not all of the boundary layer data in Reference 35 demonstrates the same characteristic. Never-the-less the theory (Eq. (60)) seems to be accepted and reasonably well established for these classical flows. In all the subsequent comparisons, therefore, the author has emphasized comparisons between the theory and the experiments only in the regions for which $\log y^+ \geq 2.0$ and has expected that the data for $\log y^+ < 2.0$ would consistently lie above the theory.

The theoretical and experimental results for Series I are compared in Figures 22(a) - (c). Series I tests are for the pure wall jet with no free stream flow. Note that these results have not been included previously. They are included in this case because the rapid decay for the pure wall jet has the strongest effect on the wall sublayer and, therefore, provides a critical evaluation of the theory. These comparisons show that the experimental and theoretical results are in excellent agreement even near the region of the maximum velocity. Applicability of the

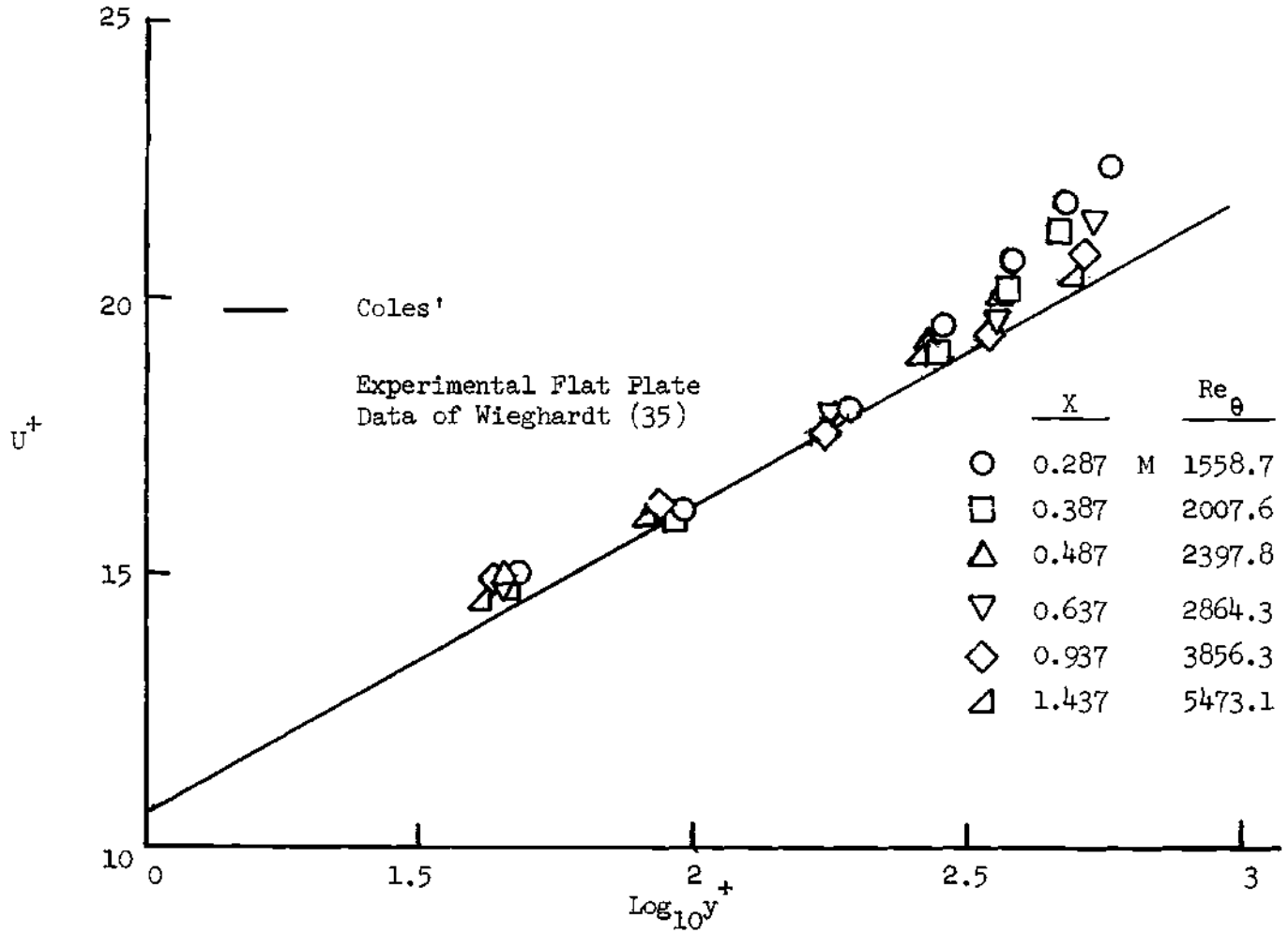

Figure 21. Wall Sublayer Velocity Profile

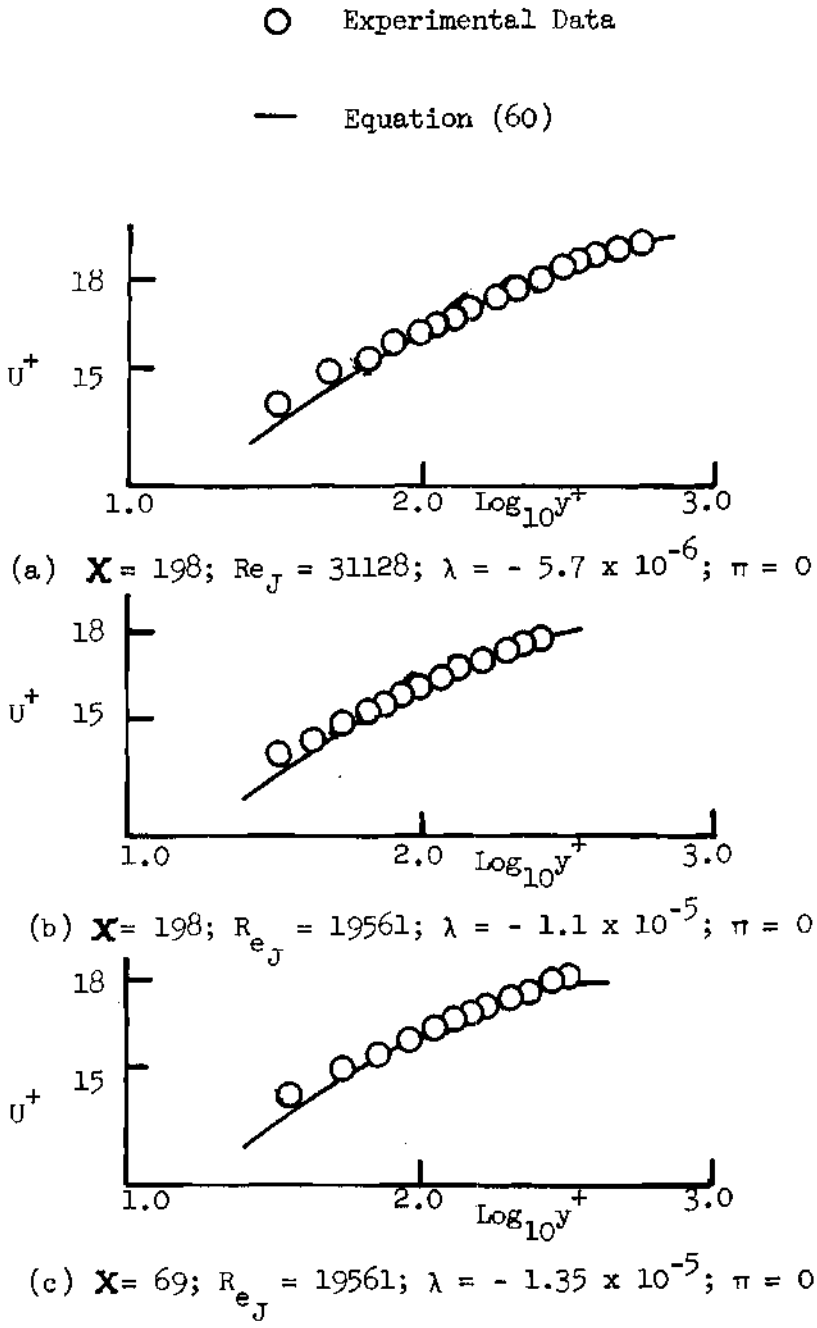

(a) $X = 198$; $Re_J = 31128$; $\lambda = -5.7 \times 10^{-6}$; $\pi = 0$

(b) $X = 198$; $R_{e_J} = 19561$; $\lambda = -1.1 \times 10^{-5}$; $\pi = 0$

(c) $X = 69$; $R_{e_J} = 19561$; $\lambda = -1.35 \times 10^{-5}$; $\pi = 0$

Figure 22. Wall Sublayer Velocity Profile
Series I, VR = ∞

theory over such a large portion of the wall layer is surprising.

The theoretical and experimental results for Series II, III, and IV are compared in Figures 23, 24, and 25. For the higher velocity ratios (Figures 23(a) and 25(a)) the data again compares well with the theory over a surprisingly large portion of the wall layer. On the other hand, for the lower velocity ratios, the data rises above the theory in the outer portion of the wall layer for which $y/\delta m$ is greater than about 0.3 to 0.4 just as in the case of an ordinary boundary layer. In these cases the wall layer is approaching that for a boundary layer. The sublayer extends over a large portion of the wall layer in these cases since δm is reduced relative to δ for a boundary layer due to the retarding effect of the jet layer on the flow near the peak velocity. Over the range of $\log y^+$ between 2 and about 2.4 the agreement between the theory and experiment is good in all cases.

The results show the assigned values of $A = 26$ and $K = .41$ are reasonable and give results which agree with the experimental data. Coles' law of the wall deviates from the experimental data if τ/τ_w varies substantially from 1.0 over the region in which the data and theory compare well.

The distribution of τ/τ_w as computed for three of the relatively extreme cases considered in the previous figures where the theory and data agree is shown in Figure 26. τ/τ_w clearly differs substantially from unity in the region where the theory is apparently applicable.

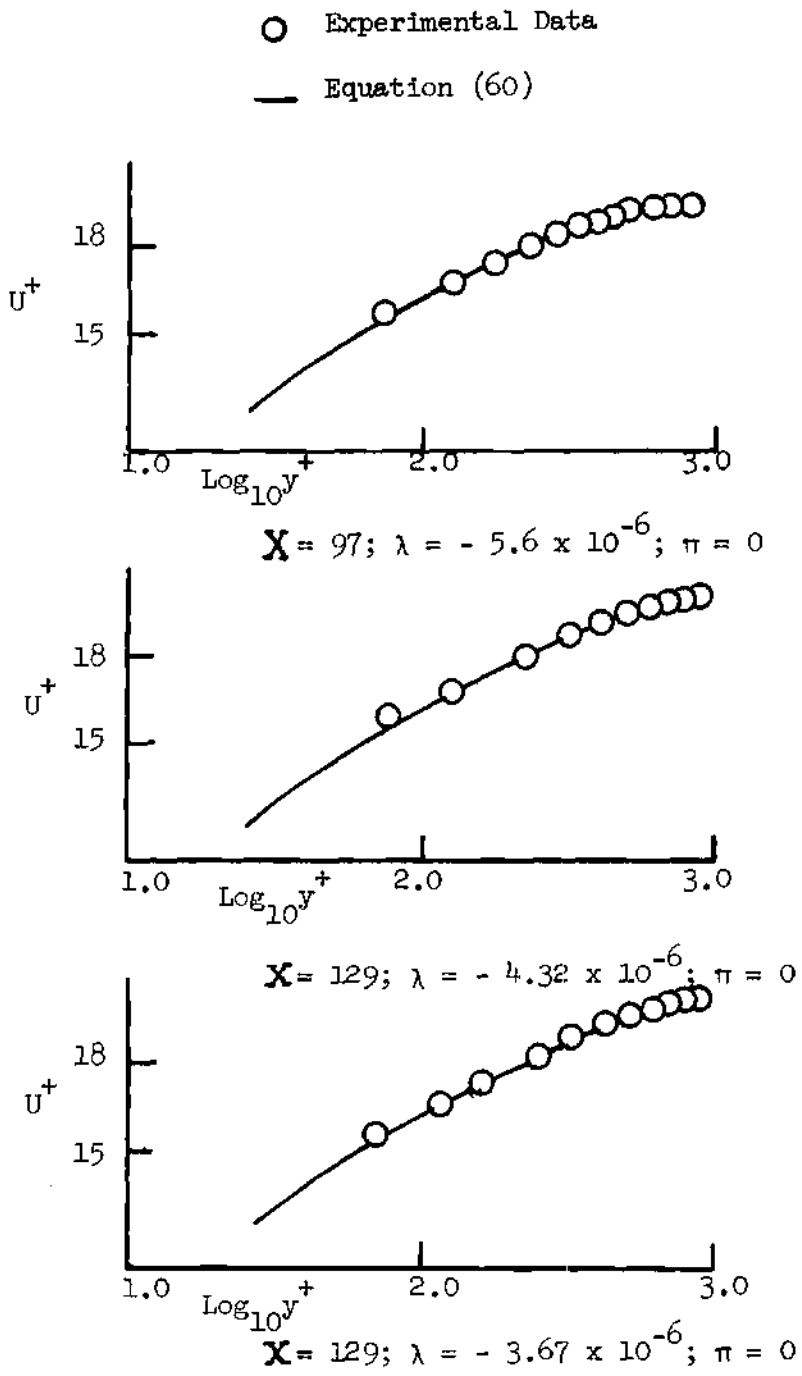

(a) Series II; VR = 4.0

Figure 23. Wall Sublayer Velocity Profile

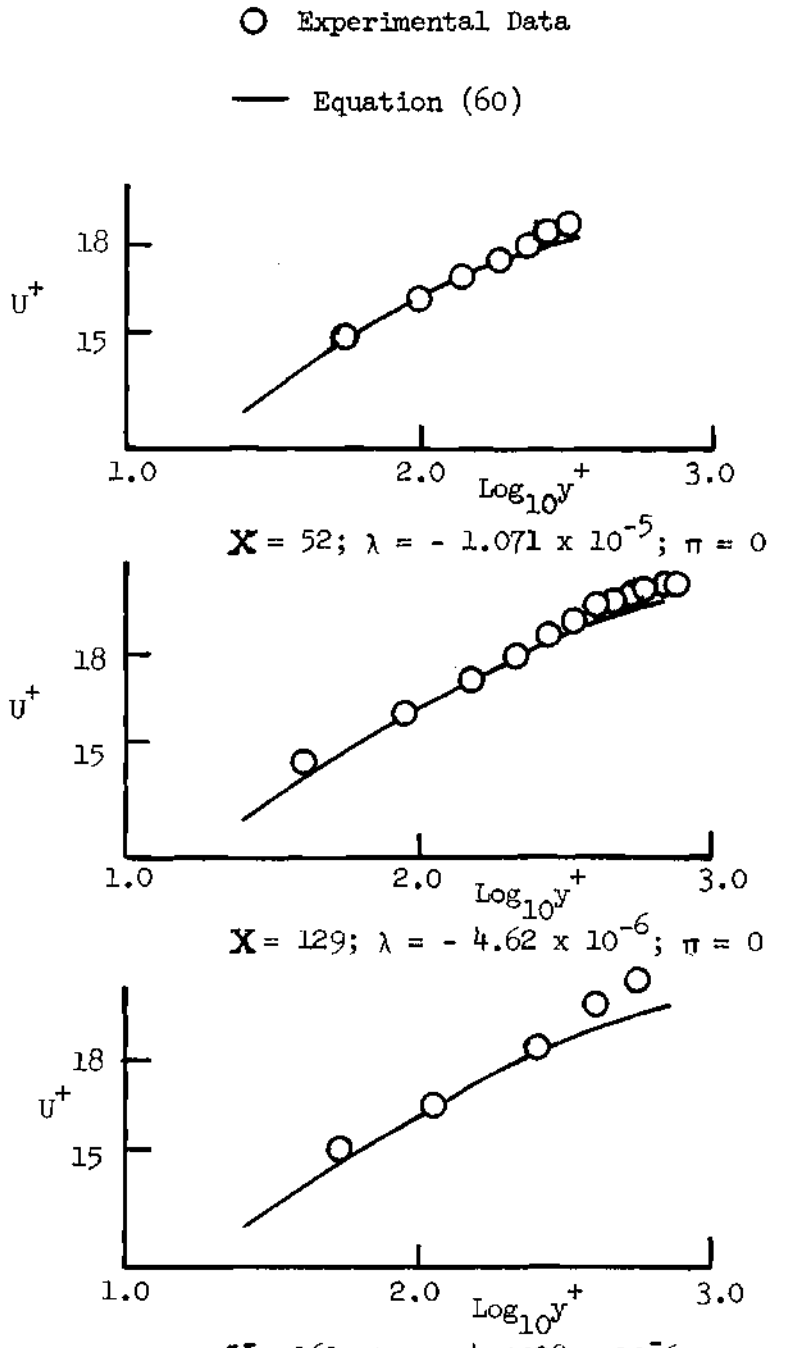

(b) Series II; VR = 2.0

Figure 23. (Continued)

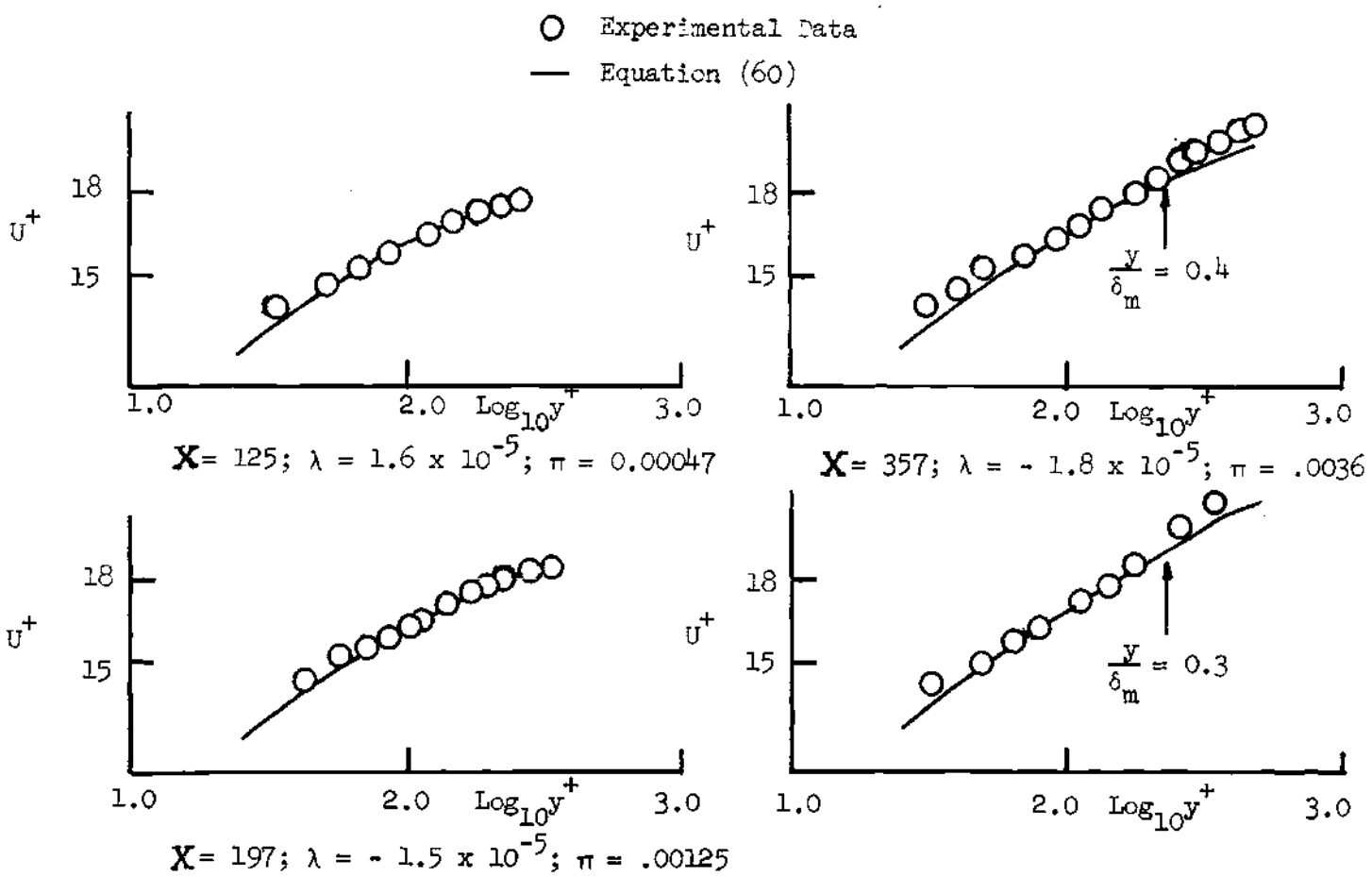

Figure 24. Wall Sublayer Velocity Profile
Series III; VR = 2.07

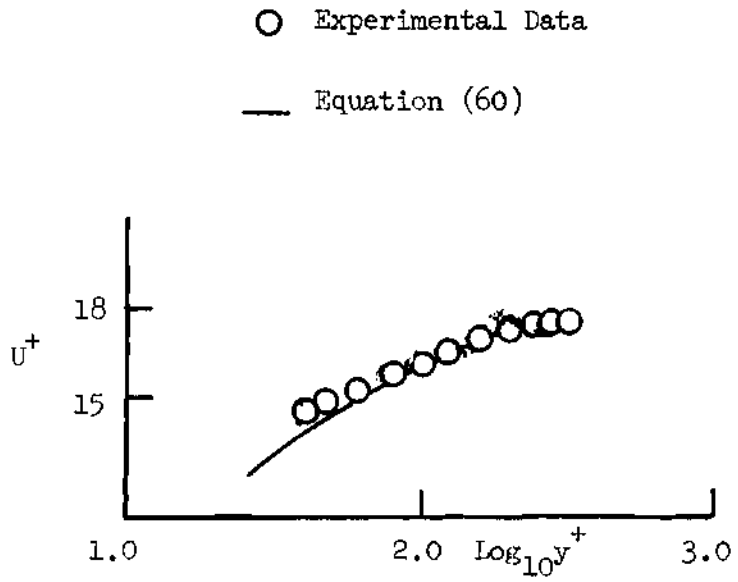

$\chi = 125$; $\lambda = -1.99 \times 10^{-5}$; $\pi = 7 \times 10^{-4}$

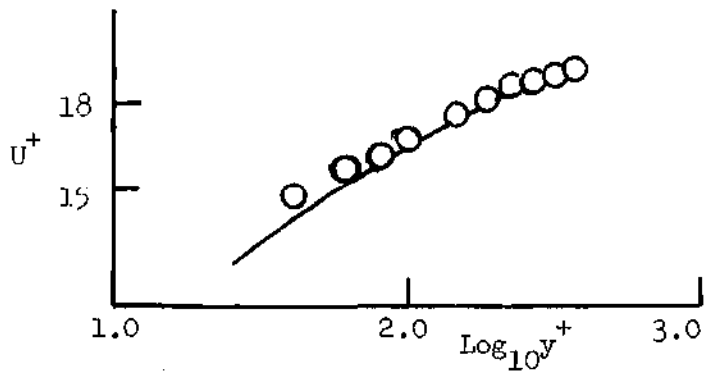

$\chi = 357$; $\lambda = -2.189$; $\pi = 3.97 \times 10^{-3}$

(a) Series IV; VR = 2.99

Figure 25. Wall Sublayer Velocity Profile

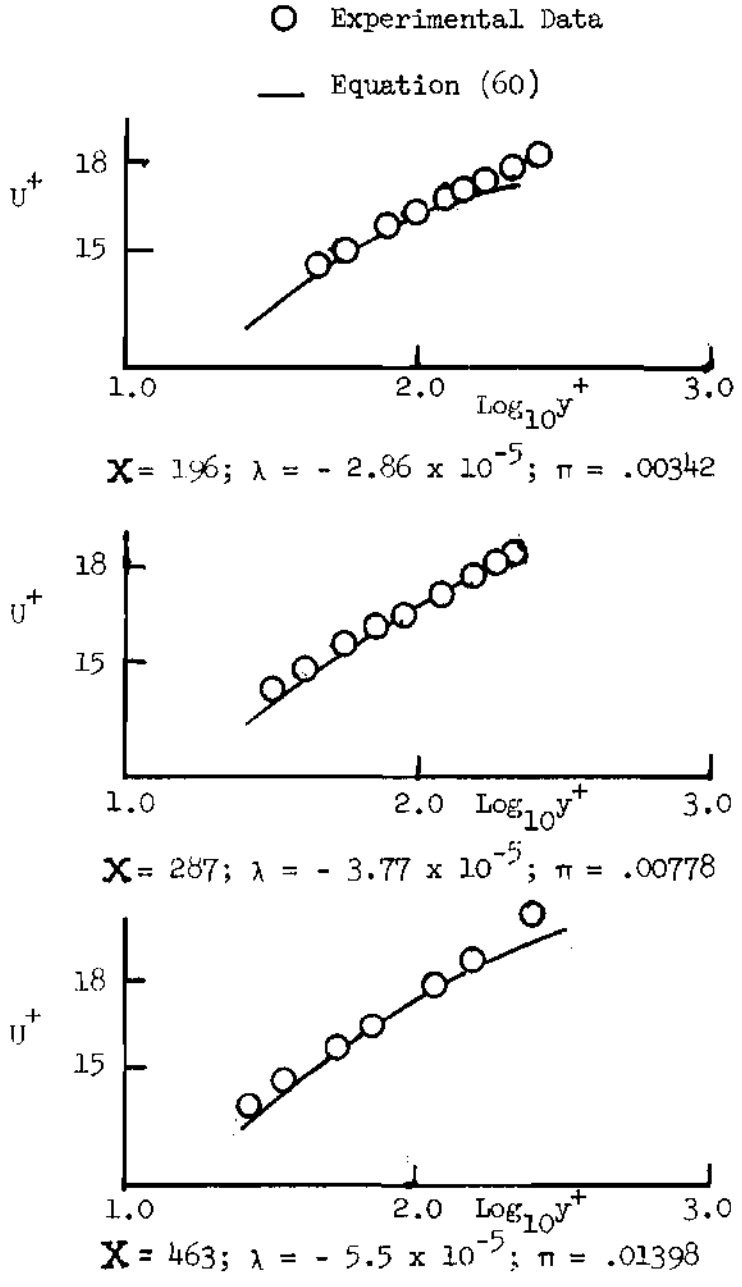

(b) Series IV; VR = 1.97

Figure 25. (Continued)

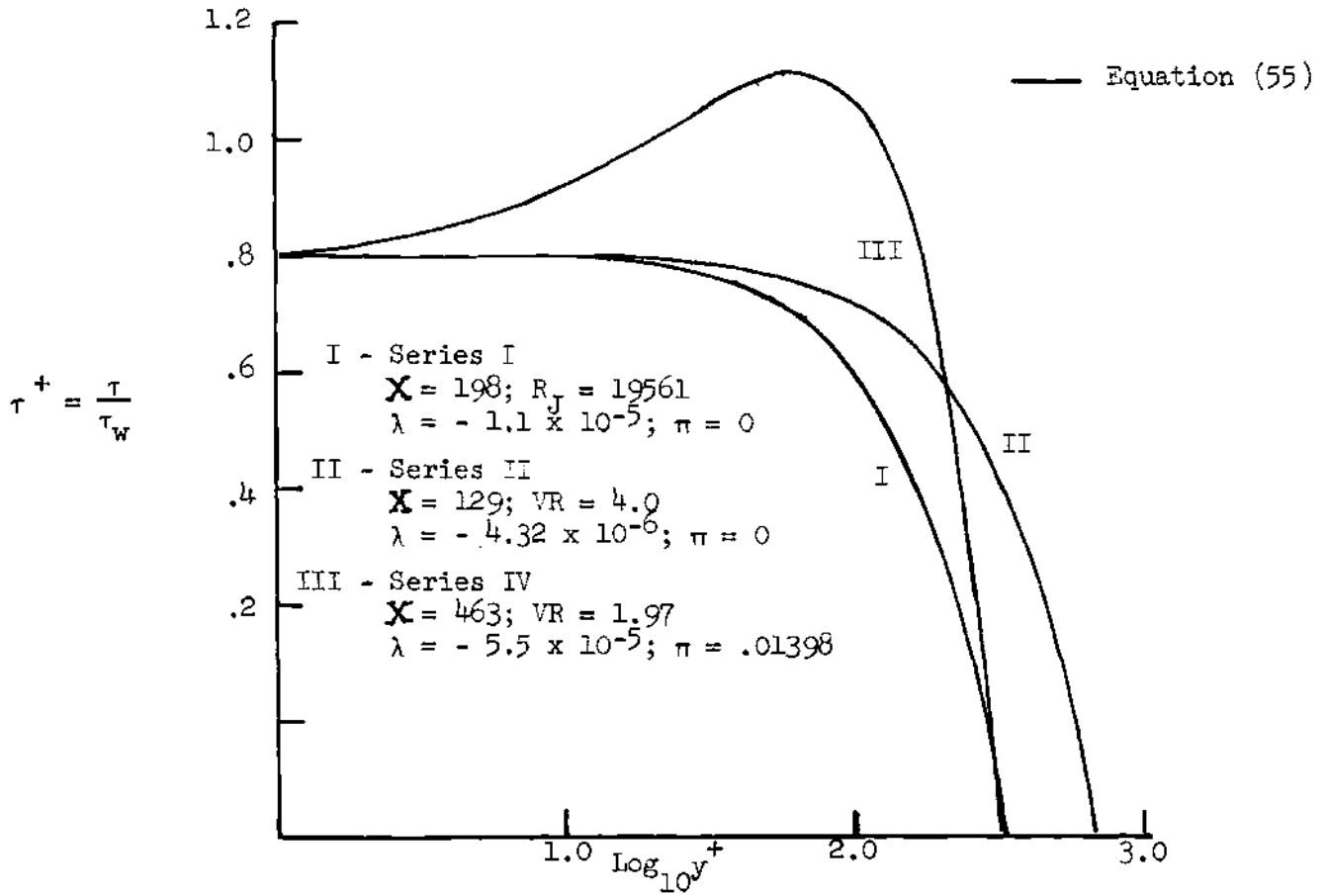

Figure 26. Wall Sublayer Shear Stress Profiles

CHAPTER IV

ANALYTICAL SOLUTION

A method for analyzing turbulent wall jets is developed and then tested against experimental results in this chapter. The technique is based upon the results and conclusions established from the analyses of the experimental data. In general, a wall-jet flow must asymptotically degenerate into an ordinary boundary-layer flow far downstream. Therefore, the solution has been designed so that it is applicable for and, in fact, can degenerate into a boundary layer solution. It is emphasized, however, that the present study is primarily concerned with establishing the feasibility of the solution technique. Little effort is devoted to refining the technique or establishing an efficient numerical scheme.

Basic Technique and Assumptions

The wall-jet shear flow is considered to be subdivided into an "inner shear layer", a "submerged shear layer", and an "outer shear layer" as shown in Figure 10. The inner shear layer is further subdivided into the "wall sublayer" as considered in Chapter III and an "inner shear layer similarity zone".

The velocity profile in the "wall sublayer" is given by Equation (60) and depends upon the wall shear stress, the wall shear stresses gradient and the pressure gradient as expressed by U_τ, λ, and π.

The shear stress distribution is specified for the "inner shear

layer similarity zone". For the wall-jet flows this could be given by the similarity function g, as tabulated in Table 3. As an alternative which provides the flexibility for adapting the procedure to a boundary-layer flow, it is assumed that the similarity function can be represented by a cubic, that is

$$g\left(\frac{y}{\delta}\right) = \frac{\tau - \tau_w}{\tau_m - \tau_w} = (1 + a + 2b) - (2a + 3b)\frac{y}{\delta} + a\left(\frac{y}{\delta}\right)^2 + b\left(\frac{y}{\delta}\right)^3 \tag{61}$$

which satisfies the conditions

$$g(1) = 1, \text{ and } g'(1) = 0 \tag{62}$$

The constants a and b are determined so that the shear stress and the shear stress gradient are continuous at the interface between the "wall sublayer" and this "inner shear layer similarity zone". They are to be evaluated from the wall sublayer equation for τ/τ_w (i.e., Eq. (55)) applied at the match point or interface. Letting

$$\beta = y/\delta \text{ at the match point,}$$

$$\tau_\beta^* = \tau/\tau_w \text{ at the match point,} \tag{63}$$

and

$$\tau_\beta^{*\prime} = (\tau/\tau_w)' \text{ at the match point}$$

Equation (61) then becomes

$$g\left(\frac{y}{\delta}\right) = 1 - \tau_\beta^* \frac{(1-3\beta)}{(1-\beta)^3} + \tau_\beta^* \frac{\beta}{(1-\beta)^2} - \left[6\tau_\beta^* \frac{\beta}{(1-\beta)^3} - \tau_\beta^{*\prime} \frac{(1+2\beta)}{(1-\beta)^2}\right]\frac{y}{\delta} + \left[3\tau_\beta^* \frac{(1+\beta)}{(1-\beta)^3} + \tau_\beta^{*\prime} \frac{(2+\beta)}{(1-\beta)^2}\right]\left(\frac{y}{\delta}\right)^2 - \left[2\tau_\beta^* \frac{1}{(1-\beta)^3} + \tau_\beta^{*\prime} \frac{1}{(1-\beta)^2}\right]\left(\frac{y}{\delta}\right)^3 \qquad (64)$$

Results computed from Equation (64) are compared with both wall jet and boundary layer data in Figures 27(a) - (b). The values of g for the wall jet are from typical data presented earlier. Those for Wieghardt's data were also obtained by integrating the momentum and continutiy equations using the experimental mean flow data. Those for Bradshaw's data are experimental values (36). The values obtained from Equ. (64) are for matching at $\beta = 0.2\ \delta_m/\delta$ (the approximate outer limit of the boundary layer wall layer for which $\delta_m = \delta$) and with τ_β^* and $\tau_\beta^{*\prime}$ determined directly from the data. The agreement between the cubic profile and the experimental distribution is reasonable good. In ann cases the cubic profile underestimates the stress in the outer portion of this shear layer. Undoubtedly, an improved analytical expression (or a numerical tabulation) could be obtained (this should involve a much more comprehensive study of boundary layer data). However, for the purposes of the present exploratory study the agreement is considered satisfactory. For all the subsequent results the match point is also taken to be at $\beta = 0.2\ \delta_m/\delta$.

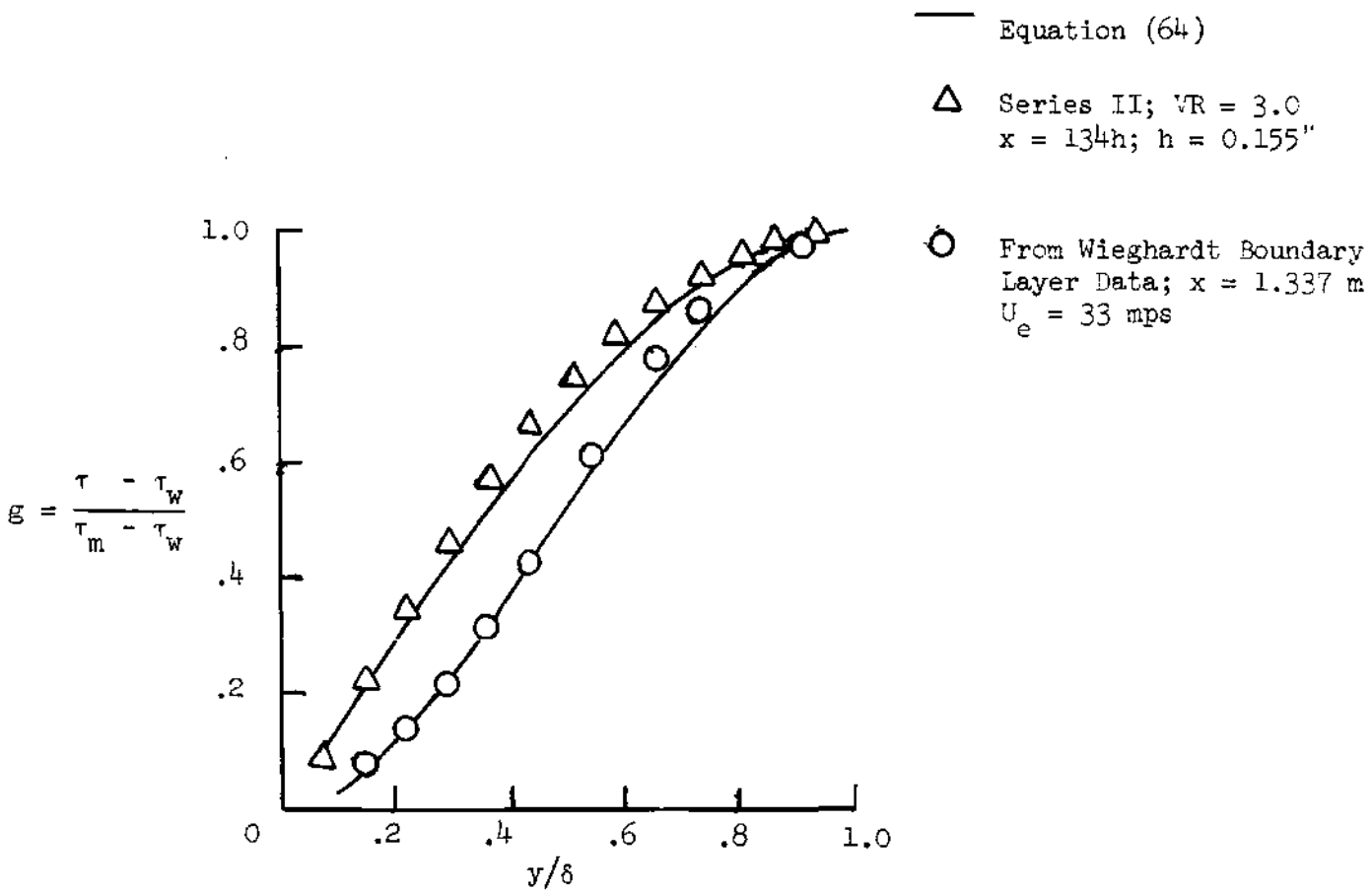

(a) Constant Pressure Flows

Figure 27. Comparison of Shear Stress Cubic Profile with Experimental Data

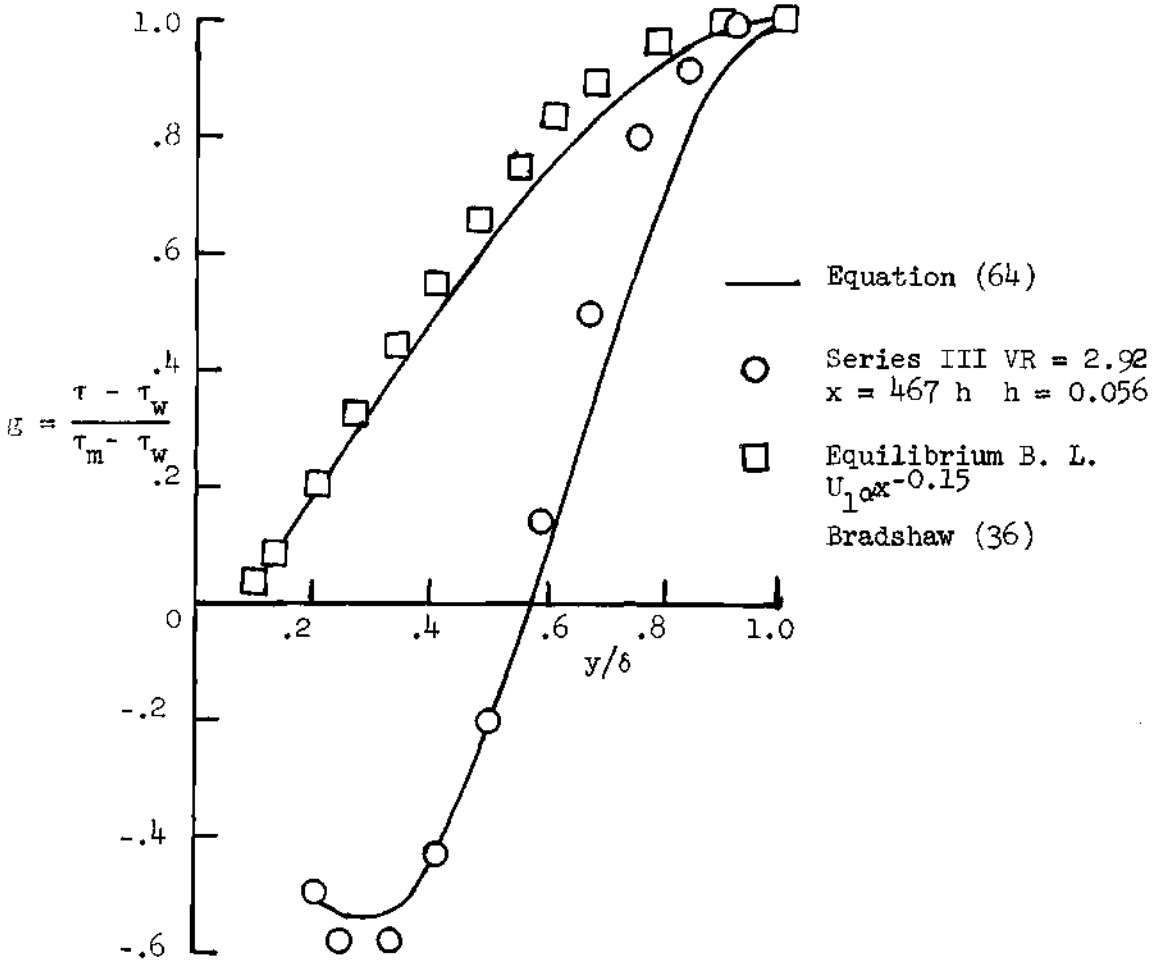

(b) Flows with Adverse Pressure Gradients

Figure 27. (Continued)

The shear stress distributions are also specified for the "submerged shear layer" and the "outer shear layer". These are given by the similarity functions g_2 (for the submerged shear layer) and g_3 (for the outer shear layer) as tabulated in Table 3. These shear stress distributions are matched (in value and slope) at the interface between the two layers.

The normalized shear stress functions g, g_2, and g_3 involve the shear stresses τ_w, τ_m and τ_2. τ_w is determined by evaluating U_τ (as related to the wall layer velocity profile by Eq. (60)) simultaneously with the entire velocity profile as discussed subsequently τ_m and τ_2 are related to the mean flow via the eddy viscosities (Eq. (30) and (31). The eddy viscosities are in turn related to the mean flow properties via the turbulent Reynolds numbers R_{T_J} and R_{T_w}. R_{T_J} is evaluated from the mean flow properties using Eq. (50). No explicit relationship was developed for R_{T_w}, however. Therefore, values of R_{T_w} have been determined directly from Figures 16 (a) and (b).

Numerical Solution

Numerical Notation and Specified Conditions

The finite difference notation used in the numerical analysis from the axial station i to i + 1 is shown in the sketch on the next page. The outer edge of the wall sublayer is at j = 0. The outer edge of the entire shear layer ($y = \delta sL$) where $U = U_e$ is at j = N.

The following boundary and flow conditions are specified:

1. $y/\delta = \beta = 0.2\ y/\delta_m$ at j = 0, i + 1
2. All conditions at i (i.e., U_i, U_{τ_i}, λ_i, and π_i)

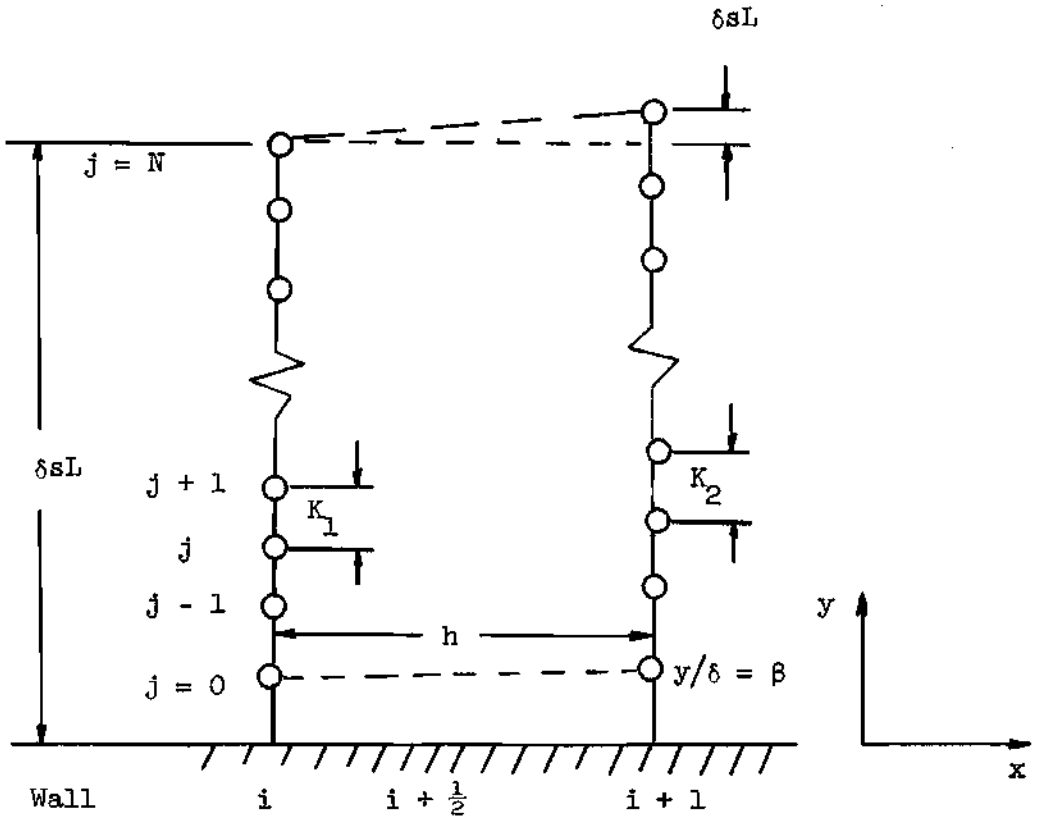

3. $U = V = 0$ at $y = 0$

4. $\tau = f(y_{i,j})$ for $j = 0 \ldots N$ ($f = g$ for inner shear layer (Eq. (64)), $f = g_2$ for submerged shear layer (Table 3), and $f = g_3$ for outer shear layer (Table 3)).

5. $\lambda_{i+1} = \lambda_{i+\frac{1}{2}}$ (i.e., λ lags behind by $\frac{1}{2}$ the station increment. This eliminates a double interation)

Solution for Wall Sublayer

The velocity profile and the shear stress in the wall sublayer are computed by numerically solving Eqs. (55) and (60) using linear steps. Since $U_{\tau_{i+1}}$ and λ_{i+1} at station $i + 1$ are initially unknown, they are first estimated. These first estimates are then used to determine the first approximation for $U_{\tau_{i+1}}$ (and hence $\lambda_{i+\frac{1}{2}}$) simultaneously

with $U_{i+1,j}$ in the entire outer layer. The detailed procedure for obtaining the first approximation is as follows:

1. Assume that $\lambda_{i+1} = \lambda_i$

2. Estimate $U_{\tau_{i+1}}$ using

$$U_{\tau_{i+1}} = U_{\tau_i} + \left[\frac{U_{\tau_i}^2}{\nu} \lambda_i \right] h \tag{65}$$

3. Assume that $\delta_{m_{i+1}} = \delta_{m_i}$

4. Estimate $y_{i+1,o}$ using

$$y_{i+1,o} = \frac{\beta \delta_{m_{i+1}} U_{\tau_{i+1}}}{\nu} \tag{66}$$

5. Compute $y_{i,o}$ for $y_{i,o} = y_{i+1,o}$ using

$$y^+_{i,o} = y^+_{i+1,o} \frac{U_{\tau_i}}{U_{\tau_{i+1}}} \tag{67}$$

6. Compute $y_{i,o} = y_{i+1,o}$ using

$$y_{i,o} = y_{i+1,o} = y^+_{i,o} \nu / U_{\tau_i} \tag{68}$$

7. Compute $V_{i+\frac{1}{2},o}$ using

$$V_{i+\frac{1}{2},o} = \frac{\int_o^{y_{i,o}} U^+_i \, dy - \int_o^{y_{i+1,o}} U_{i+1} \, dy}{h}$$

$$= \frac{\nu}{h}\left[\int_{o}^{y_{i,o}} U^{+}_{i}\, dy^{+} - \int_{o}^{y_{i+1,o}} U^{+}_{i+1} dy^{+}\right] \tag{69}$$

where integrals are evaluated numerically using Equation (60) for U^{+}.

8. Using Eq. (60) numerically compute

$$U_{i+1,o}/U_{\tau_{i+1}} = f_2(y^{+}_{i+1,o}) \tag{70}$$

$U_{i+1,o}$ and $U_{\tau_{i+1}}$ in Eq. (70) are considered as unknowns. They can finally be evaluated using a solution for $U_{i+1,j}$ in the entire outer layer.

Solution for Outer Layer

The boundary conditions applied at $j = 0$ are U_{i+1} and $V_{i+\frac{1}{2}}$ as given by Eq. (69) and (70). The detail procedure is as follows:

1. Assume $\tau_{i+\frac{1}{2},j} = \tau_{i,j}$ where the values of $\tau_{i,j}$ are given by the functions g, g_2 and g_3.

2. Solve the boundary layer equations (Eqs. (10) and (11)) using the finite difference form

$$\rho \frac{(U_{i+1,j} + U_{i,j})}{z}(U_{i+1,j} - U_{i,j})/h$$

$$- \rho\left[\int_{o}^{j} \frac{\partial U}{\partial x}\, dy + V_{i+\frac{1}{2},o}\right]\Big(U_{i,j+1} - U_{i,j-1}$$

$$+ U_{i+1,j+1} - U_{i+1,j-1}\Big)/4k = -\frac{dP}{dx} + \frac{\partial \tau}{\partial y} \tag{71}$$

Equation (70) and (71) are N + 1 equations for N + 1 unknowns $U_{i+1,o}$, . . . $U_{i+1,N-1}$ and $U_{\tau_{i+1}}$. These equations are solved simultaneously by matrix inversion.

With a first approximation for $U_{\tau_{i+1}}$, the entire procedure is repeated again starting with the wall sublayer but using the new value of $U_{\tau_{i+1}}$ and using $\lambda_{i+1} = \lambda_{i+\frac{1}{2}}$ where

$$\lambda_{i+\frac{1}{2}} = \frac{\nu}{\left(\frac{U_{\tau_{i+1}} + U_{\tau_i}}{2}\right)^2} \frac{(U_{\tau_{i+1}} - U_{\tau_i})}{h} \tag{72}$$

Iteration is then continued until the solution converges.

The boundary layer thickness is finally calculated by integrating the boundary layer equations to give

$$\Delta\delta = \frac{\frac{\tau_w}{\rho} - u\int_o^{\delta_i} \frac{\partial u}{\partial x}\,dy + \int_o^{\delta_i} \frac{\partial u^2}{\partial x}\,dy + \frac{1}{\rho}\frac{dP}{dx}\delta_i}{\left(u\frac{\Delta u}{\Delta x}\right)_{y=\delta_i+\frac{1}{2}\Delta\delta} - \left(\frac{\Delta u^2}{\Delta x}\right)_{y=\delta_i+\frac{\Delta\delta}{2}} - \frac{1}{\rho}\frac{dP}{dx}} \tag{73}$$

where $\Delta\delta = \delta_{i+1} - \delta_i$. An initial guess for $\Delta\delta$ is necessary. Starting with the initial guess the calculations are iterated until the solution converges. δ_{i+1} is then computed using $\delta_{i+1} = \delta_i + \Delta\delta$.

Numerical Results

The analysis was first tested for typical boundary-layer flows. This test was considered to be essential since in most cases a wall-jet flow asymptatically approaches a boundary-layer flow. It is important, therefore, that a wall-jet analysis behave properly in this asymptatic limit. The analysis was then tested for typical wall-jet

flows.

Results computed for Wieghardt's flat plate flow (35) are compared with the experimental data in Figures 28 (a) - (c). The numerical calculations were started at x = 1.087 m using the experimental data for the initial velocity profile. However, the initial value of U_τ was computed by fitting the experimental velocities near the wall to the wall sublayer equation.

Results computed for Ludwieg and Tillmann's flow (35) with mild adverse pressure gradients are compared with the experimental data in Figures 29 (a) - (b). The numerical calculations are started at x = 1.282 m using the experimental data and again evaluating U_τ at this point so that the data were consistent with the wall sublayer equation.

Results computed for two cases of wall-jet flows are compared with the experimental results in Figures 30 (a) - (d), and 31 (a) - (c). The calculations for Figures 30 (a) - (d) (Series II) were started at X = 52 while those of Figures 31 (a) - (c) (Series III) were started at X = 197. Again, in both cases the initial velocity profiles were specified by the experimental data and U_τ was selected to be consistent with the wall sublayer equation.

As shown by the comparisons in Figures 28, 29, 30 and 31, the present method is reasonably successful in predicting the flow field produced by either a wall jet or a boundary layer. It is concluded that the similarity approach is quite plausible and encouraging. The differences between the analytically and experimental results are primarily attributed to the choice of the matching point at the interface

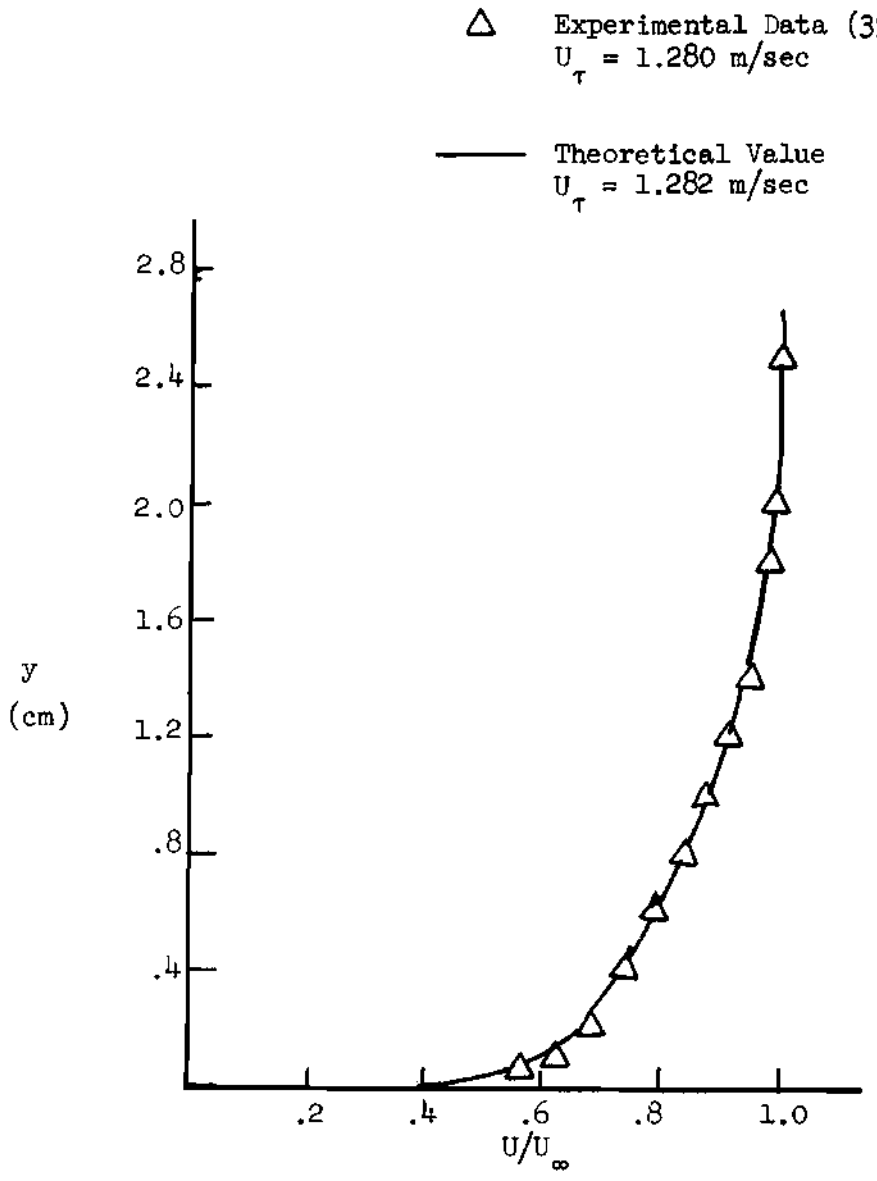

(a) x = 1.237 m

Figure 28. Boundary Layer Velocity Profile for Wieghardt Flat Plate Flow; U_∞ = 33 m/sec

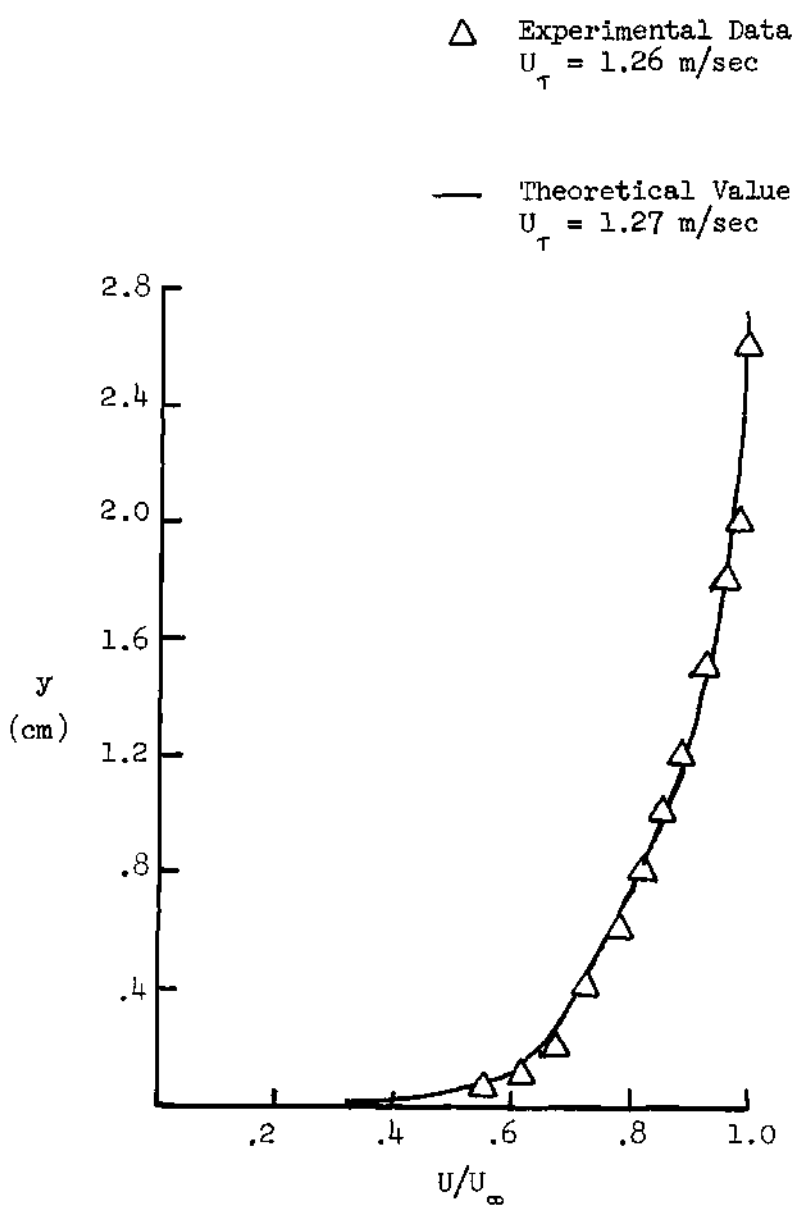

(b) x = 1.437 m

Figure 28. (Continued)

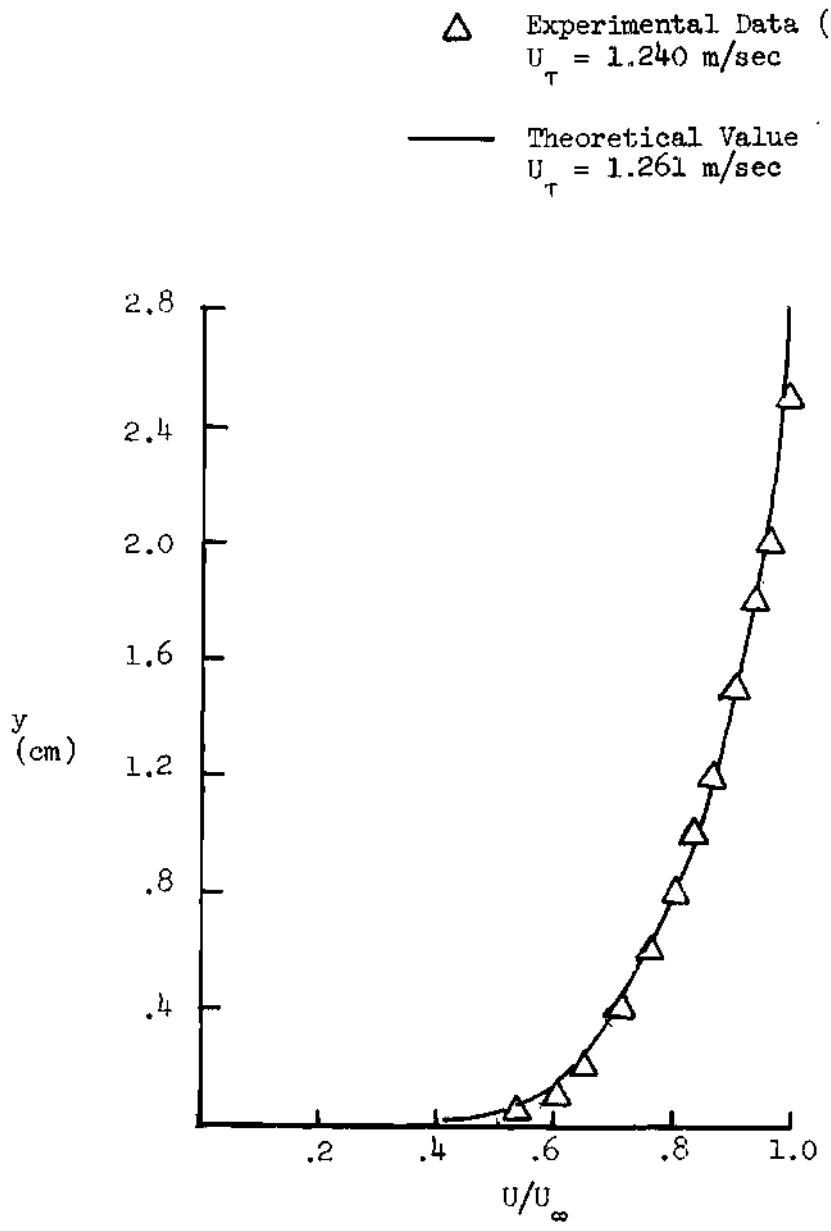

(c) x = 1.687 m

Figure 28. (Continued)

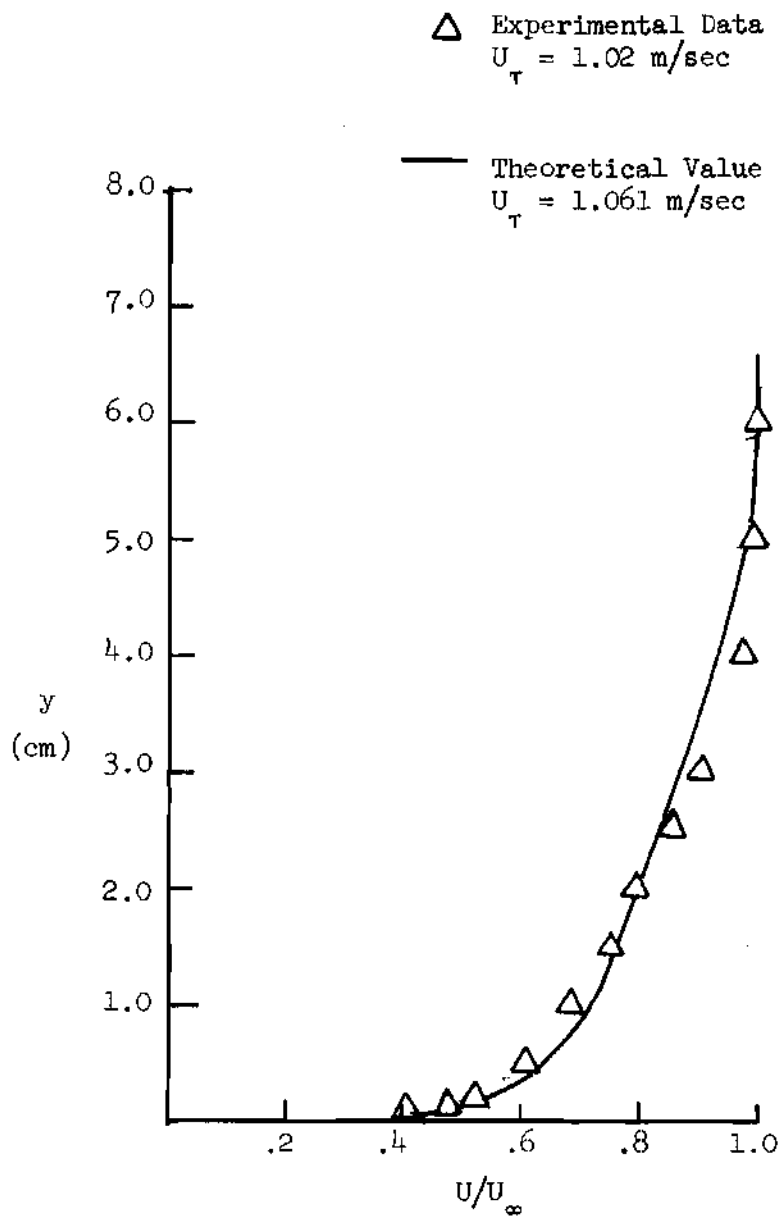

(a) x = 1.782 m; U_∞ = 30.7 m/sec

Figure 29. Boundary Layer Velocity Profile for Ludwiegand Tillmann Mild Adverse Pressure Gradient

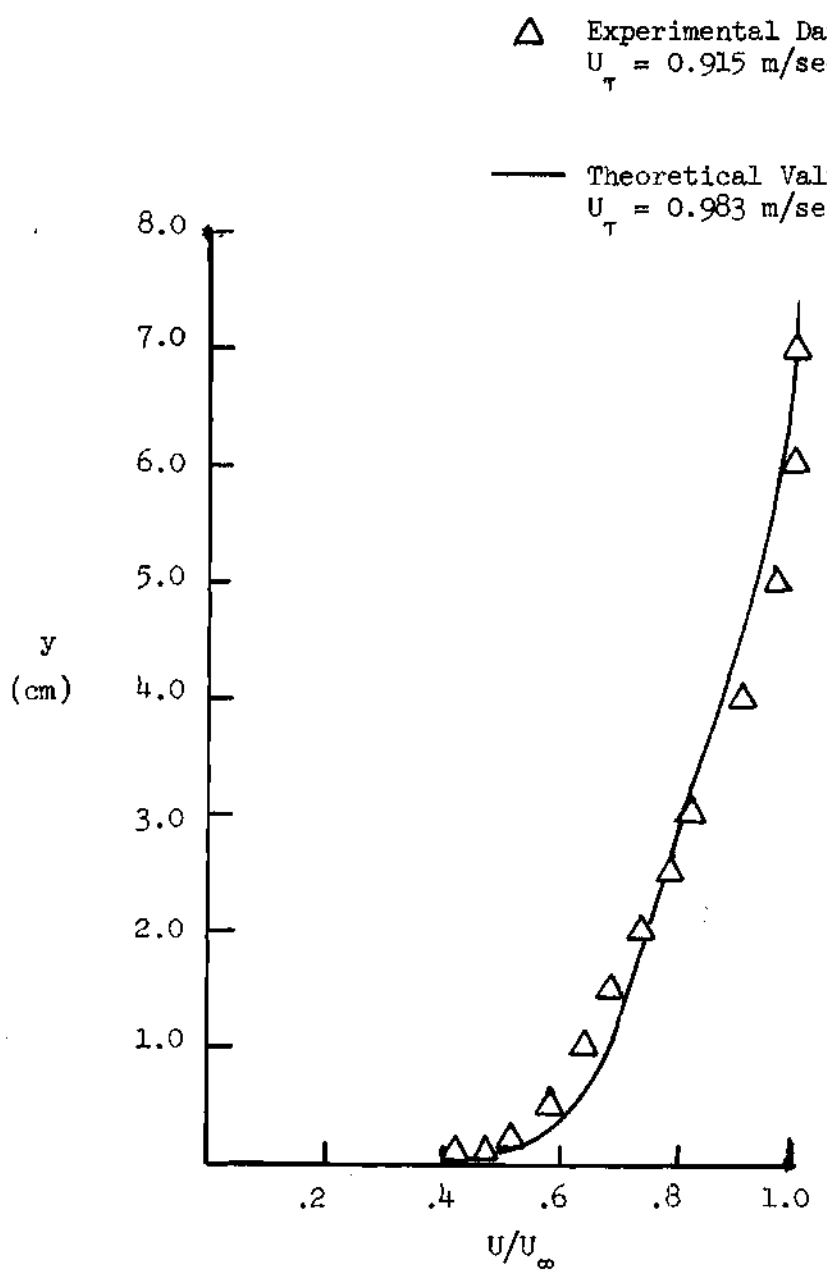

(b) x = 2.282 m; U_∞ = 28.6 m/sec

Figure 29. (Continued)

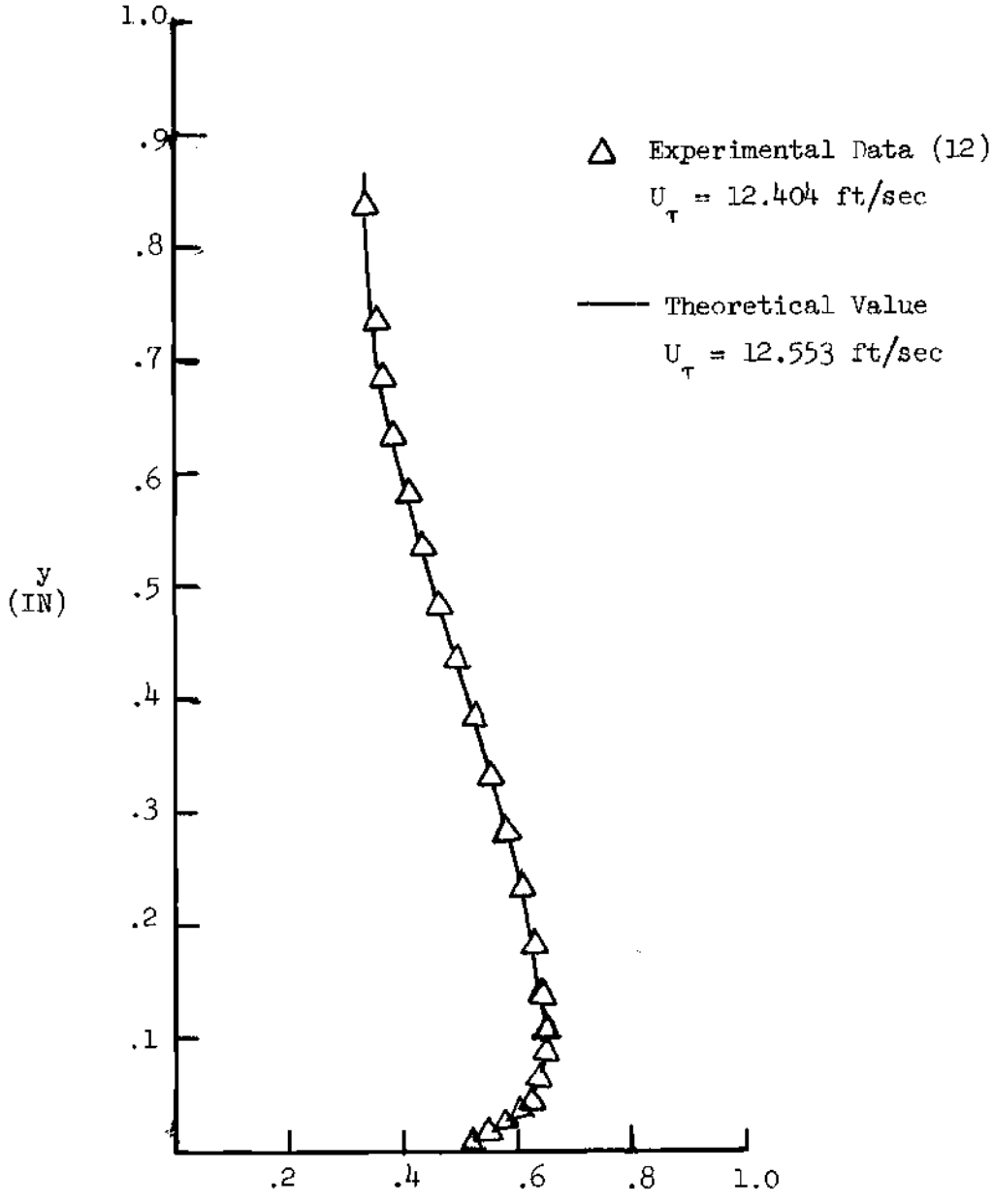

(a) X = 65

Figure 30. Wall-Jet Velocity Profile
Series II; VR = 3

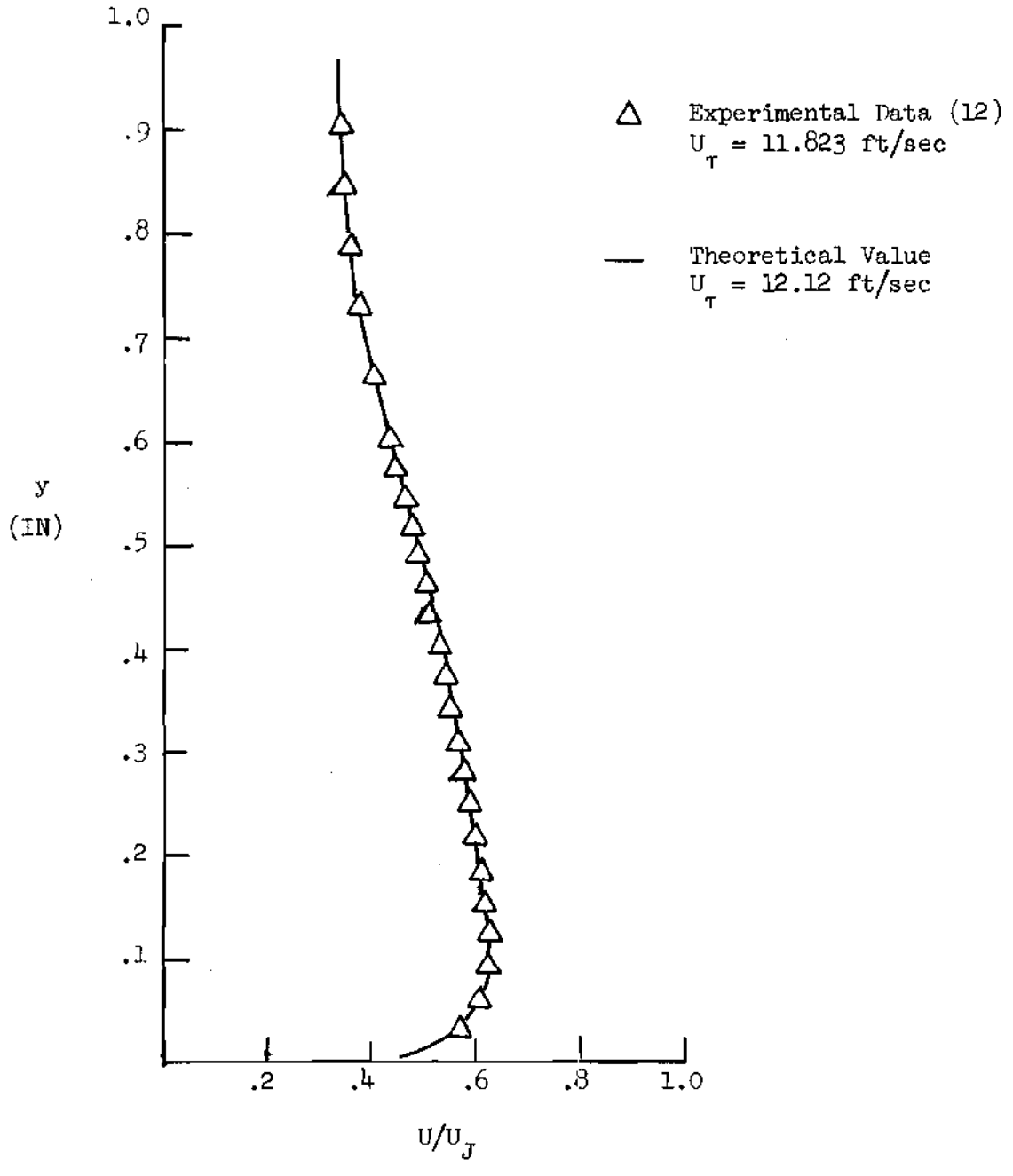

(b) X = 75

Figure 30. (Continued)

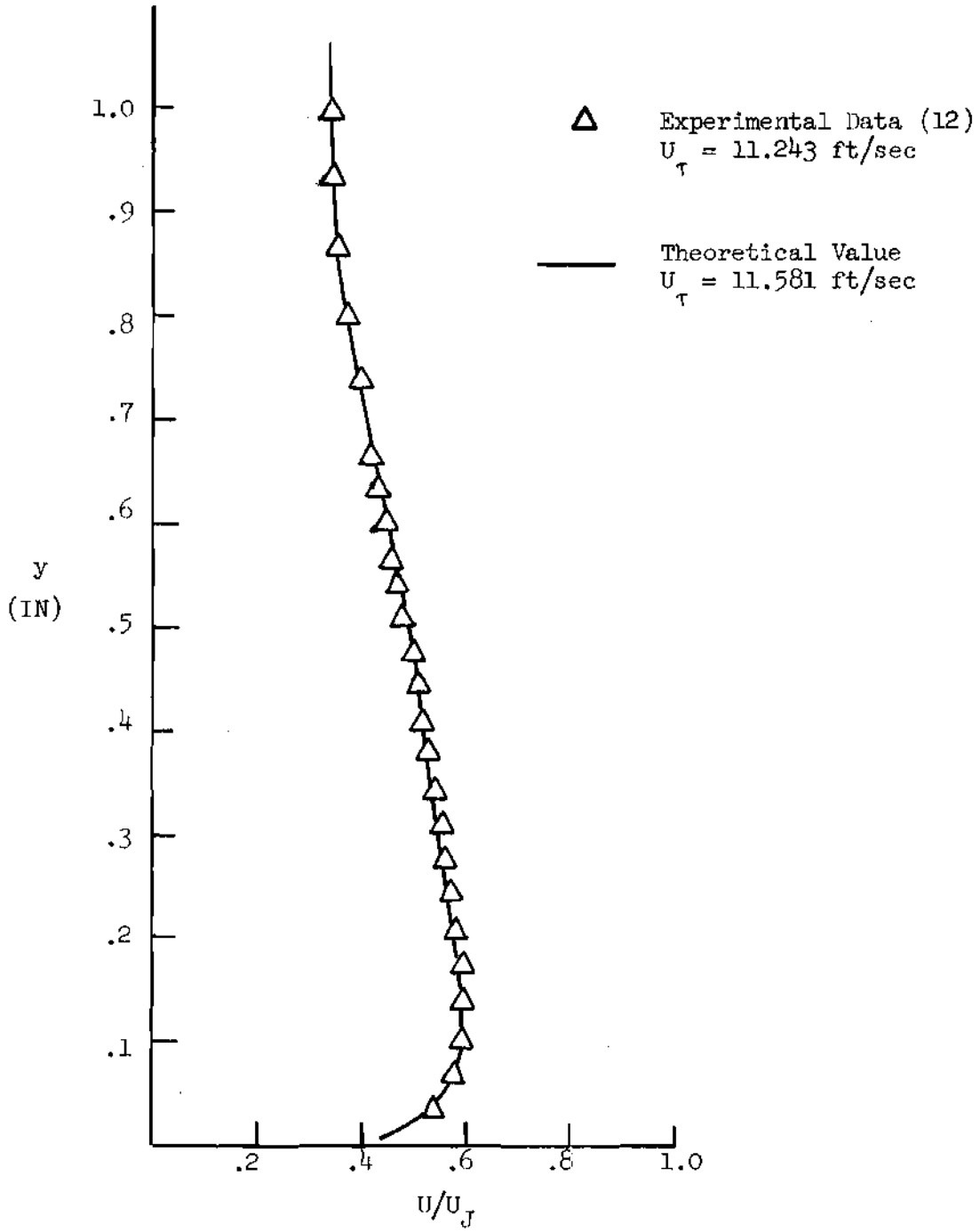

(c) X = 85

Figure 30. (Continued)

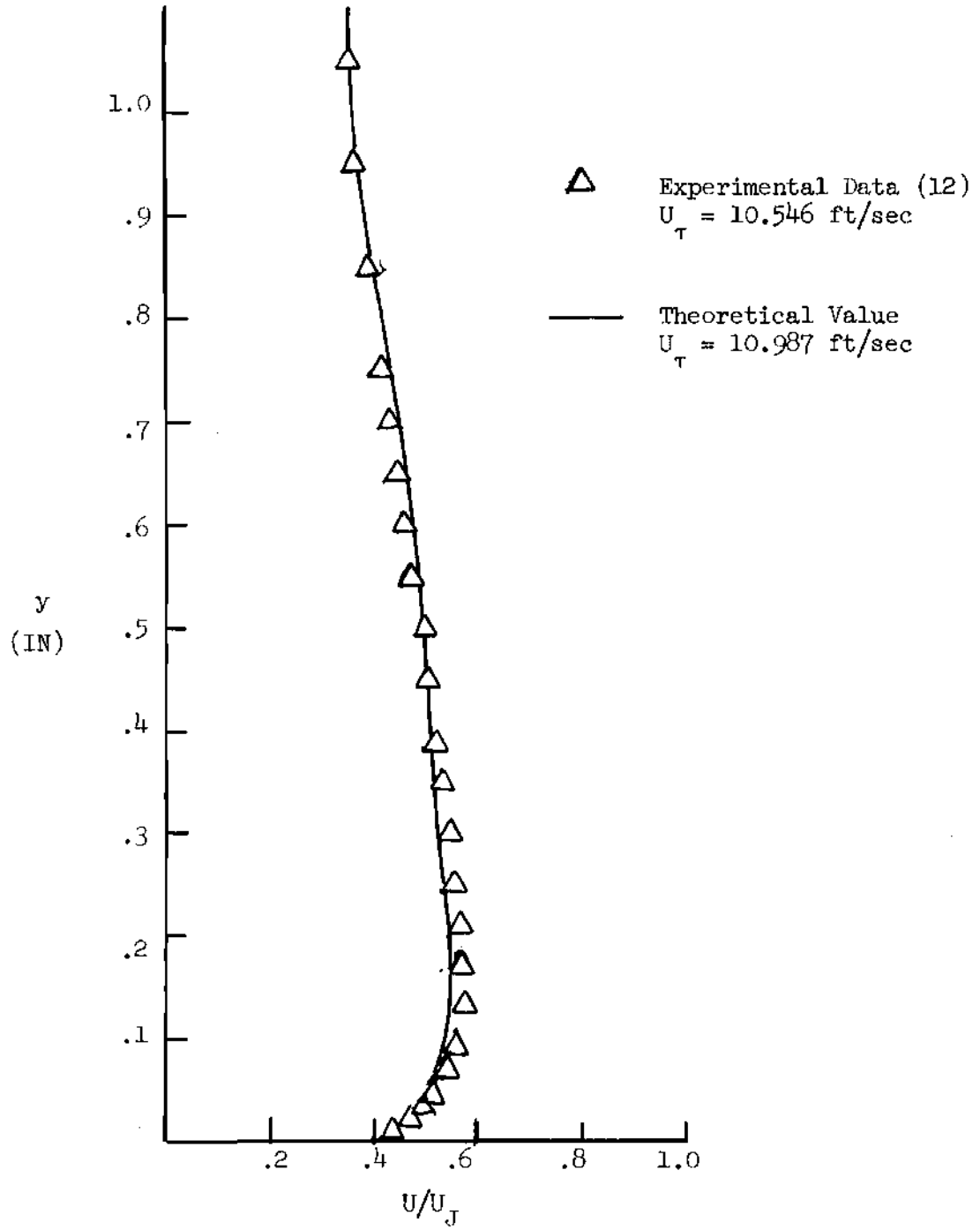

(d) X = 97

Figure 30. (Continued)

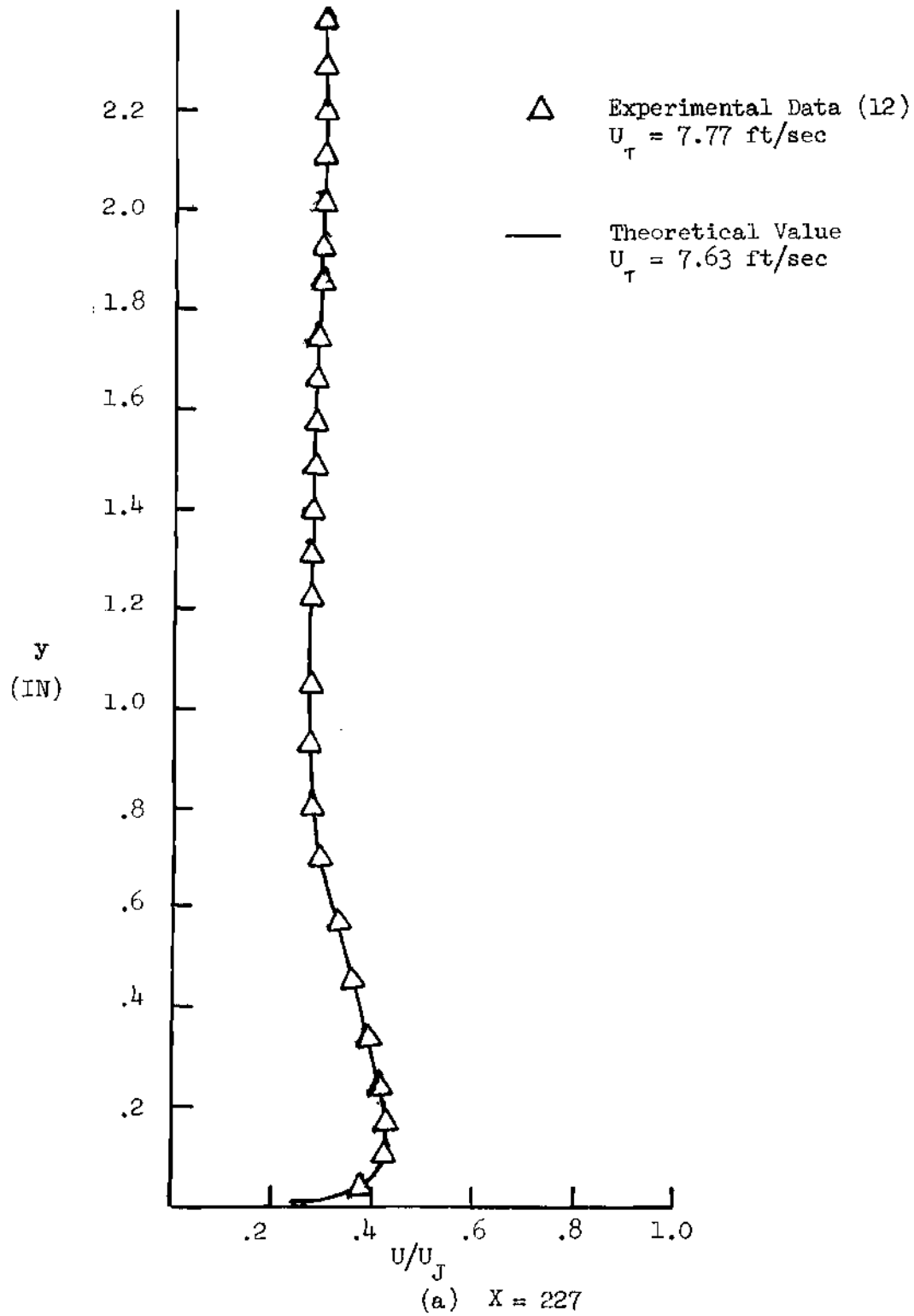

(a) X = 227

Figure 31. Wall-Jet Velocity Profile Series III; VR = 2.92

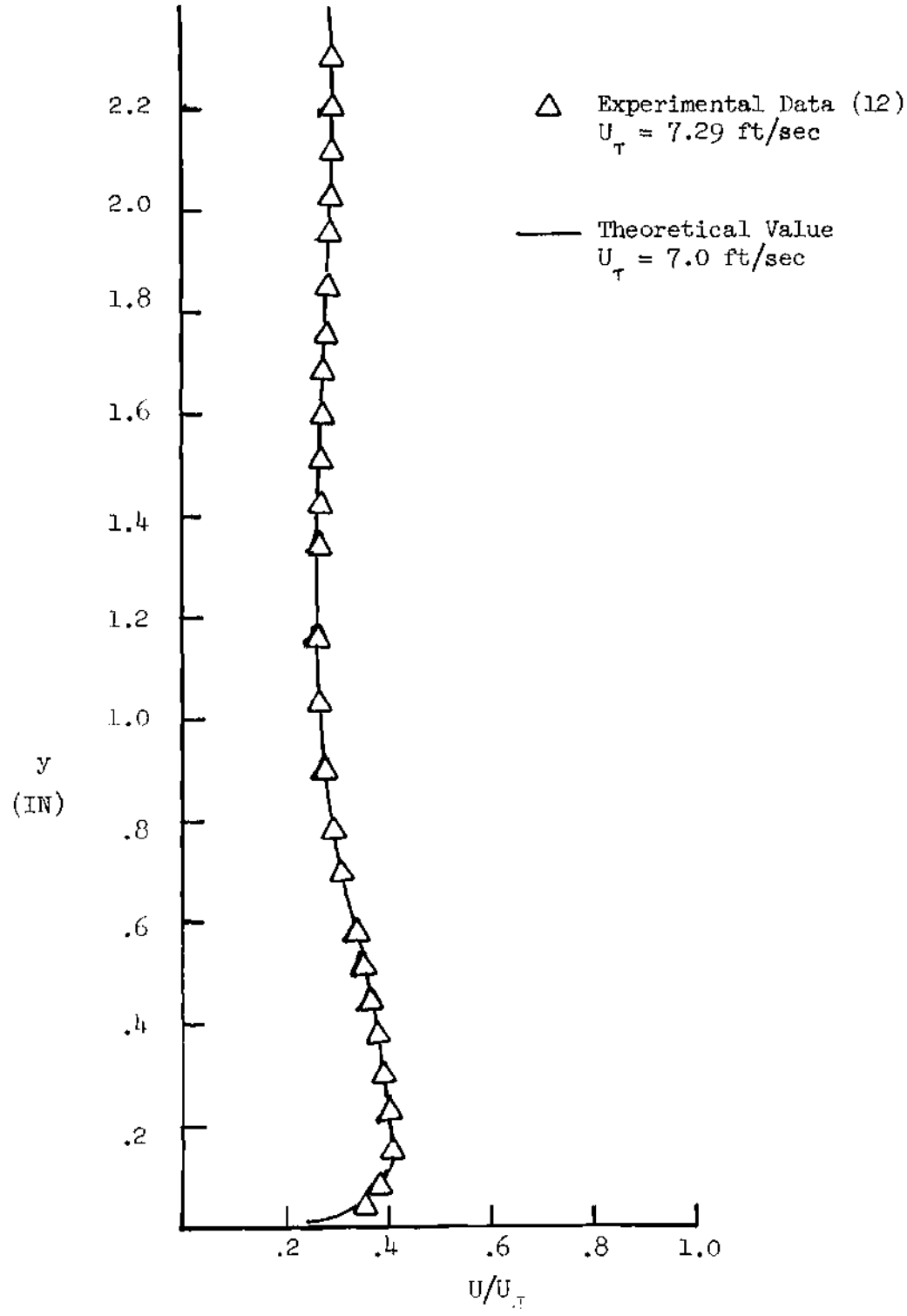

(b) X = 257

Figure 31. (Continued)

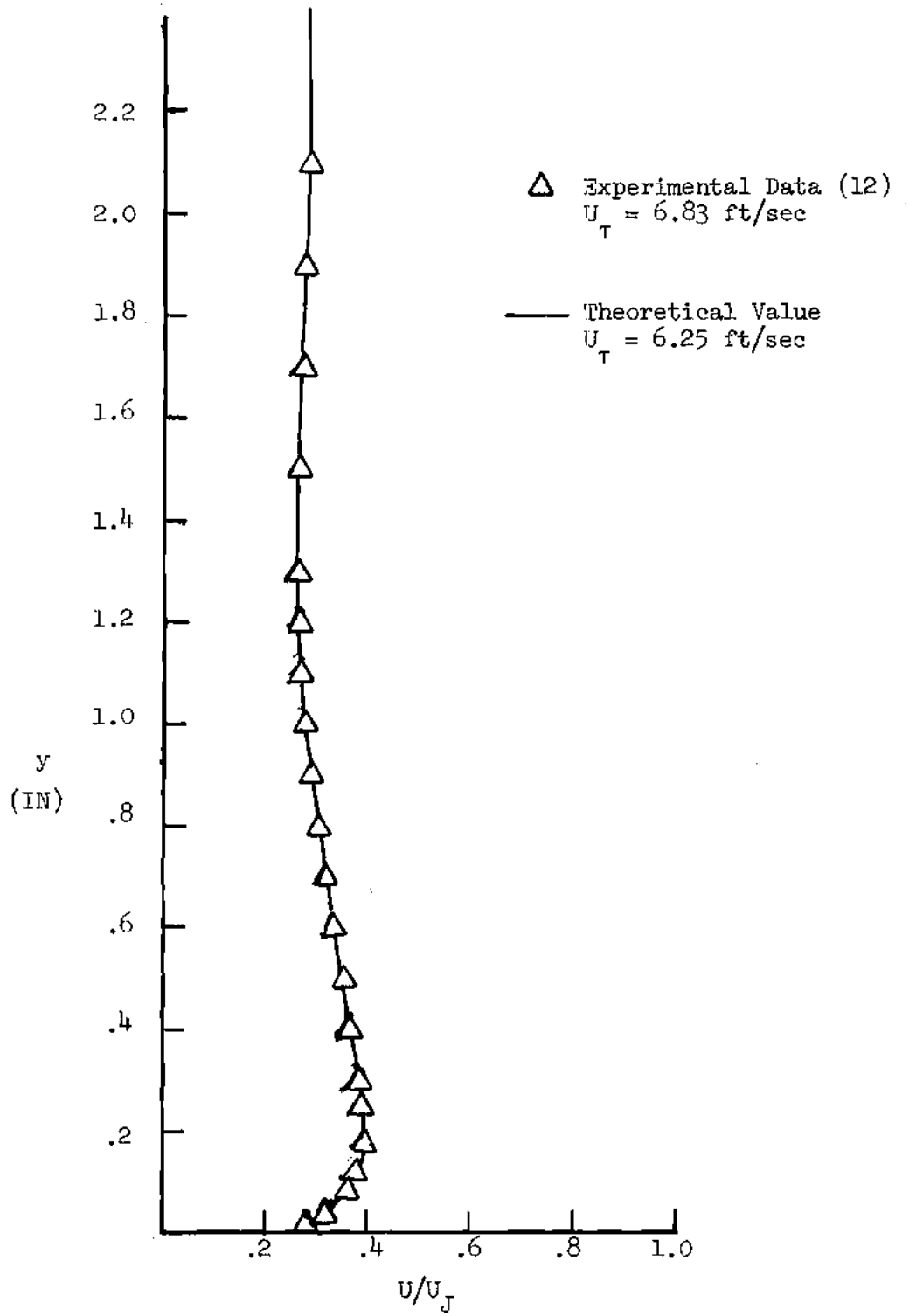

(c) X = 286

Figure 31. (Continued)

between the "wall sublayer" and the "inner shear stress similarity zone" and the numerical solution.

It is believed that a better matching condition would particularly improve the results for the Ludwieg and Tillmann flow (in this case the shear stress near the wall first rises and then decreases similar to that shown in Figure 29 (b)).

For example, it is readily possible to allow the matching point to float by specifying that the shear stress at the interface be equal to that predicted using the Clauser relation for an eddy viscosity which uses the wall-layer displacement thickness as the length scale and the maximum wall-layer velocity as the velocity scale. For this condition, it is expected that the boundary layer results would be very similar to those predicted by the method of Reference (37).

The numerical solution is relatively inefficient and as a result it was not reasonable to properly evaluate the step sizes and convergence (for the present calculations relatively large steps were used in the streamwise direction).

In the authors opinion, considerable improvement can and should be made by refining the numerical solution and developing a more definitive matching technique.

CHAPTER V

CONCLUSIONS AND RECOMMENDATIONS

Results from detailed analyses of experimental turbulent wall-jet data yield the following conclusions:

1. Similarity of velocity profiles in the jet and wake layers is observed when the velocities and lengths are appropriately scaled. This holds true even in the presence of a pressure gradient.

2. Similarity of shear stress profiles in the inner, jet and wake layers is observed when the stresses and lengths are appropriately scaled. This holds true even in the presence of a pressure gradient.

3. The wall sublayer velocities and shear stresses can be calculated from the similarity form of the viscous sublayer equations. The velocity profile and the wall shear stress agree quite well with the experimental data. The results incidentally show that the viscous sublayer is more strongly affected by streamwise shear-stress gradients than is the rest of the inner layer.

4. The turbulent energy equation can be converted into a differential equation for the maximum shear stress, along the line of maximum shear stress by defining three empirical functions relating the turbulent intensity, diffusion and dissipation to the shear stress profile. A resulting closed form expression for R_T agrees reasonably well with experimental data.

5. A cubic profile for approximating the inner shear layer

stress distribution outside the wall sublayer was developed for wall jets and boundary layers. Although it is believed that a better similarity function can be developed, the cubic profile as an initial try agrees reasonably well with experimental data. This similarity approach provided a more general basis for predicting the turbulent flow.

6. The shear-stress similarity approach for analyzing turbulent wall jets appears very promising. This approach not only can reduce the partial differential equation from second order to first order but also can avoid the singularity at zero shear stress which appears in the eddy viscosity approach. These advantages in conjunction with the preliminary finite-difference scheme used herein provide a reasonably successful method for the prediction of two-dimensional turbulent boundary layers and wall jets developing over a flat plate in constant or adverse pressure gradient.

The results presented herein are sufficiently promising to warrant additional fundamental studies. In particular the following additional studies are recommended:

1. Turbulent boundary layer data for a wide range in flow conditions should be analyzed in detail and compared with the present wall-jet results in order to establish an improved similarity function for the shear stress distribution in the porition of the inner shear layer outside the wall sublayer. This study should also consider the problem of matching this similarity function with the wall sublayer solution.

2. Additional experiments and analyses should be made to

improve the method of predicting the maximum shear stresses in the jet and wake layers of wall jets. Experimental measurements of the turbulence quantities, including the Reynolds stresses, in the regions around these maximum stresses should be made.

3. The numerical analysis for calculating the wall-jet development should be refined.

REFERENCES

1. Kacker, S. E., Pai, B. R. and Whitelaw, J. H., "The Prediction of Wall-Jet Flows with Particular Reference to Film Cooling", Progress in Heat and Mass Transfer, Vol. 2, Pergamon Press, London, 1969.

2. Quinn, B., "Compact Ejector Thrust Augmentation," Journal of Aircraft, Volume 10, No. 8, August 1973.

3. Forthmann, E., "Turbulent Jet Expansion," NACA TM 789, 1936.

4. Bakke, P., "An Experimental Investigation of a Wall Jet," Journal of Fluid Mechanics, Vol. 2, July 1957.

5. Glauert, M. B., "The Wall Jet," Journal of Fluid Mechanics, Volume 1, 1956.

6. Patel, R. P., and Newman, B. G., "Self Preserving, Two-Dimensional Jets and Wall Jets in a Moving Stream" McGill University Report No. Ae5, September 1961.

7. Kruka, V., and Eskinazi, S., "The Wall Jet in a Moving Stream" Syracuse University, Mechanical Engineering Department, Report No. ME 937-6309 F, August 1963.

8. Bradshaw, P., and Gee, M. T., "Turbulent Wall Jets with and without and External Stream", Aeronautical Research Council Reports and Memoranda, No. 3252, June, 1960.

9. Erian, F., and Eskinazi, S., "The Wall Jet in a Longitudinal Pressure Gradient", Syracuse University, Mechanical Engineering Department, Report No. ME 937-6410 F, October 1964.

10. Kacker, S. C., and Whitelaw, J. H., "Some Properties of the Two-Dimensional, Turbulent Wall Jet in a Moving Stream," Journal of Applied Mechanics, Transactions of the ASME, December 1968.

11. Gartshore, I. S., and Newmann, B. G., "The Turbulent Wall Jet in an Arbitrary Pressure Gradient," The Aeronautical Quarterly, February 1969.

12. Neale, D. H., "Experimental Study of Two-Dimensional Turbulent Wall Jet Development with and without Longitudinal Free-Stream Pressure Gradient," Ph.D. Dissertation, Georgia Institute of Technology, Atlanta, Ga., June 1971.

13. Sigalla, A., "Measurements of Skin Friction in a Plane Turbulent Wall Jet," Journal of the Royal Aeronautical Society, Vol. 62, December 1958.

14. Currieve, P. and Eichelbrenner, E. A., "Theory of Flow Reattachment by a Tangential Jet Discharging Against a Strong Adverse Pressure Gradient," Boundary-Layer and Flow Control, Pergamon Press, London, 1961.

15. Harris, G. L., "The Turbulent Wall Jet in a Moving Stream," Proceedings of Specialists Meeting Sponsored by AGARD Fluid Dynamics Panel, May 1965.

16. Patankar, S. V. and Spalding, D. B., Heat and Mass Transfer in Boundary Layers, International Textbook Company Ltd., London, England, 1970.

17. Myers, G. E., Schauer, J. J. and Eustis, R. H., "Heat Transfer to Plane Turbulent Wall Jet," ASME Paper 62-1-1T-33, 1962.

18. Schwartz, W. H. and Cosart, W. P., "The Two-Dimensional Turbulent Wall Jet," Journal of Fluid Mechanics, 10, p. 481, 1961.

19. Verhoff, A., "Steady and Pulsating Two-Dimensional Turbulent Wall Jets in a Uniform Stream," Princeton University Report No. 723, March 1970.

20. Hubbartt, J. E., and Bangert, L. H., "Turbulent Boundary Layer Control by a Wall Jet," AIAA Paper No. 70-107, Jan. 1970.

21. Goradia, S. H., "Confluent Boundary Layer Flow Development with Arbitrary Pressure Distribution," A Ph.D. Thesis, Georgia Institute of Technology, August, 1971.

22. Lighthill, M. J., "Introduction. Real and Ideal Fluids," Laminar Boundary Layers, edited by L. Rosenhead, Clarendon Press, Oxford, pp. 1-45, 1963.

23. Liepmann, H. W. and Roshko, A, Elements of Gasdynamics, John Wiley & Sons, Inc., New York, London, Sydney, 1956.

24. Schlichting, H., Boundary Layer Theory, Fourth edition, McGraw-Hill Book Company, Inc., New York, 1960.

25. Bradshaw, P., "The Understanding and Prediction of Turbulent Flow," Aeronautical Journal, PP. 403, July 1972.

26. Townsend, A. A., "The Structure of Turbulent Shear Flows," Cambridge University Press, 1956.

27. Bradshaw, P., Ferriss, D. H. and Atwell, N. P., "Calculation of Boundary-Layer Development Using the Turbulent Energy Equation," J. Fluid Mech., Vol. 23, 1967.

28. Hubbartt Private Communication

29. Coles, D., "The Turbulent Boundary Layer in a Compressible Fluid," R-403-PR, Rand Corp, Santa Monica, Calif., Sept. 1962.

30. Simpson, R. L., "Characteristics of Turbulent Boundary Layers at Low Reynolds Numbers with and without Transpiration," Journal of Fluid Mechanics, Vol. 42, Pt. 4, pp. 769-802, July 1970.

31. Cebeci, T. and Mosinskis, G. T., "Computation of Incompressible Turbulent Boundary Layers at Low Reynolds Numbers," AIAA Journal Vol. 9, No. 8, pp. 1632-1634, Aug. 1971.

32. Herring, H. J. and Mellor, G. L., "A Method of Calculating Compressible Turbulent Boundary Layers," NASA CR-1144, Sept. 1968.

33. Huffman, D. G. and Bradshaw, P., "A Note on Von Karman's Constant in Low Reynolds Number Turbulent Flows," Journal of Fluid Mechanics, Vol. 53, Pt. 1, pp. 45-60, May 1972.

34. Cebeci, T. "Kinematic Eddy Viscosity at Low Reynolds Numbers," AIAA, Vol. 11, No. 1, pp. 102, August 30, 1972.

35. Coles, D. E., and Hirst, E. A., "Computation of Turbulent Boundary Layers," Proceedings of the 1968 AFOSR-IFP-Stanford Conference, Vol. II Compiled Data, Stanford University Press, Stanford, Calif., 1969.

36. V. C. Patel and M. R. Head, "A Simplified Version of Bradshaw's Method for Calculating Two-Dimensional Turbulent Boundary Layers," AFOSR-IFP-Stanford 1968 Conference Proceedings, Stanford University, California, August 1970.

37. Cebeci, T., Smith, A. M. O., and Wang, L. C., "A Finite-Difference Method for Calculating Compressible Laminar and Turbulent Boundary Layer," Douglas Aircraft Company Report No. DAC-67131, March 1969.

VITA

Jaunan Liaw was born in I-Lan, Taiwan, China, on September 14, 1942.

He attended elementary school in I-Lan, Taiwan. He graduated from I-Lan high school in June, 1962. Mr. Liaw entered the University of Chengkung in Tainan, Taiwan, and he received the B.S. in M.E. in June, 1966 and M.S. in M.E. in June 1968. Mr. Liaw entered China Navy Academy as an instructor to serve the R.O.T.C. in July 1968.

He entered the Georgia Institute of Technology in September 1969 and was awarded a research assistantship to study under the doctoral program in the Department of Aerospace Engineering. He is a member of ASME, and Sigma Xi.

During his doctoral studies, Mr. Liaw was employed by Lockwood Greene Engineering Company and he joined Midrex Corporation as a Mechanical Design Engineer on January 2, 1975.

In August 1969 Mr. Liaw was married to the former Meichih Wu, Taiwan. They have a son, Henry, Linzu.